2014

Voltage and reactive power regulation by photovoltaics in distribution systems

Pedram Jahangiri
Iowa State University

Voltage and reactive power regulation
by photovoltaics in distribution systems

by

Pedram Jahangiri

A dissertation submitted to the graduate faculty
in partial fulfillment of the requirements for the degree of
DOCTOR OF PHILOSOPHY

Major: Electrical Engineering

Program of Study Committee:
Dionysios C. Aliprantis, Co-Major Professor
Colin Christy, Co-Major Professor
Venkataramana Ajjarapu
James D. McCalley
Leigh Tesfatsion
Zhengdao Wang

Iowa State University
Ames, Iowa
2014

DEDICATION

I would like to dedicate this dissertation to my parents, Lotfallah Jahangiri and Pooran Khorooshi, my wife Elham and my sister Pegah for their unconditional love and support in every way possible throughout the process of this course, this dissertation and beyond.

TABLE OF CONTENTS

LIST OF TABLES

LIST OF FIGURES

ACKNOWLEDGMENTS

I would like to to express my thanks to those who helped me with various aspects of conducting research and the writing of this dissertation.

First and foremost, I express my sincere gratitude to Dr. Dionysios C. Aliprantis, the major advisor of my Ph.D. studies, for his guidance, patience, and support throughout my research work and the writing of this dissertation.

Special thanks to my committee members, Dr. Colin Christy, Dr. Venkataramana Ajjarapu, Dr. James D. McCalley, Dr. Leigh Tesfatsion, and Dr. Zhengdao Wang for their efforts and contributions to my success.

Further, I acknowledge the financial support from the Electric Power Research Center of Iowa State University and the American Public Power Association (APPA) Demonstration of Energy & Efficiency Developments (DEED) program.

ABSTRACT

This research focuses on the design and implementation of two novel controllers within rooftop photovoltaic (PV) inverters. The main objective of the first control scheme is to eliminate the voltage violation (induced voltage rise due to reverse power flow) and to maintain the voltages within acceptable bounds, at essentially no extra investment cost to the PV owner. The second controller can significantly reduce real energy losses in the distribution feeder and reactive energy demand at the substation. Besides, reducing reactive demand at substation leads to loss reduction of substation transformer and transmission network. It can also relieve congestion in transmission network and improve the voltage stability. A significant advantage of the proposed controllers is that they do not require communication or cooperation with other PV inverters. The control objectives are attained by exploiting the inherent reactive power capability of the inverters and the dispatch of their reactive power is calculated in an autonomous fashion. In this context, important theoretical aspects of control design are investigated and a general framework for stability analysis of these types of systems is established. In addition, this work reports on the development of a distribution test feeder with smart-grid functionality. The test feeder is based on an actual distribution feeder. Case studies involving simulations of real (the developed feeder) and realistic distribution feeders with hundreds of households and their appliances modeled in high detail are performed to study the impacts of the proposed controllers on the distribution system. It is shown that implementation of these controllers could have a significant beneficial impact upon the efficiency and operation of the power grid.

1. GENERAL INTRODUCTION

1.1 Introduction

There is an increased pressure by regulatory agencies on utilities to accommodate higher levels of renewables for their distribution system and to speed up the interconnection process [1]. On the other hand, photovoltaics (PV) are expected to be the quickest increasing renewable technology due to the availability of solar resources in the world and the U.S [2]. Distributed PV (residential rooftop PV system) can be quickly interconnected at distribution level. The average residential PV systems range from 1 kW to 10 kW and can be simply mounted on rooftops of residential customers [3–5]. These residential PV systems are perfect for mitigating some of the major loads of residential customers. Additionally, recent reports [6–8] confirm that the capacity of PV installation continues to proliferate worldwide. It can be due to strong customer demand (because of increases in electricity prices), falling PV costs and financial incentives from the governments.

High penetration level of PV on distribution system present several opportunities and challenges for power distribution utilities. The utilities must ensure that the quality of service to their customers will not be violated due to integrating PV into their distribution systems [9, 10]. Major adverse impacts of high PV penetration are on system voltages (steady state voltage rises) [11–17]. In the United States, the ANSI Standard C84.1 [18] states that the voltage of residential loads should remain within five percent from its nominal value (120 V) under normal operating conditions. The severity of

these voltage issues depend on the penetration level, location, and the size of distributed PV systems and the configuration and characteristic of distribution feeders. This bad impact decreases the allowed PV hosting capacity[1] of the distribution system and is a serious barrier for further PV integration into the grid. Several techniques to alleviate the voltage rise issue have been proposed [19, 20]. The approach considered herein is by exploiting the inherent reactive power capability of the PV inverters to offset the voltage rise in distribution networks. Using reactive power capability could defer the need for new assets and grid reinforcements.

In general, PV systems use inverters to convert DC power from PV arrays to 60 Hz (or 50 Hz) AC power grid standard [21, 22]. In addition to the basic inversion function, there are more functions and features that are common to grid-tied PV inverters such as: Maximum Power Point Tracking (MPPT), grid disconnection, phase-locked loop for tracking the terminal voltage and anti-islanding detection scheme. Some of these functions are required by interconnection codes and standards, such as UL 1741 [23] and IEEE Std. 1547 [24]. Moreover, some modern PV inverters have the capability to supply or absorb reactive power, independently of their production of real power, at essentially no extra cost. PV systems that are capable of providing reactive power support to the grid are now commercially available [25, 26]. Retrofitting of some existing old inverters is also possible. For example, inverter manufacturer SolarEdge, claims it is possible to upgrade the reactive power capability for an old inverter without this capability [27]. Additionally, inverters are robust solid state devices that many of their electrical characteristics can be modified through software settings and commands [28]. The reactive power capability of PV inverters represent a significant opportunity to improve the operation, and efficiency of the electric power distribution system, particularly as PV systems become integrated into the grid at higher penetration levels. The reactive power capability can be exploited in a number of ways, for instance, for reducing the voltage rise

[1] How much PV can be integrated in a distribution system without violating power quality or security issues.

phenomenon due to the reverse power flow in distribution feeders [29]. Alternatively, PV inverters can be operated as local VAr compensators (LVArC), that is, when they are providing the reactive power consumed by local loads as measured at their point of common coupling (PCC). VAr compensation by PV inverters, reduces transmission loss, maximizes power transmission capability, enhances stability, and helps support the supply voltage. Consequently, the reactive power functionality of inverters (if designed and used accurately) could have a significant beneficial impact upon the efficiency and operation of the power system grid. This study considers the design and implementation of two controllers within rooftop PV inverters. The main objective of the first control scheme is to eliminate the aforementioned voltage violation and to maintain the voltages within acceptable bounds. The second controller reduces real energy losses in the distribution feeder and reactive energy demand at the substation. A significant advantage of the proposed controllers is that they do not require communication or cooperation with other PV inverters. The control objectives are attained by exploiting the inherent reactive power capability of the inverters and the dispatch of their reactive power is calculated in an autonomous fashion.

In order to properly evaluate the adverse impacts of PV systems and beneficial impacts of deployments of the proposed controllers on the distribution system, it is necessary to model the grid with high detail and conduct detailed time-series analysis. Currently, many utilities rely on commercial simulation tools to run the steady state power flow that are constrained to snapshots of critical time periods, such as the peak and minimum load points [30]. However, modern distribution systems with high penetration of PV systems and the potential interaction with their control systems cannot be adequately analyzed with these snapshot tools. Hence, there is an increased need for simulation tools and models arising from the evolution of today's electrical system to tomorrow's with high penetration of renewables and "smarter" grid. In this work, one of the objectives is to develop and simulate realistic representative power distribution

feeders with high fidelity (in terms of electrical topology, household loads and smart appliances, and environmental parameters) in order to eventually perform detailed analysis of PV generation at the distribution level with the proposed controllers. In particular, part of this dissertation focuses on the modeling of a future grid that will include a significant amount of distributed renewable energy generation, mainly from PV systems. The simulations in this dissertation are run using GridLAB-D [31], which is an open-source software platform and a time-series power distribution system simulation.

Another issue of considerable importance is analysing the system stability of the distribution system with multiple distributed controllers in the quasi steady-state operating points. Because, even as distributed controllers operate to improve local and system level performance, their control algorithm should be able to separate their dynamic responses from other controllers to limit their interference. If it cannot be attained, the dynamic interaction of distributed controllers can compromise the system stability and oscillations could result. For example, as pointed out in [32, 33] a bad choice of controller parameters can significantly affect the dynamic response for local and system voltage regulation, and may lead to oscillatory and an unstable response. However, in the aforementioned works and prior related research papers, theoretical system analysis of distribution system stability was not investigated when distributed controllers are used. The use of distributed controllers represent a new paradigm in the active control of the distribution system and less is known about the stability analysis of such controllers in quasi steady-state operating points. As a result, the construction of a framework for active distribution system stability analysis seems absolutely necessary. In the present study, rigorous theoretical analysis of system stability, including multiple proposed controllers acting independently of each other is investigated. This analysis can also provide a useful framework for studying system stability with other types of distributed controllers.

1.2 Dissertation Organization

The dissertation's chapters correspond to journal and conference papers that I have co-authored.

Chapter 2 provides an agent-based implementation of a distribution test feeder with a high-fidelity representation of electrical topology, environmental parameters, and loads arising from households equipped with smart appliances and dispersed generation units. The availability of such realistically rendered distribution test feeders facilitates the study of "smart" distribution systems. The agent-based distribution test feeder (ABDTF) uses GridLAB-D to simulate a distribution feeder that incorporates various smart-grid technologies. It is based on an actual feeder from an electric utility in Iowa, with detailed specifications for distribution feeder equipment (such as fuses, switches, overhead and underground conductors, and service transformers) as well as for residential and/or commercial customers. Houses are virtually equipped with various smart-grid enabled technologies, such as rooftop PV generation and price-responsive demands in the form of Plug-in electric vehicles (PEV) and intelligently controlled A/C systems. Effects of cloud-passing on PV generation output are also considered. The ABDTF is used for case studies[2] in Chapter 3 and Chapter 4.

Chapter 3 describes the implementation of a voltage control loop within PV inverters that maintains the voltage within acceptable bounds by absorbing or supplying reactive power. In principle, this can be considered to be a form of distributed Volt/VAr control, which is conventionally performed by coordinated control of capacitor banks and transformer tap changers. Comprehensive simulation studies on detailed feeder models are used to demonstrate that the proposed control scheme will mitigate voltage rises. One of the main objective of this analysis is to provide evidence through comprehensive sim-

[2]In its original implementation, the feeder was equipped with an array of intelligent "agents," such as price-responsive air-conditioning units and plug-in electric vehicles, hence the name of the feeder. However, this type of functionality has been disabled in Chapter 3 and Chapter 4, and the feeder only contains conventional non-price-responsive load.

ulation studies that this control scheme will mitigate voltage rise, at essentially no extra investment cost to the consumer. In all cases that were analyzed, voltage violations were completely eliminated. Also a general framework for stability analysis of these types of controllers is established in this chapter.

Chapter 4 studies the behavior of distribution feeders with high penetration level of rooftop PV, in the case where PV inverters compensate the reactive power consumption of local households loads. In this context, some important theoretical aspects of control design are investigated and a rigorous theoretical analysis framework of system stability is established. Case studies involving simulations of realistic distribution feeders with hundreds of households and their appliances modeled in high detail are performed to study the distribution system impacts of the proposed controller. It is shown that this control typically leads to a reduction of real power losses, and helps to decrease congestion at the transmission side.

Chapter 5 summarizes the contributions of this work and recommends further investigations for future work.

2. Development of an Agent-Based Distribution Test Feeder with Smart-Grid Functionality

A paper published in the *Proceedings of the IEEE Power and Energy Society General Meeting*, San Diego, CA, July 22-26, 2012.

Pedram Jahangiri [1], Di Wu, Wanning Li, Dionysios C. Aliprantis, and Leigh Tesfatsion

Abstract

This paper reports on the development of an agent-based distribution test feeder with smart-grid functionality. The test feeder is based on an actual distribution feeder with various additional features incorporated, including rooftop photovoltaic generation and price-responsive loads (e.g., plug-in electric vehicles and intelligent air-conditioning systems). This work aims to enable the integrated study of wholesale electric power markets coupled with detailed representations of the retail-side distribution systems.

2.1 Introduction

TODAY most consumers of electric power face fixed retail rates, hence their demands are independent of day-to-day variations in wholesale power prices. Consequently, for many purposes, wholesale power market researchers can treat demands for power as fixed inputs, avoiding the need for any detailed modeling of distribution

[1] Primary researcher and author.

systems. Nevertheless, the validity of conducting decoupled studies of wholesale and retail power system operations could be dramatically reduced in the near future with the development of smart-grid features such as demand response, dynamic-price retail contracting, distributed generation, and energy storage systems. These developments will lead to increased feedbacks between retail and wholesale power system operations that must be captured if empirical verisimilitude is to be attained. Realizing this need, an agent-based test bed has been developed for the integrated study of retail and wholesale power markets operating over transmission and distribution networks with smart-grid functionality [34, 35]. The current study reports on one aspect of this ongoing research: the development of an agent-based distribution test feeder (ABDTF) for evaluating the impacts of smart-grid market designs on distribution feeders.

The ABDTF will implement a detailed model of a distribution feeder with smart-grid functionality, including rooftop photovoltaic (PV) generation and price-responsive loads such as plug-in electric vehicles (PEV) and intelligent air-conditioning (A/C). The ABDTF will thus facilitate the study of the impacts of smart-grid technologies on distribution feeders. More broadly, however, the ABDTF will permit the performance evaluation of smart-grid market designs at both wholesale and retail levels.

The IEEE Distribution Test Feeder Working Group and the CIGRE Task Force C6.04.02 have developed several test feeders and network benchmarks [36–39]. However, the high-fidelity modeling of load is beyond the scope of these studies, whose purpose has been to provide common data sets to test and validate new algorithms for the analysis of distribution systems. For example, typically only load values or generic profiles are provided, but the load's dependence on the time of day or the weather is not accurately modeled. Environmental (e.g., temperature) and house parameters (e.g., ceiling height and area) are not accessible either. In consequence, these test feeders are not detailed enough for the evaluation of smart-grid market designs.

Researchers at the Pacific Northwest National Laboratory (PNNL) have developed a

taxonomy of 24 prototypical feeder models that contain the fundamental characteristics of radial distribution feeders found in the U.S., based on 575 distribution feeders from 151 separate substations from different utilities across the U.S. [40, 41]. Each prototypical feeder is characterized by climate region, primary distribution voltage level, and other features. The feeder information is provided in a form that can be directly used in GridLAB-D [31], which is an open-source software platform developed by DOE at PNNL for the simulation of electric power distribution systems. Nevertheless, smart-grid technologies such as intelligent A/C systems, PEV and PV generation (with a consideration of cloud-passing effects) are still under development for the PNNL feeder models and are not yet available. Moreover, the PNNL feeder models are missing geographical coordinates of the feeder components important for the realistic rendering of dispersed PV generation units with a consideration of cloud patterns.

The ABDTF uses GridLAB-D to simulate a distribution feeder that incorporates various smart-grid technologies. It is based on an actual feeder from an electric utility in Iowa, with detailed specifications for distribution feeder equipment (such as fuses, switches, overhead and underground conductors, and service transformers) as well as for residential and/or commercial customers. Houses are virtually equipped with various smart-grid enabled technologies, such as rooftop PV generation and price-responsive demands in the form of PEVs and intelligently controlled A/C systems. Effects of cloud-passing on PV generation output are also considered. Realistic travel pattern data obtained from a 2009 National Household Travel Survey [42] are used to model PEV load.

The ABDTF is agent-based in the sense that some of the distribution feeder components are modeled as interacting agents whose actions are determined by individually specified objectives or purposes subject to financial and/or physical constraints. For example, the actions of a household resident agent might involve the determination of optimal inter-temporal comfort/cost trade-offs conditional on retail energy prices, envi-

ronmental conditions, and equipment limitations. The actions of a PEV agent might involve the minimization of energy costs subject to feasible travel routes, time constraints, and charger rating. The actions of a PV agent might involve the maximization of harvested solar power subject to panel surface area and weather conditions (e.g., cloud cover).

The remainder of this paper is organized as follows. Section 2.2 describes the ABDTF topology and its main characteristics. Section 2.3 provides more details about the agents of the test feeder. In Section 2.4, an example is provided to illustrate how the developed test feeder can be used in a market analysis, with emphasis on the distribution system variables. Section 2.5 concludes the paper.

2.2 Distribution Feeder Description

The distribution feeder is providing electricity to a residential neighborhood in the state of Iowa. Its technical data were obtained from the electric utility that operates it. Fig. 2.1 depicts a schematic of the feeder's topology that includes all branches at the medium voltage level. Exact geographic coordinates of its components are also known, but are not reflected in the figure. Fig. 2.2 shows a small representative section of the feeder, including part of the substation. The other branches have similar characteristics. Therefore, the feeder is modeled with as much accuracy as possible, including asymmetry in the lines and the loads. The feeder's electrical component data are entered into a GLM file for use by GridLAB-D, which solves a sequence of three-phase power flows throughout the simulated time period at a user-defined time step.

The feeder's peak power at the substation is reported by the utility to be approximately 14 MVA. It consists of 316 medium voltage (13.2 kV) lines; 301 are overhead and 15 are underground. In terms of overhead lines, the feeder contains 7 different types of conductors, and has 98 three-phase plus neutral (ABCN) lines, 2 two-phase (ACN)

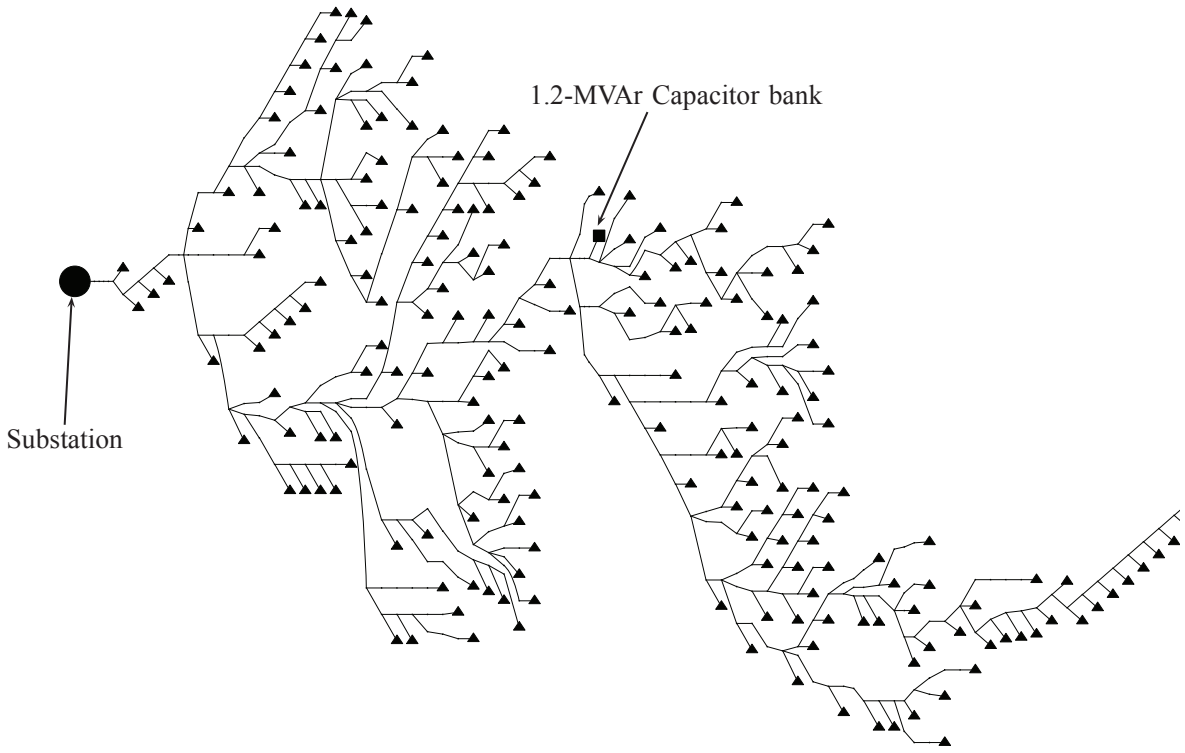

Figure 2.1 Schematic of the feeder topology (this is not an accurate geographic representation). The triangles at the leaves of this tree represent distribution transformers.

lines, and 73 AN, 60 BN, and 68 CN single-phase lines. In terms of underground cables, there are 2 different conductor types, and 13 ABCN, 1 AN, and 1 CN cable. The main parameters of the overhead lines and underground cables are listed in Table 2.1. The length of the lines varies between 5 and 522 feet. There are 175 single-phase center-tapped transformers rated 7621/240 V and 25 to 75 KVA, mounted on utility poles or concrete pads, with parameters listed in Table 2.2. (Some of these parameters were obtained from [43].) Finally, the end-load consists of 1370 houses. For the modeling of the PV and A/C systems, it is necessary to know the floor area and number of stories for each house, as well as the area of the south-facing part of the roof of each house (where PV panels are typically installed). To this end, these parameters were estimated using Google earth [44] based on the geographic coordinates of the distribution transformers.

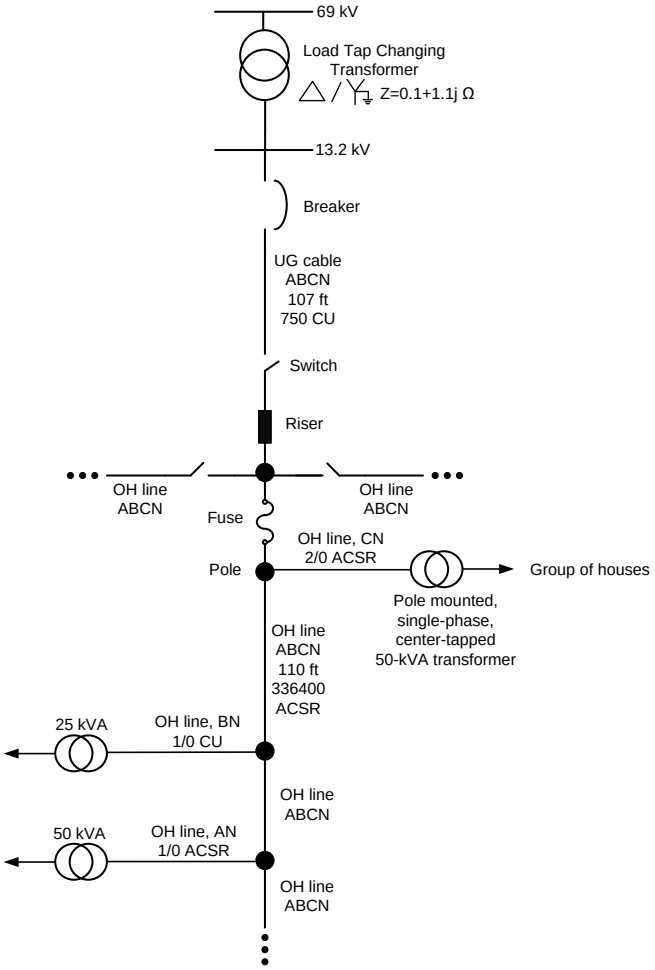

Figure 2.2 One-line diagram of a small representative section of the feeder.

2.3 Description of Agents

The end-use loads of the households are divided into two groups. The first group includes loads such as conventional thermostatically controlled A/C, water heaters, TV sets, fans, lights, ovens, and other common electric devices. These constitute a background non-price-responsive load, which is determined automatically by GridLAB-D's internal load modeling algorithms. The second group contains two kinds of "intelligent" loads, namely: (i) a new class of A/C controller that operates based on a varying retail price signal and the household resident's cost-comfort tradeoff preferences, and (ii) PEVs

Table 2.1 Parameters of Overhead Lines and Underground Cables

ID	Type	AWG/kcmil	Rating (A)
1	OH-ACSR	336.4	639
2	OH-AL	336.4	585
3	OH-CU	1/0	291
4	OH-ACSR	1/0	285
5	OH-ACSR	2	215
6	OH-CU	4	155
7	OH-CU	6	116
8	UG-CU	750	550
9	UG-AL	1/0	200

Table 2.2 Parameters of Single-Phase Center-Tapped Transformers

Type	Rating (kVA)	Z_{series}(pu)	Z_{shunt}(pu)
Pole mounted	25	0.016+0.023j	339.6+331.8j
Pole mounted	50	0.014+0.024j	391.8+428.1j
Pole mounted	75	0.0135+0.030j	470.0+454.6j
Pad mounted	25	0.016+0.023j	339.6+295.5j

whose charging is performed overnight based on the same retail price signal as the A/C. The feeder also has a large penetration of distributed generation in the form of rooftop PV panels. It should be noted that the electric power and energy consumption of A/C systems and PEVs accounts for a substantial portion of the total feeder load. If installation costs continue to decline, it is also possible that rooftop solar will become much more prevalent in the near future in the United States. Each one of these technologies on its own merit has potential to impact distribution feeder reliability to a significant degree due, for example, to transformer overloading or unacceptable voltage deviations. In particular, the test feeder described herein allows us to study the behavior of such systems when responding to market-based price signals, and hence to evaluate the impact of market policies at the distribution level. Additional details about these smart-grid agents are provided in the following subsections.

2.3.1 Intelligent Air-Conditioning Systems

Households are equipped with a recently proposed intelligent A/C system with smart-grid functionality [45]. The qualifier "intelligent" means that the A/C controller has advanced computational capabilities and uses an array of environmental and occupancy parameters in order to provide optimal intertemporal comfort/cost trade-offs for the household residents, conditional on retail energy prices and environmental conditions. The term "smart-grid functionality" means that retail energy prices are allowed to vary throughout the day. They are transmitted to the A/C controller each day (say, at 6pm daily), thus allowing the controller to schedule its energy consumption for 24 hours in advance (starting at midnight). It should be noted that the entity (e..g, utility or A/C aggregator) that is responsible for providing the retail prices to the A/C systems (different from the fixed retail price that conventional uncontrollable loads pay) is another (profit-maximizing) agent which could be modeled within the wholesale power market simulation software.

2.3.2 Plug-in Electric Vehicles

Plug-in electric vehicles can help reduce dependence on petroleum and transportation costs. In addition, they can be aggregated to provide an array of ancillary services to the power grid with appropriate control [46]. Therefore, they could be an important ingredient in tomorrow's smart distribution systems, but they represent a substantial additional load to the system. In the ABDTF, PEV load is estimated using a stochastic formulation that takes into account spatial and temporal diversity [47]. When developing the PEV power consumption, various factors are modeled, for example, PEV fleet characteristics such as charge-depleting range and fraction of tractive energy from electricity in charge-depleting mode [48,49], charging circuits [50], travel patterns [42,49], and PEV load control and management strategies [51–53]. Similar to the A/C system, the PEV aggregator entity (or entities) could be modeled as a separate agent (or agents) in the

wholesale market simulation.

2.3.3 Rooftop Solar Generation

Each house can have installed rooftop PV panels. The maximum amount of PV capacity is determined by the house's southern roof area. Each PV installation is represented as a separate agent with its own attributes and methods (rules of operation). The attributes include power rating and installation parameters such as tilt angle, cover area, and efficiency rating. The inverter is assumed to be operating in a quasi steady-state, under maximum power point tracking control [54]. In response to environmental inputs, such as solar radiation and ambient temperature, the PV panel reacts by generating different amounts of real power. The solar radiation pattern for each house is generated by moving over the feeder area a synthesized cloud pattern similar to the one shown in Fig. 2.3. Also, the PV inverter has the capability to supply or absorb reactive power from the grid in order to improve the local distribution system voltage profile. The design of algorithms for determining the appropriate reactive power compensation by the PV inverters is the subject of ongoing work.

2.4 Illustrative Example

The ABDTF is seamed with AMES [55], an open-source agent-based platform previously developed by a team of researchers at Iowa State University for the study of strategic trading in restructured wholesale power markets with congestion managed by locational marginal prices (LMPs). The resulting seamed platform will be used to conduct controlled computational experiments to investigate a number of important issues relating to smart-grid developments, such as how the penetration of price-responsive demand, PEVs, and distributed generation (e.g., PV) affects load profiles at the wholesale level.

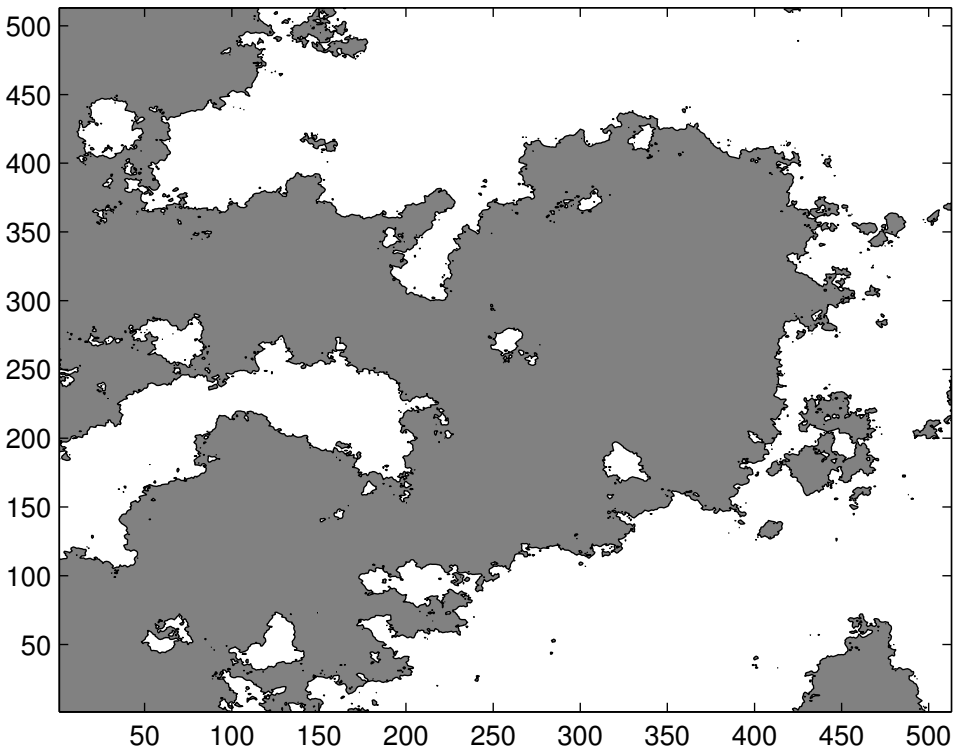

Figure 2.3 Example of synthetic cloud cover used in the simulation, which moves over the distribution feeder area at constant velocity. The axes units are pixels, and one pixel represents 7 meters. Hence, this square area has a 3.5-km side. The cloud is represented by the gray area.

Here a simple example that illustrates how the resulting seamed platform might be used to study feedback effects between retail and wholesale power system operations is presented. As shown in Fig. 2.4, the current implementation of such a study involves four main components, namely, the ABDTF running in GridLAB-D, a Data Management Program (DMP), a MySQL database server, and AMES running in Java.

The DMP has the following three tasks: (i) to receive environmental parameters (weather data and cloud pattern), household occupancy parameters, and 24-hour day-ahead wholesale energy prices (LMPs), and to map this data into retail energy prices (REPs); (ii) to send all information obtained in (i) to the ABDTF in comma-separated values (CSV) format; and (iii) to collect simulation results (aggregated load data) from the ABDTF output and transmit these results to the MySQL database server. The

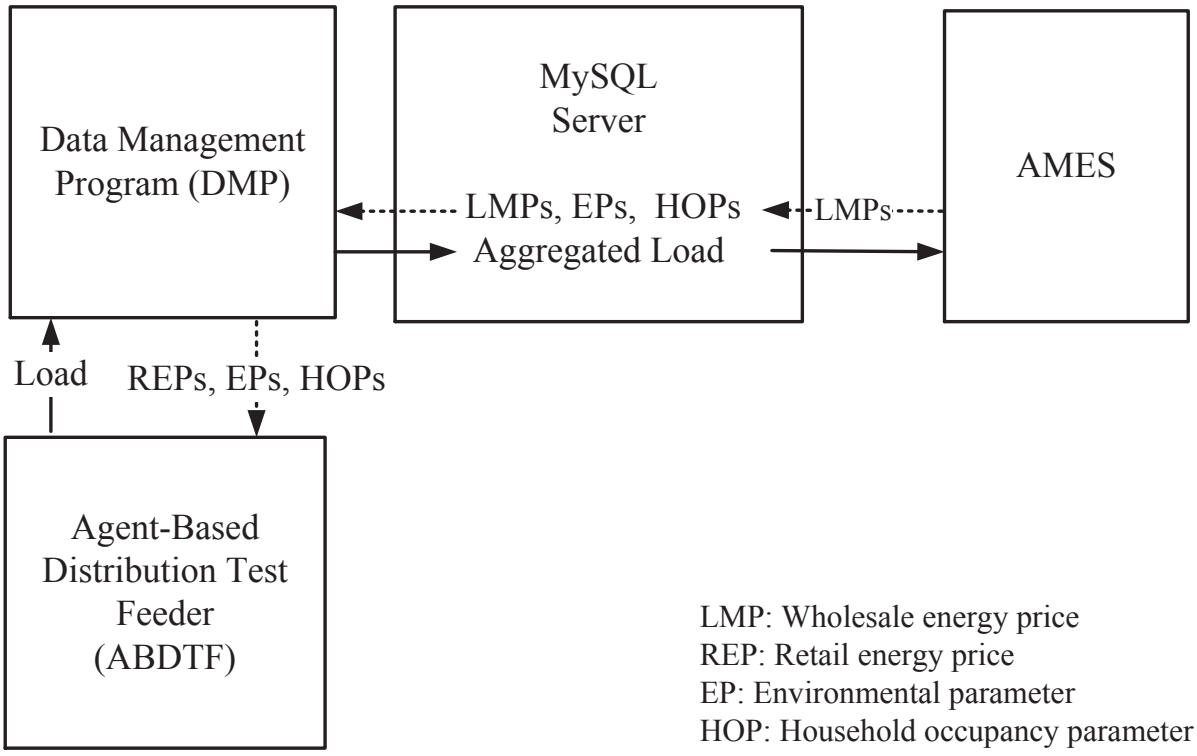

Figure 2.4 Illustration of data flow for the integrated study of retail and wholesale power market operations.

functionality of the DMP basically represents the communication between distribution-level components (e.g., advanced meters) and entities that exist at a higher level (e.g., transmission/distribution utilities, load serving entities, aggregators of demand response, or aggregators of plug-in electric vehicles). The MySQL database server maintains two repeatedly-updated information storage tables, one for storage of the LMPs obtained from AMES, and one for storage of the load data obtained from the ABDTF.

In what follows, simulation results are presented for a hot and cloudy summer day. The variation of environmental parameters used for day-ahead scheduling and real-time simulations is depicted in Fig. 2.5. A crudely predetermined schedule of appliances is used to construct the internal heat flow rate for the day-ahead scheduling of the A/C systems. A finer variation of appliances and occupant activity is assumed to occur in real-time. The retail price for this day, which is communicated to the smart A/C systems and

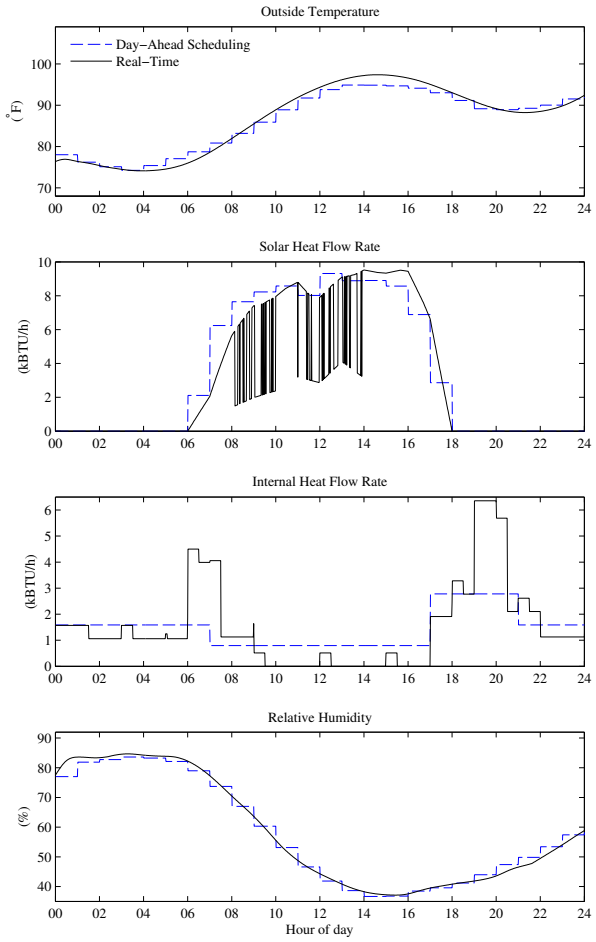

Figure 2.5 Variation of environmental parameters for day-ahead scheduling and real–time simulation. The solar irradiation and internal heat flow rates differ for each house.

the PEVs, is the day-ahead LMP (this could be obtained from AMES) plus a mark-up of 5 cents/kWh, shown in Fig. 2.6.

Figs. 2.7(a) and 2.7(b) depict the total real and reactive power load at the substation. The reversal of real power flow at the substation during the daytime is due to the high penetration of PV units in this case. For this example, a 100% penetration level was assumed for the rooftop PV units, where penetration level is defined as the total PV panel area divided by the total available south roof area. Figs. 2.7(c) and 2.7(d) show the total real power consumption from the smart A/C systems and the PEVs, respectively. The penetration level of PEVs in this case is 25%, i.e., one out of four vehicles is randomly

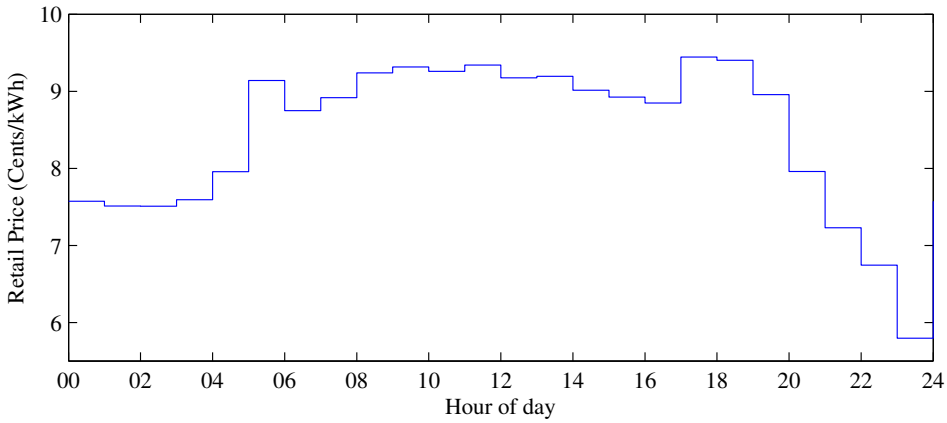

Figure 2.6 Retail price variation.

selected to be a PEV. Half are charged at off-peak hours with a minimum-cost control algorithm, whereas the other half start charging at the time when they return home paying the usual flat electricity price. Fig. 2.7(e) presents the total real power generated from the PV units. Finally, Fig. 2.8 shows the real power losses on the various types of feeder components.

Fig. 2.9 illustrates maximum, minimum and average voltages at the meters of the residential loads. As can be seen, the maximum voltages become significantly higher than 126 V for some residential customers due to the reverse power flow caused by the PV units. The ANSI Standard C84.1 [56] requires that the voltage at residential loads remains within five percent (114–126 V) from its nominal value (120 V).

2.5 Conclusion

Ideally, smart-grid technologies should be thoroughly evaluated prior to their deployment. The primary goal of this project is to supply researchers with an agent-based implementation of a distribution test feeder that provides a high-fidelity representation of electrical topology, environmental parameters, and loads arising from households equipped with smart appliances and dispersed generation units. The availability of such

realistically rendered distribution test feeders should facilitate the study of market design at the retail level. Moreover, as discussed in previous sections, the agent-based distribution test feeder can be seamed with agent-based platforms implementing wholesale power market operations, such as the AMES platform [55], thus permitting the integrated study of retail and wholesale power market operations.

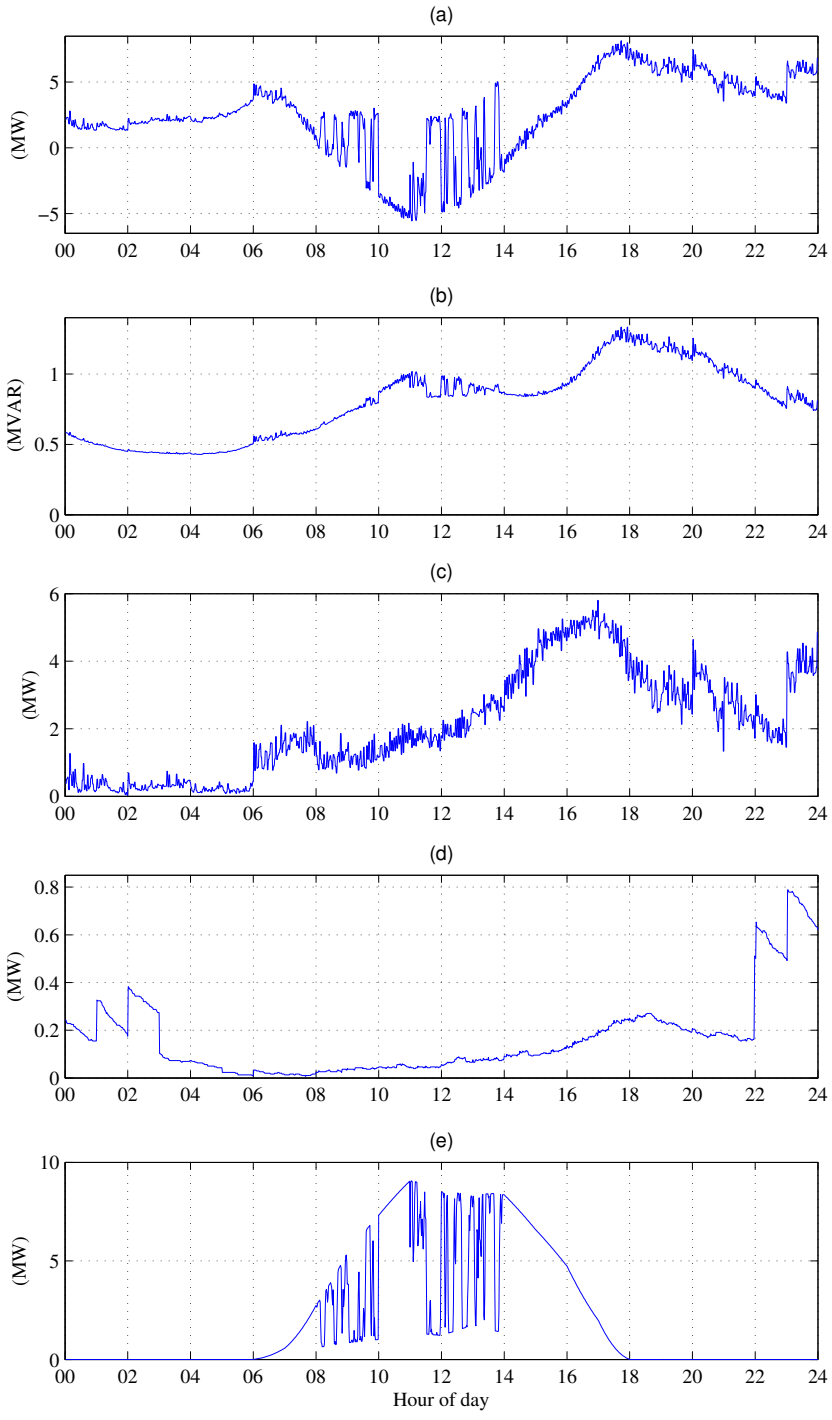

Figure 2.7 (a) Real power at the substation, (b) Reactive power at the substation, (c) Real power consumption from all smart A/C systems, (d) Real power consumption from all PEVs, (e) Real power generation from all PV units.

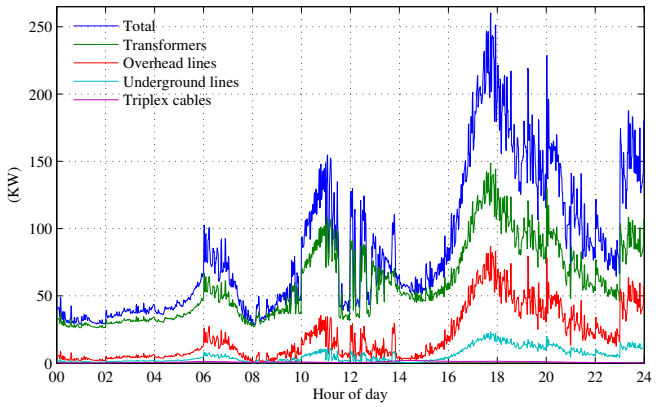

Figure 2.8 Real power losses.

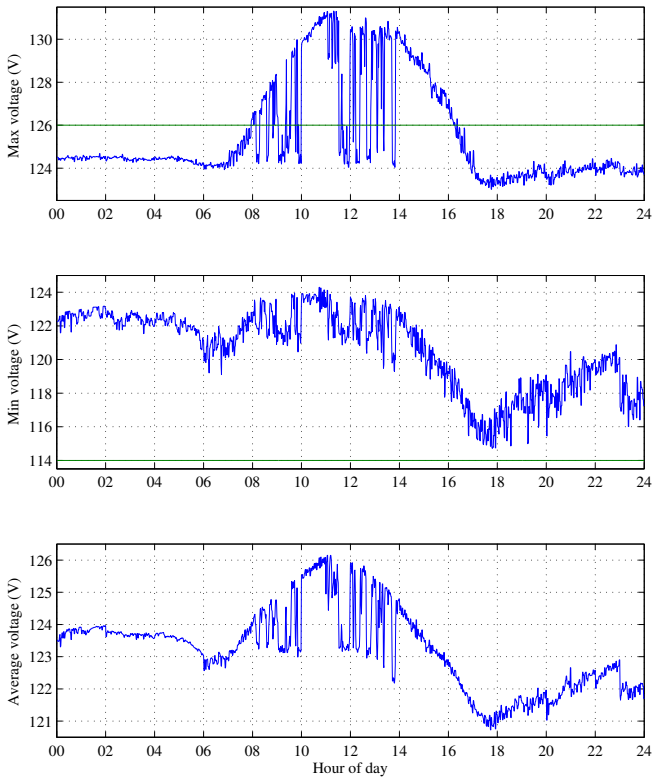

Figure 2.9 Maximum, minimum, and average voltages of residential loads.

3. Distributed Volt/VAr Control by PV Inverters

Modified from a paper published in the *IEEE Transactions on Power Systems*, vol. 28, no. 3, pp. 3429-3439, AUGUST 2013.

Pedram Jahangiri [1], and Dionysios C. Aliprantis

Abstract

A major technical obstacle for rooftop photovoltaics (PV) integration into existing distribution systems is the voltage rise due to the reverse power flow from the distributed PV sources. This paper describes the implementation of a voltage control loop within PV inverters that maintains the voltage within acceptable bounds by absorbing or supplying reactive power. In principle, this can be considered to be a form of distributed Volt/VAr control, which is conventionally performed by coordinated control of capacitor banks and transformer tap changers. Comprehensive simulation studies on detailed feeder models are used to demonstrate that the proposed control scheme will mitigate voltage rises.

3.1 Introduction

THE INSTALLED capacity of embedded rooftop photovoltaic (PV) generation in residential distribution systems is rising rapidly worldwide [57], driven by reductions in costs, increases in electricity prices, and higher sensitivity about sustainability. Under the premise that this exponential trend will continue unabated, power distribution

[1]Primary researcher and author.

utilities must ensure that the quality of service to their customers will not be compromised [9,10]. For instance, the increased penetration of distributed PV sources has been cause of concern for harmonic pollution, but this issue can be resolved with standardization regarding harmonic distortion limits and the use of appropriate power electronic topologies.

A major obstacle for further PV integration into existing medium/low-voltage networks is the induced voltage rise due to the reverse power flow along the distribution feeders [11–17]. This phenomenon is bound to be exacerbated under higher penetration of PV sources. In the United States, the ANSI Standard C84.1 [18] states that the voltage of residential loads should remain within five percent from its nominal value (120 V) under normal operating conditions.

Several techniques to alleviate the voltage rise issue have been proposed. These can be employed by the utility itself or by its customer-owners of distributed PV generation (in this case, either appropriate financial incentives or regulation might be necessary). One simple solution is to lower the setpoint of the on-load tap changer at the high-voltage/medium-voltage substation, or to use a voltage regulator [19]. However, this method cannot guarantee that the voltage profile will be within acceptable bounds throughout the feeder. In addition, other feeders that might be connected to the same transformer may be adversely impacted by this action [11]. Alternatively, the utility can choose to reinforce the distribution grid, by increasing conductor sizes to reduce the resistance of medium- and low-voltage lines. In Germany, where installed capacity of PV systems increased at a much faster rate than the development of new controllers or the updating of grid codes, this practice has led to high costs [11,16]. Yet another solution is to curtail real power feed-in from PV units at times of low demand. For instance, in the Japanese grid code, when the voltage at the point of common coupling exceeds the upper limit, the PV system is required to reduce its active power output [14,16,20,58,59]. The disadvantage of this technique is that it causes the spilling of solar energy, which is not

economically attractive to the PV panel owners.

The approach considered herein is to absorb reactive power using the PV inverters themselves, in a distributed fashion.[2] This is feasible even though the X/R ratio in distribution systems is typically smaller than in transmission systems and therefore, reactive power has a relatively lower impact on voltage magnitude. Nevertheless, as will be demonstrated in this paper as well, appropriate reactive power control can offset the voltage rise in distribution networks, while reducing or deferring the need for new assets or grid reinforcements [14–16, 58, 61].

This study considers the implementation of a voltage control loop within rooftop PV inverters, to maintain the voltage within acceptable bounds by reactive power injection or absorption. In principle, this can be considered to be a form of Volt/VAr control, which is conventionally performed by coordinated control of capacitor banks located along the feeder and transformer tap changers. In the proposed implementation, the voltage control objective is accomplished with a piecewise linear droop characteristic, which determines the reactive power injection as a function of the voltage magnitude at the PV inverter terminals. This control strategy has been studied in [13, 15, 62, 63], and by other researchers. Notably, the control is simple to implement, and does not require communication or cooperation among the PV inverters [58, 64].

The main objective of this analysis is to provide evidence through comprehensive simulation studies that this control scheme will mitigate voltage rise, at essentially no extra investment cost to the consumer. In all cases that were analyzed, voltage violations were completely eliminated. Previous work on this topic is extended in the following ways: (i) Studies are performed by means of computer simulations of several realistic distribution feeders with hundreds of households and their appliances modeled in high

[2]Controlling real and reactive power output implies that PV units actively participate in grid voltage control. The grid codes of some countries, such as the United States (based on the IEEE Standard 1547 series), prohibit active voltage regulation of PV units at the point of common coupling [16]. Deliberations to relieve this constraint are under way, in light of new technologies and emerging higher penetrations of distributed energy resources [60].

detail. To our knowledge, this is the first time that this type of controller is demonstrated with such degree of modeling verisimilitude, since past work has used feeder models of limited size and fidelity. The simulations are run using GridLAB-D [31], which is an open-source software platform developed by the U.S. Department of Energy at the Pacific Northwest National Laboratory (PNNL) for the simulation of electric power distribution systems. GridLAB-D has a comprehensive library of precise load models, including their dependence on voltage levels. The original inverter source code of GridLAB-D was modified to represent the proposed control. (ii) The dynamic interactions between a large number of inverters operating in tandem are taken into account. In particular, a transfer function that helps stabilize the system by eliminating unwanted oscillatory (hunting) behavior is introduced in the control path. This phenomenon has not been previously mentioned in the PV literature, but it was revealed by our simulations. (iii) The reactive power capability of the inverter is modeled accurately, as dynamically dependent on the real power generation. This is important because during times of peak PV power generation, reactive power generation capability is limited the most, exactly when it is most needed by the system. (iv) The inverter losses are accounted for with a simple model. (v) The cumulative side-effects of the proposed scheme at the substation are observed.

The remainder of this paper is organized as follows. Section 3.2 sets forth the proposed controller and discusses its stability. Section 3.3 describes the system model and metrics that are used for case studies. Illustrative findings from computer simulations are reported in Section 3.4. Concluding remarks are provided in Section 3.5. In the Appendices, the reader may find system parameters and comprehensive tabulated results from the simulation studies.

3.2 Control Strategy

This section discusses the envisioned practical implementation of the proposed voltage controller as a discrete-time dynamic system, including its stability properties. Fig. 3.1 shows the proposed modification to an otherwise standard PV inverter with maximum power point tracking (MPPT) functionality.

3.2.1 Reactive Power Support Function

The MPPT algorithm determines the desired real power output at each period n, $\hat{P}_n$, whereas the actual output accounts for the loss in the inverter, $P_n^{\text{inv}} = \hat{P}_n - P_{\text{loss},n}$. The desired reactive power output $\hat{Q}_n$ is determined by the proposed controller using the function $q(V^{\text{meas}}, Q^{\text{max}})$, which is depicted in Fig. 3.2. The actual reactive power output is $Q_n^{\text{inv}} \approx \hat{Q}_n$. The reactive power compensation loop could be automatically turned off overnight since under normal conditions, feeders operate within the acceptable voltage range in the absence of PV generation. Of course, the controller would have other functions that are not shown here, such as a phase-locked loop for tracking the terminal voltage and anti-islanding detection schemes. The generation of an additional reactive power component is relatively simple to implement (for example, using qd reference frame theory), and amounts to injecting the appropriate current component ninety degrees out of phase with the voltage.

The droop characteristic is a piecewise linear function of the voltage. It is dynamically changing due to its dependence on the maximum reactive power capability, Q^{max}, which in turn depends on the variable real power output of the inverter. In general, the droop characteristic can be defined in terms of four parameters, V^a, V^b, V^c, and V^d, or by three parameters V^a, D (deadband width), and V^d, if the deadband is symmetric around the nominal voltage value. These parameters can be hard-coded, or programmed at the time of installation by a technician (according to the recommendations of the

i

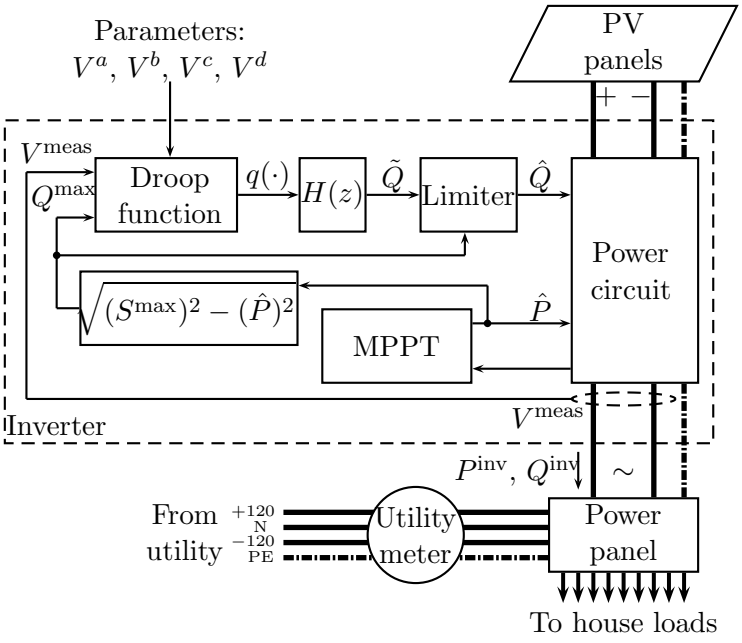

Figure 3.1 Block diagram of a PV inverter with voltage controller (for a United States-based system).

distribution system utility). It is also conceivable in a future "smart grid" scenario that these parameters could be dynamically adjusted by the distribution system operator via a communications network, which opens interesting opportunities for system performance optimization on a regular basis, for instance, as seasons and load patterns change, or if the feeder topology is modified (e.g., due to feeder growth).

The maximum reactive power capability of the inverter at period n, which essentially reflects a current limitation, is defined by

$$Q_n^{\max} = \sqrt{(S^{\max})^2 - (\hat{P}_n)^2}\,. \tag{3.1}$$

This is recomputed at every period based on the real power generation and the apparent power rating of the inverter $S^{\max}$. Inside the deadband, $q(\cdot) = 0$ since the voltage is close to its nominal value. When the measured voltage exceeds V^c, the converter starts absorbing reactive power, in a bid to lower the voltage. At V^d and beyond, the inverter is asked to absorb the maximum possible reactive power. This is the most common

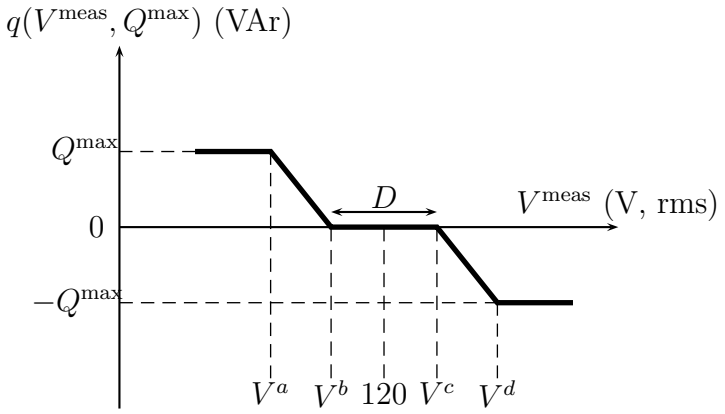

Figure 3.2 Droop control function (for a United States-based system).

operating mode, due to the voltage rise phenomenon by PV generation. Nevertheless, this controller can also contribute to the mitigation of low-voltage occurrences, e.g., for locations far away from the substation under heavy load conditions, when the voltage drops below V^b.

It is interesting to note that the $q(\cdot)$ characteristic does not have to be symmetric. In fact, variations of this function have been proposed in the past. For instance, a "transmission VAr support" mode has been proposed [60], where the PV inverter will not absorb reactive power for voltages higher than V^b, if signaled to do so by the utility. Another modification would be to use constant slope (rather than a dynamically changing one) below V^b and above V^c, until $\pm Q^{\text{max}}$ is reached. The constant slope method could be interesting from a theoretical standpoint, since one could relate this slope to the Jacobian of the power flow, and possibly determine its optimal value analytically. However, such study is left for future work. Yet another example would be the necessary modification of the characteristic for utilities adopting a Conservation Voltage Reduction scheme [65], where an asymmetric function might be desirable. In addition, in cases where the reactive power control scheme fails to regulate voltages within acceptable bounds, then an outer loop that would curtail PV real power production could be activated. In any case, all studies performed here utilize the "canonical" droop characteristic of Fig. 3.2.

If the PV system uses a central inverter, which is typically installed in close proximity to the main power panel, then the voltage at its terminals would be approximately equal to the voltage at the point of interconnection with the utility. Some newer PV systems use micro-inverters, embedded into the panels themselves, in which case the control scheme should be modified to account for the voltage drop in the wires connecting the inverters to the power panel. Alternatively, it is conceivable that an advanced meter might have the capability to communicate its voltage measurement to the inverters via a home area network, as proposed in [62]. In our implementation, central inverters are considered, and they are assumed to be wired to the 240 V, rms[3] coming from a center-tapped distribution transformer. (A division of the measured voltage by a factor of two takes place in the control loop.)

3.2.2 Instability Concerns

A simple digital implementation of the control scheme shown in Fig. 3.1 can be modeled as a discrete-time system with a "Type-A" transfer function $H_A(z) = z^{-1}$. It was observed that this led to an undesirable oscillatory behavior. To mitigate this, a "Type-B" transfer function, whose response resembles that of a continuous-time transfer function of the form $1/(1+\tau s)$, is defined by:

$$H_B(z) = \frac{1}{\left(1 - \frac{\tau}{\Delta T}\right) + \left(\frac{\tau}{\Delta T}\right) z}\,. \tag{3.2}$$

Hence, the discrete-time response can be expressed as

$$\tilde{Q}_{n+1} = \begin{cases} q(V_n^{\text{meas}}, Q_n^{\max}) & \text{for Type-A systems} \\ \left(1 - \frac{\Delta T}{\tau}\right) \tilde{Q}_n + \left(\frac{\Delta T}{\tau}\right) q(V_n^{\text{meas}}, Q_n^{\max}) & \text{for Type-B systems} \end{cases} \tag{3.3}$$

Here, the sampling time is $\Delta T = 1$ s, and the time constant is $\tau = 10$ s.

In order to demonstrate the potential instability of the simple control scheme that uses the Type-A transfer function, two simple examples have been devised, illustrated in

[3] All voltages in the paper are provided as rms values.

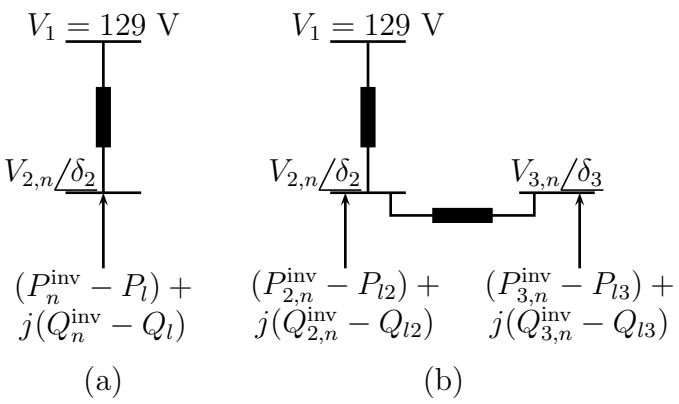

Figure 3.3 Two-bus and three-bus system examples.

Fig. 3.3, with parameters provided in Appendix A. The reader may refer to Section 3.2.3 for a theoretical analysis of system stability.

First, consider the hypothetical two-bus single-phase system of Fig. 3.3(a). Bus 1 is the slack bus and bus 2 is a load (PQ) bus with a PV system.[4] Initially, the PV system is generating zero real power, and since the voltage of bus 2 (124.90 V) is inside the deadband, the inverter is not injecting reactive power. During period 6, the real power generation is stepped from 0 to 1 kW, which causes the voltage to rise, and an oscillation to begin as the inverter tries to mitigate this. As can be observed from Fig. 3.4(a), the voltage at bus 2 is oscillating between 125.61 V and 124.11 V, with the corresponding reactive power injections shown in Fig. 3.4(b). Fig. 3.4(a) also illustrates the response when the controller includes the Type-B transfer function. Now the oscillations are damped and the system reaches a stable operating point ($V_2 = 125.18$ V, $Q^{\text{inv}} = -197.32$ VAr).

The second example (see Fig. 3.3(b)) demonstrates the potential instability caused by two inverters interacting with each other when their control schemes use the type-

[4]The commonly used notation for synchronous generator buses in standard power flow formulations, where real power and voltage are given, and which are thus termed 'PV' buses, conflicts with the abbreviation of the word 'photovoltaic.' It is important to stress that photovoltaic inverters are *not* modeled as PV buses, but as PQ buses, where real and reactive power output change in every period n. Hence, the analysis is based on a sequence of quasi-steady-state power flow solutions.

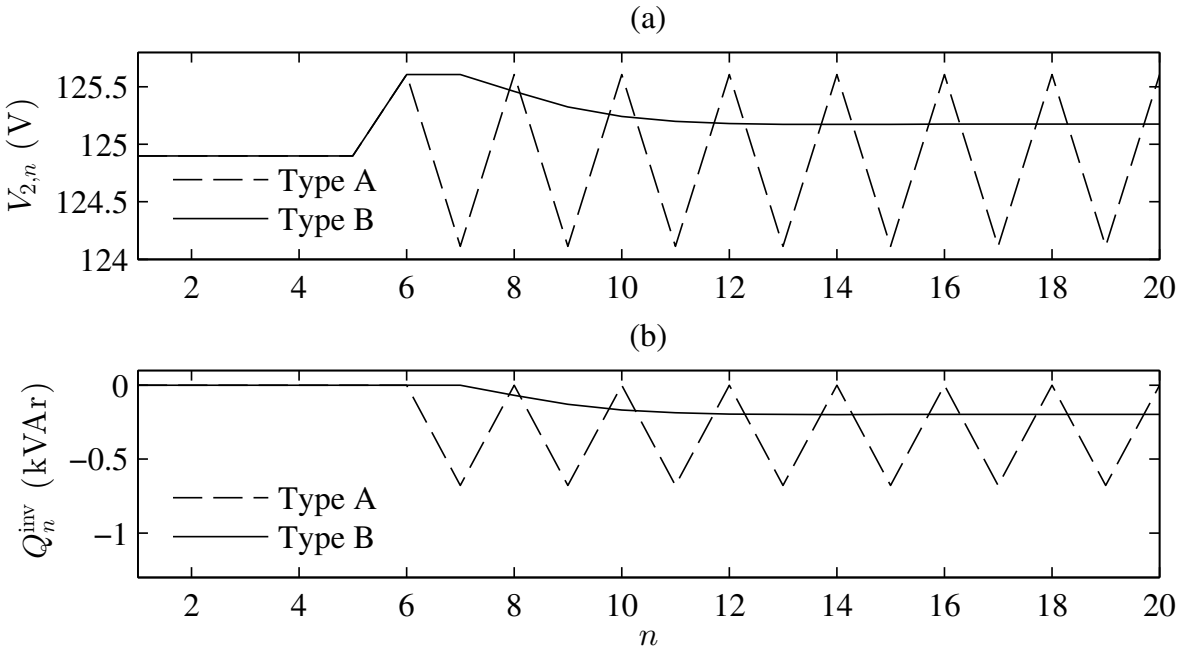

Figure 3.4 Two-bus system: voltage magnitudes and reactive power injections from PV inverter.

A transfer function. In practice, the two inverters will not be necessarily acting in a synchronized manner, so here they are evenly staggered for simplicity: the bus-2 inverter acts in odd periods, whereas the bus-3 inverter acts in even periods. Initially, the PV systems are not generating real power, and since the voltages of bus 2 and bus 3 are inside the deadband ($V_2 = 124.90$ V, $V_3 = 124.69$ V), their inverters are not injecting reactive power. During period 6, the real power generation of both inverters is stepped from 0 to 1 kW, which causes the voltages to rise, and oscillations to begin as the inverters try to mitigate them. As can be observed from Figs. 3.5(a) and 3.5(b), the voltages at buses 2 and 3 are oscillating, with corresponding reactive power injections shown in Figs. 3.5(c) and 3.5(d). The response of the system when the Type-B transfer function is used is superimposed in Fig. 3.5. Now the oscillations are damped and the system reaches a stable operating point ($V_2 = 125.28$ V, $Q_2^{\text{inv}} = -318.16$ VAr, $V_3 = 125.12$ V, $Q_3^{\text{inv}} = -132.82$ VAr).

Similar oscillations have been observed in the simulations of the realistic feeders

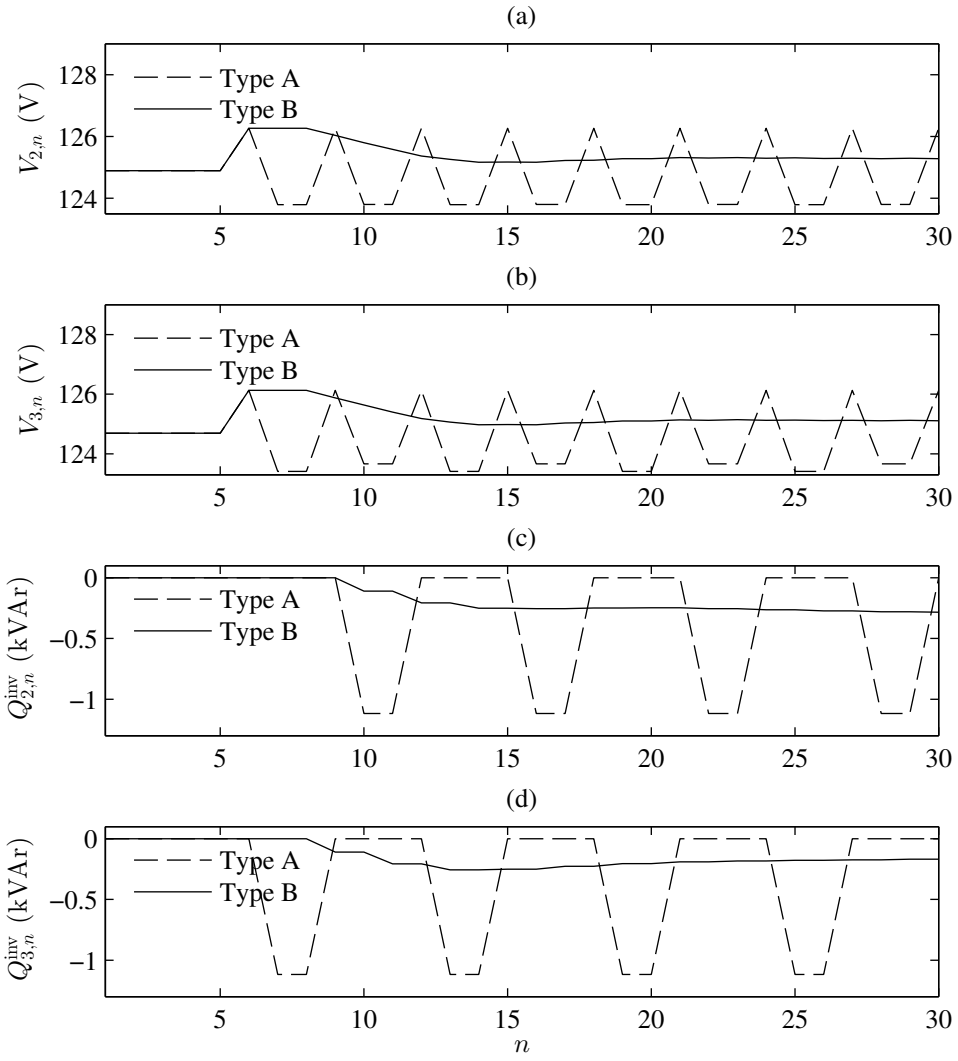

Figure 3.5 Three-bus system: (a) and (b) voltage magnitudes; (c) and (d) reactive power injections from PV inverters.

described in the next section. However, due to space limitations, such results are not shown here. Using the Type-B transfer function eliminated this type of hunting behavior in all cases. A more general framework for stability analysis of these types of systems is established in the next subsection.

3.2.3 Stability Analysis

Consider the general case of an N-bus distribution feeder system with a constant-voltage slack bus representing the substation, and $N-1$ load buses with PV inverters, i.e.,

$N-1$ PQ buses. For simplicity, let this be a single-phase system, and let all inverters act in a synchronized manner. (The analysis can be extended to the general case of a three-phase unbalanced feeder with staggered inverter actions, but this will be unnecessarily complicated, and will distract the reader from the main purpose of this section, which is to illustrate why the system is inherently unstable and how it is stabilized.) Assume that the real power output of each inverter remains constant, so that the droop characteristic only depends on the measured voltage. Voltage measurement errors are neglected. Also assume that the limiter blocks are not activated, i.e., $\hat{Q} = \tilde{Q}$, and that the reactive power output of the inverter is equal to the commanded value, i.e., $Q^{\text{inv}} = \hat{Q}$.

This dynamic system has $N-1$ states representing the reactive power output of each inverter during period n, contained in a column vector $\hat{Q}_n = [\hat{Q}_{2,n}\ \hat{Q}_{3,n}\ \cdots\ \hat{Q}_{N,n}]^T$. The state equation is

$$\hat{Q}_{n+1} = f(\hat{Q}_n) = \begin{cases} q(V(\hat{Q}_n)) & \text{for Type-A systems} \\ \left(1 - \frac{\Delta T}{\tau}\right) \hat{Q}_n + \left(\frac{\Delta T}{\tau}\right) q(V(\hat{Q}_n)) & \text{for Type-B systems} \end{cases} \tag{3.4}$$

The vector $q(V(\hat{Q}_n)) = [q_2(V_2(\hat{Q}_n))\ \cdots\ q_N(V_N(\hat{Q}_n))]^T$ contains the droop control function outputs of each inverter as functions of the local bus voltages. These voltages are in turn related to the reactive power injections of all inverters through the power flow equations of the network. It can be readily shown that both Type-A and Type-B system stationary states (or fixed points) $\bar{Q} = [\bar{Q}_2\ \bar{Q}_3\ \cdots\ \bar{Q}_N]^T$ satisfy the nonlinear equation:

$$\bar{Q} = f(\bar{Q}) = q(V(\bar{Q}))\,. \tag{3.5}$$

The stability of a nonlinear discrete-time system in the vicinity of its stationary states can be determined using the following theorem [66]:

> *Theorem:* For the discrete-time system $X_{n+1} = \phi(X_n)$, suppose $\phi : \mathbb{U} \to \mathbb{U}, \mathbb{U} \subseteq \mathbb{R}^m$, is continuously differentiable in some neighborhood of a fixed point $\bar{X} \in \mathbb{U}$. Let $J = [\partial\phi/\partial X]_{X=\bar{X}}$ be the Jacobian matrix of ϕ, evaluated at $\bar{X}$. Then:

- $\bar{X}$ is asymptotically stable if all eigenvalues of J have magnitude less than 1.
- $\bar{X}$ is unstable if at least one eigenvalue of J has magnitude greater than 1.

In our application, the Jacobian matrix of (3.4) becomes

$$J = \left[\frac{\partial f}{\partial \hat{Q}}\right]_{\hat{Q}=\bar{Q}} = \begin{cases} \left[\frac{\partial q}{\partial V}\right]\left[\frac{\partial V}{\partial \hat{Q}}\right] & \text{for Type-A systems} \\ \left(1-\frac{\Delta T}{\tau}\right)\mathbb{I} + \left(\frac{\Delta T}{\tau}\right)\left[\frac{\partial q}{\partial V}\right]\left[\frac{\partial V}{\partial \hat{Q}}\right] & \text{for Type-B systems} \end{cases} \tag{3.6}$$

where $[\partial q/\partial V]$ is a diagonal matrix:

$$\left[\frac{\partial q}{\partial V}\right] = \begin{bmatrix} \frac{\partial q_2}{\partial V_2} & & 0 \\ & \ddots & \\ 0 & & \frac{\partial q_N}{\partial V_N} \end{bmatrix}. \tag{3.7}$$

The diagonal elements represent the slopes of the individual droop control functions. They can have zero or negative value, depending on the segment in which the stationary point happens to be located.[5] The matrix $[\partial V/\partial \hat{Q}]$ contains the partial derivatives:

$$\left[\frac{\partial V}{\partial \hat{Q}}\right] = \begin{bmatrix} \frac{\partial V_2}{\partial \hat{Q}_2} & \frac{\partial V_2}{\partial \hat{Q}_3} & \cdots & \frac{\partial V_2}{\partial \hat{Q}_N} \\ \frac{\partial V_3}{\partial \hat{Q}_2} & \frac{\partial V_3}{\partial \hat{Q}_3} & \cdots & \frac{\partial V_3}{\partial \hat{Q}_N} \\ \vdots & \vdots & & \vdots \\ \frac{\partial V_N}{\partial \hat{Q}_2} & \frac{\partial V_N}{\partial \hat{Q}_3} & \cdots & \frac{\partial V_N}{\partial \hat{Q}_N} \end{bmatrix}. \tag{3.8}$$

Define $A = [\partial q/\partial V][\partial V/\partial \hat{Q}]$, and let an eigenvalue of the Type-A Jacobian matrix be denoted by λ, satisfying $Ax = \lambda x$. From the Type-B expression of (3.6), we have:

$$\begin{aligned} \left[\left(1-\frac{\Delta T}{\tau}\right)\mathbb{I} + \left(\frac{\Delta T}{\tau}\right)A\right]x &= \left(1-\frac{\Delta T}{\tau}\right)x + \left(\frac{\Delta T}{\tau}\right)Ax \\ &= \left[\left(1-\frac{\Delta T}{\tau}\right) + \left(\frac{\Delta T}{\tau}\right)\lambda\right]x\,. \end{aligned} \tag{3.9}$$

[5] Application of the theorem to the special case where the stationary point happens to be exactly on a corner point of the droop characteristic (V^a, V^b, V^c, or V^d) is problematic, since the function f is not differentiable. However, this issue can be readily resolved by adding a slight curvature to $q(\cdot)$ around these points.

This implies that the corresponding eigenvalue of the Type-B Jacobian matrix will be

$$\mu = \left(1 - \frac{\Delta T}{\tau}\right) + \left(\frac{\Delta T}{\tau}\right)\lambda\,. \tag{3.10}$$

For example, if $\Delta T = 1$ s, and $\tau = 10$ s, then $\mu = 0.9 + 0.1\lambda$.

It is interesting to note what happens if the stationary point of the inverter on bus i lies on the flat region of the droop characteristic. In this case, the corresponding $\partial q_i/\partial V_i$ term is equal to zero. This, in turn, implies that row $(i-1)$ of the Jacobian J will be zero for Type-A systems, or that it will only contain a $\left(1 - \frac{\Delta T}{\tau}\right)$ element in the diagonal for Type-B systems. The former case leads to a zero eigenvalue; the latter case leads to an eigenvalue of the same value as the element itself. In both cases, the corresponding eigenvalue is a real number less than one, hence stability is not adversely affected.

To calculate $[\partial V/\partial \hat{Q}]$, we first write the power flow equations as implicit functions of the reactive power injections by the PV inverters $\hat{Q}$:

$$P(\delta(\hat{Q}), V(\hat{Q})) - (P^{\text{inv}} - P_l) = 0 \tag{3.11}$$

$$Q(\delta(\hat{Q}), V(\hat{Q})) - (\hat{Q} - Q_l) = 0 \tag{3.12}$$

Here, the vector functions $P = [P_2\ P_3\ \ldots\ P_N]^T$ and $Q = [Q_2\ Q_3\ \ldots\ Q_N]^T$ represent real and reactive power injections, respectively. The other variables, P^{inv}, P_l, and Q_l, are constant vectors. The power injections at each load bus, P_i and Q_i, $i = 2, 3, \ldots, N$, are given by

$$P_i = \sum_{j=1}^{N} V_i V_j |Y_{i,j}| \cos(\delta_j - \delta_i + \theta_{i,j}) \tag{3.13}$$

$$Q_i = -\sum_{j=1}^{N} V_i V_j |Y_{i,j}| \sin(\delta_j - \delta_i + \theta_{i,j}) \tag{3.14}$$

where the elements of the nodal admittance matrix of the system are denoted by $Y_{i,j} = |Y_{i,j}|\underline{/\theta_{i,j}}$. Hence, from (3.11)–(3.12), we obtain:

$$\left[\frac{\partial P}{\partial \hat{Q}}\right] = \left[\frac{\partial P}{\partial \delta}\right]\left[\frac{\partial \delta}{\partial \hat{Q}}\right] + \left[\frac{\partial P}{\partial V}\right]\left[\frac{\partial V}{\partial \hat{Q}}\right] = 0 \tag{3.15}$$

$$\left[\frac{\partial Q}{\partial \hat{Q}}\right] = \left[\frac{\partial Q}{\partial \delta}\right]\left[\frac{\partial \delta}{\partial \hat{Q}}\right] + \left[\frac{\partial Q}{\partial V}\right]\left[\frac{\partial V}{\partial \hat{Q}}\right] = \mathbb{I} \tag{3.16}$$

Manipulation of (3.15)–(3.16) yields

$$\left[\frac{\partial V}{\partial \hat{Q}}\right] = \left\{\left[\frac{\partial Q}{\partial V}\right] - \left[\frac{\partial Q}{\partial \delta}\right]\left[\frac{\partial P}{\partial \delta}\right]^{-1}\left[\frac{\partial P}{\partial V}\right]\right\}^{-1}. \tag{3.17}$$

This expression is based on the four submatrices of the Jacobian of the power flow problem (not to be confused with the Jacobian of the dynamic system function f), which have well-known expressions that can be computed from (3.11)–(3.12) or found in a power systems textbook.

This analysis is illustrated using the two simple systems that were introduced in the previous section.

3.2.3.1 Stability of Two-Bus Example

The two-bus system example is a one-dimensional discrete-time system. Its stationary state is $\bar{Q}_2 = -197.32$ VAr. This point corresponds to the fourth segment of the droop control function (between V^c and V^d), which implies that

$$\frac{\partial q_2}{\partial V_2} = \frac{-Q^{\max}}{V^d - V^c} = -1118 \text{ VAr/V}. \tag{3.18}$$

The power flow solution at the fixed point is: $\bar{V}_2 = 125.18$ V, $\bar{\delta}_2 = -0.0275$ rad. The matrix $[\partial V/\partial \hat{Q}]$ is just a scalar, and can be evaluated from (3.17):

$$\frac{\partial V_2}{\partial \hat{Q}_2} = \left\{\frac{\partial Q_2}{\partial V_2} - \left(\frac{\partial Q_2}{\partial \delta_2}\right)\left(\frac{\partial P_2}{\partial \delta_2}\right)^{-1}\left(\frac{\partial P_2}{\partial V_2}\right)\right\}^{-1} = 0.00219 \text{ V/VAr}. \tag{3.19}$$

According to (3.6), the Jacobian matrix evaluates to:

$$J = \begin{cases} -2.448 & \text{for a Type-A system} \\ 0.655 & \text{for a Type-B system} \end{cases} \tag{3.20}$$

The Jacobian J is a scalar, so its eigenvalue is the same number. Therefore, the Type-A system is unstable, whereas the Type-B system is locally asymptotically stable.

3.2.3.2 Stability of Three-Bus Example

The three-bus example is a two-dimensional discrete-time system, with stationary state $\bar{Q} = \begin{bmatrix} -318.16 & -132.82 \end{bmatrix}^T$ VAr. Both points correspond to the fourth segment of the droop control function (between V^c and V^d), so $\partial q_2/\partial V_2 = \partial q_3/\partial V_3 = -1118$ VAr/V. The fixed point steady-state voltage magnitudes and angles are: $\bar{V}_2 = 125.28$ V, $\bar{\delta}_2 = -0.0097$ rad, $\bar{V}_3 = 125.12$ V, and $\bar{\delta}_3 = -0.0103$ rad. Using (3.17), one may obtain

$$\left[\frac{\partial V}{\partial \hat{Q}}\right] = \begin{bmatrix} 0.002196 & 0.002201 \\ 0.002199 & 0.002418 \end{bmatrix} \text{ V/VAr}\,. \tag{3.21}$$

The Jacobian matrix (3.6) of the Type-A system is

$$J = \begin{bmatrix} -2.4552 & -2.4608 \\ -2.4586 & -2.7034 \end{bmatrix}, \tag{3.22}$$

with eigenvalues $\lambda_1 = -0.116$ and $\lambda_2 = -5.042$. Hence, the Type-A system is unstable. On the other hand, the Jacobian matrix of the Type-B system is

$$J = \begin{bmatrix} 0.6545 & -0.2461 \\ -0.2459 & 0.6297 \end{bmatrix}, \tag{3.23}$$

with eigenvalues $\mu_1 = 0.888$ and $\mu_2 = 0.396$, which can alternatively be obtained by applying (3.10). Hence, the Type-B system is locally asymptotically stable.

3.3 System Model

This section explains modeling of rooftop PV systems, the metrics that are used to evaluate the performance of the proposed controller and details about the distribution systems that are used for the case studies.

3.3.1 Modeling of Rooftop PV Panels

The incident solar radiation on a tilted PV array is calculated using classical formulas [67], implemented in GridLAB-D. The calculation involves various types of irradiance

adjusted for time of day, the site latitude, and the orientation and tilt angle of the PV panels.

In the simulations, PV panels are virtually installed on residential rooftops according to a PV penetration level parameter, which is defined as:

$$\text{penetration level} = \frac{\text{residential customers with PV systems}}{\text{total number of residential customers in the feeder}} \tag{3.24}$$

The houses are assumed to have two types of orientation, namely, north-south and east-west. The orientation of houses with PV systems is split in a 3:1 ratio, signifying that there is higher probability that PV panels will be installed on a south-facing rather than on a west-facing roof in the northern hemisphere. The roof angle is uniformly selected from a set with pitch equal to $x/12$, where $x = \{0, 3, 4, \ldots, 12\}$. If the roof is flat ($x = 0$), the solar panels are assumed to be facing south and tilted to a degree equal to the site latitude; otherwise, solar panels are assumed to be installed parallel to the roof.

The southern or western part of the roof area is set equal to

$$\text{south- or west-facing roof area} = (0.5) \cdot (\text{floor area}) / \cos(\text{roof angle})\,. \tag{3.25}$$

Then the total panel area is randomly generated according to a uniform distribution within 50% to 90% of the south- or west-facing roof area. For a given PV panel area value, the nominal apparent power rating of the inverter should satisfy:

$$\begin{aligned} S^{\max} &\geq (\text{CF}) \cdot (\text{panel efficiency}) \cdot (\text{rated insolation}) \cdot (\text{area}) \\ &= (1.15) \cdot (0.15) \cdot (1000\ (\text{W/m}^2)) \cdot (\text{area}\ (\text{m}^2))\,, \end{aligned} \tag{3.26}$$

where CF represents a corrective factor, since in certain cases the rated insolation can be exceeded. $S^{\max}$ is selected from a list that has been compiled from commercially available inverters (up to 30 kVA) [68], as the next higher value in the list. In other words, the most economical inverter that can handle the rated real power for any given PV installation is still being selected, so that additional investment costs for providing reactive power support are not incurred to the customer.[6]

[6]The additional functionality of reactive power support should not increase the cost of inverters

3.3.2 Metrics for Evaluating Results

In this subsection, the metrics that are used to evaluate the performance of the proposed controller are described. The proposed metrics represent either extreme values or integrals of various time-varying quantities of interest, observed over a span of 24 hours at a time interval of 60 seconds.

The first set of metrics is related to voltage. The Voltage Violation Ratio (VVR) is defined as the maximum ratio of residential consumers with voltage limit violation (higher than 126 V or lower than 114 V). Ideally, VVR should be equal to zero, indicating no voltage violation throughout the day. Two other voltage-related metrics are the maximum and minimum voltage magnitudes ($V_{\max}$, $V_{\min}$) that appear at the meters of all residential consumers.

The second set of metrics is related to energy. These are the energy consumed by all loads (E_{load}), the energy losses of the network (E_{loss}), the energy generated by all PV systems (E_{PV}), and the energy measured at the substation (E_{SS}). Also, by integrating reactive power, "reactive energy" metrics can be defined, measured in MVAr-h. These are the reactive energy measured at the substation (E^{Q}_{SS}) and the reactive energy generated by all PV systems (E^{Q}_{PV}). The difference in an energy metric between the case where the PV inverters are actively regulating the voltage and the base (uncontrolled) case is denoted by "ΔE."

In general, we expect to obtain negative values for ΔE^{Q}_{PV}, whereas typically positive ΔE_{loss} and ΔE^{Q}_{SS} represent increased real and reactive energy losses throughout the distribution feeder. ΔE_{PV} should be negative because of extra inverter losses due to the reactive power current component. Also, since the voltages are decreased, this usually results in lower power consumption (from voltage-dependent loads) thus yielding negative values of ΔE_{load}. Finally, it is interesting to note that the change in substation energy

significantly. Any standard inverter can be made to absorb/supply reactive power, with only slight modifications in its controller code, and with exactly the same power electronics circuit as before.

ΔE_{SS} can be either positive or negative. This is because $\Delta E_{\mathrm{SS}} = \Delta E_{\mathrm{load}} + \Delta E_{\mathrm{loss}} + (-\Delta E_{\mathrm{PV}})$, is determined by the sum of quantities of different sign (negative, positive, and positive, respectively).

In the simulations, the real power loss of the inverter is modeled as a linear function of its apparent power:

$$P_n^{\mathrm{inv}} = \hat{P}_n - (0.04)\sqrt{(\hat{P}_n)^2 + (\hat{Q}_n)^2}\,. \tag{3.27}$$

3.3.3 Distribution Feeders

This subsection provides some details about the distribution systems that are used for the case studies. The houses are virtually equipped with rooftop PV systems using the method described above at various penetration levels. All feeders are connected to a high-voltage bus through a substation transformer with an impedance of $0.009+j0.06$ pu. Voltage regulators are deactivated. The voltage at the transmission side of the substation transformer for all feeders is assumed to be constant and equal to 1.05 pu, except for feeders R1-1247-2 and R1-2500-1, where it is 1.04 pu, and feeder R5-1247-3, where it is 1.02 pu.

3.3.3.1 Agent-based distribution test feeder

A so-called "agent-based distribution test feeder" (ABDTF) has been developed by the authors [69], based on an actual feeder of an electric utility in Iowa, with detailed specifications for feeder equipment (such as fuses, switches, overhead and underground conductors, and service transformers) as well as for residential and/or commercial customers, including the floor areas of the houses.[7] Fig. 3.6 depicts a schematic of the topology of the feeder that includes all branches at the medium-voltage level. Exact geo-

[7] In its original implementation, the feeder was equipped with an array of intelligent "agents," such as price-responsive air-conditioning units and plug-in electric vehicles, hence the name of the feeder. However, this type of functionality has now been disabled, and the feeder only contains conventional non-price-responsive load.

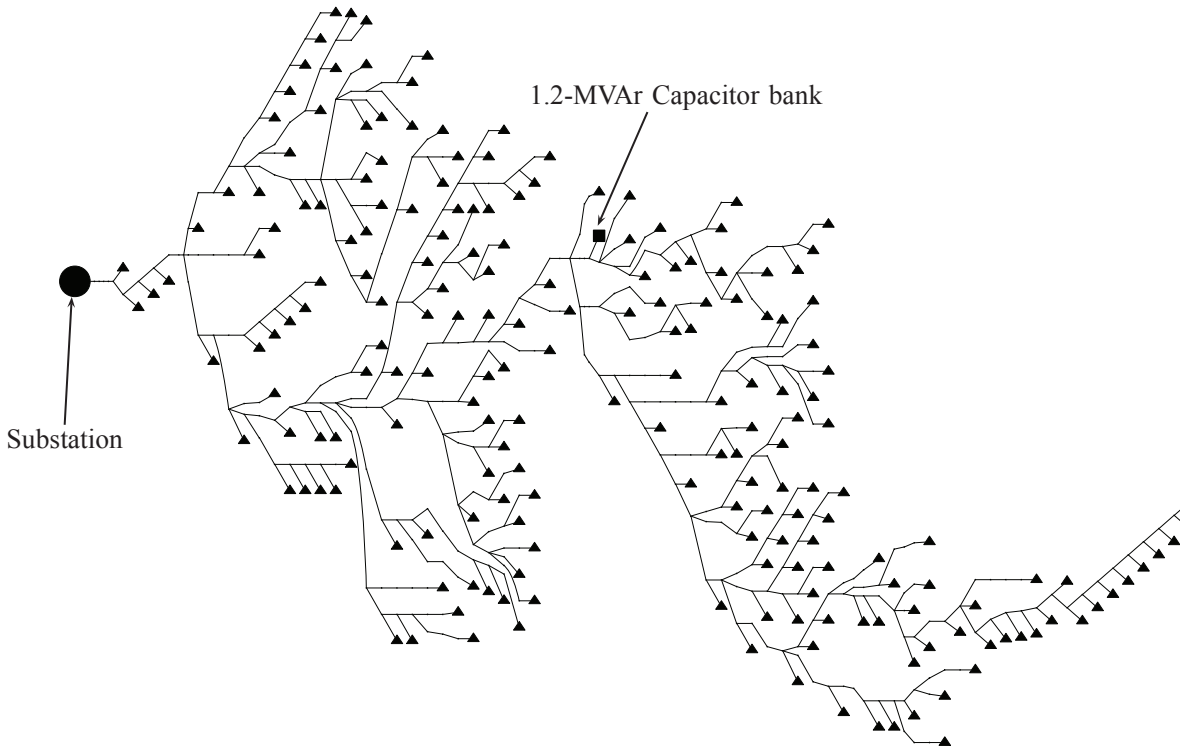

Figure 3.6 Schematic of the feeder topology (this is not an accurate geographic representation). The triangles at the leaves of this tree represent distribution transformers.

graphic coordinates of its components are also known, but are not reflected in the figure. The peak power of the feeder at the substation is reported by the utility to be approximately 14 MVA, and the primary distribution voltage is 13.2 kV. The end-use loads of the households include conventional thermostatically controlled air-conditioning, water heaters, TV sets, fans, lights, ovens, and other common electric devices. This feeder has 1372 houses.

3.3.3.2 PNNL taxonomy feeders

The so-called "taxonomy feeders" are prototypical feeders developed by researchers at PNNL. They represent the fundamental characteristics of radial distribution feeders found in the U.S., based on 575 distribution feeders from 151 separate substations

from different utilities across the U.S. Each prototypical feeder is characterized as belonging to one of five U.S. climate regions[8], by primary distribution voltage level, and other features [40, 41]. The models of the taxonomy feeders are provided as part of the GridLAB-D software package. Simulation studies were performed on all 22 taxonomy feeders that contain houses. The feeders have been modeled with high fidelity from the substation down to the individual customer meters, including detailed end-use load representations (heating, ventilation, and air-conditioning, and various other constant impedance, current, and power loads). Floor areas are provided as part of the model parameters.

3.4 Simulation Results

This section contains a distillation of results from extensive simulation studies on a wide range of distribution feeders that were modeled in very high detail. Our findings indicate that the proposed voltage controller with appropriate parameter settings would successfully control the voltages within normal bounds in all cases. In the studies described below, the "no droop" case represents a base scenario where none of the inverters is regulating the voltage, whereas in the "all droop" case all inverters are regulating their local voltage, and have the same droop function parameters. The inverters are distributed in a random fashion around the distribution feeder.

3.4.1 Sunny and clear Sky

In this section cloud effects are ignored, and all PV panels are assumed to receive the same amount of solar irradiance. A relatively temperate day with a sunny sky is selected (Feb. 27, 2011, from the Loyola Marymount University, University Hall, Los Angeles, CA site). Light load conditions with high PV power production are most likely to cause

[8]Region 1 is the U.S. west coast, region 2 is the north-central and eastern U.S., region 3 is the non-coastal southwest U.S., region 4 is the non-coastal southeast and central U.S., and region 5 is the southeast.

Table 3.1 ABDTF Metrics for 15% and 30% Penetration Level

Metrics	15% No droop	15% All droop	30% No droop	30% All droop
D (V)	N/A	10	N/A	10
VVR (%)	5.32	0.00	47.52	0.00
$V_{\max}$ (V)	126.63	125.86	127.11	125.88
$V_{\min}$ (V)	120.58	120.57	120.33	120.34
ΔE_{load} (MWh)	50.505*	−0.0127	51.027*	−0.033
ΔE_{loss} (MWh)	0.928*	0.007	0.909*	0.021
ΔE_{PV} (MWh)	9.369*	−0.008	17.286*	−0.023
ΔE_{SS} (MWh)	42.063*	0.003	34.650*	0.010
ΔE^{Q}_{SS} (MVAr-h)	16.460*	1.402	16.514*	3.474
ΔE^{Q}_{PV} (MVAr-h)	0.000*	−1.398	0.000*	−3.457

* These values represent energies for the base case.

undesirable voltage rise effects. Meteorological data are obtained from the National Renewable Energy Laboratory Measurement and Instrumentation Data Center (MIDC) database [70], which contains records of solar irradiance and air temperature recorded at 1-minute intervals from several stations. In the simulations, Volt/VAr support is not active overnight. It is activated in the morning, as soon as real PV power generation begins, and deactivated at sunset.

3.4.1.1 ABDTF

Studies are first run for two different penetration levels (15% and 30%), with constant droop function parameters (V^a = 114 V, D = 10 V, and V^d = 126 V). Table 3.1 contains the simulation metrics for these studies. Then studies are conducted for a 50% penetration level, with varying droop function parameters (same V^a, V^d as before, but different D). Table 3.2 summarizes these simulation results.

15% penetration level For this case, 231 houses are assumed to have PV systems. The maximum uncontrolled voltage ($V_{\max}$ = 126.63 V) is higher than 126 V, and causes

Table 3.2 ABDTF Metrics for 50% Penetration Level

D (V)	VVR (%)	$V_{\max}$ (V)	$V_{\min}$ (V)	ΔE_{load} (MWh)	ΔE_{loss} (MWh)	ΔE_{PV} (MWh)	ΔE_{SS} (MWh)	ΔE_{SS}^{Q} (MVAr-h)	ΔE_{PV}^{Q} (MVAr-h)
N/A	94.1	128.8	120.8	50.40*	0.94*	30.73*	20.62*	16.46*	0.00*
10	0.0	125.9	120.8	−0.080	0.056	−0.051	0.027	7.677	−7.623
9	0.0	125.9	120.8	−0.110	0.079	−0.086	0.055	10.369	−10.291
8	0.0	125.9	120.8	−0.127	0.106	−0.130	0.109	13.049	−12.942
7	0.0	125.9	120.8	−0.162	0.135	−0.179	0.152	15.572	−15.432
6	0.0	125.9	120.8	−0.176	0.165	−0.230	0.218	17.886	−17.711
5	0.0	125.9	120.6	−0.200	0.195	−0.279	0.274	19.993	−19.783
4	0.0	125.9	120.4	−0.230	0.225	−0.327	0.321	21.907	−21.660
3	0.0	125.9	120.3	−0.237	0.254	−0.372	0.389	23.650	−23.366
2	0.0	125.9	120.1	−0.250	0.283	−0.415	0.448	25.246	−24.926
1	0.0	125.9	119.8	−0.276	0.311	−0.455	0.489	26.713	−26.357

* These values represent energies for the base case.

the absorption of a minor amount of reactive power in the controlled case (E_{PV}^{Q} = −1.398 MVAr-h). The voltages in the controlled case are in compliance with ANSI Standard C84.1.

30% penetration level In this case, 433 houses are assumed to have PV systems. In the uncontrolled case, almost 50% of residential customers experience an overvoltage at some point in the day. However, the voltage controllers successfully mitigate this issue.

50% penetration level For this case, 733 houses are assumed to have PV units. As can be observed in Fig. 3.7(a), the real power flow at the substation is reversed during the daytime. Fig. 3.7(b) reflects the level of reactive power absorbed from the PV inverters. Fig. 3.8 depicts the statistical distribution of voltages at the household meters. Fig. 3.8(a) illustrates that without the droop control the maximum voltages significantly exceed the upper limit for a substantial number of residential customers. Fig. 3.8(b) shows how the proposed controllers acting in unison can offset voltage rise

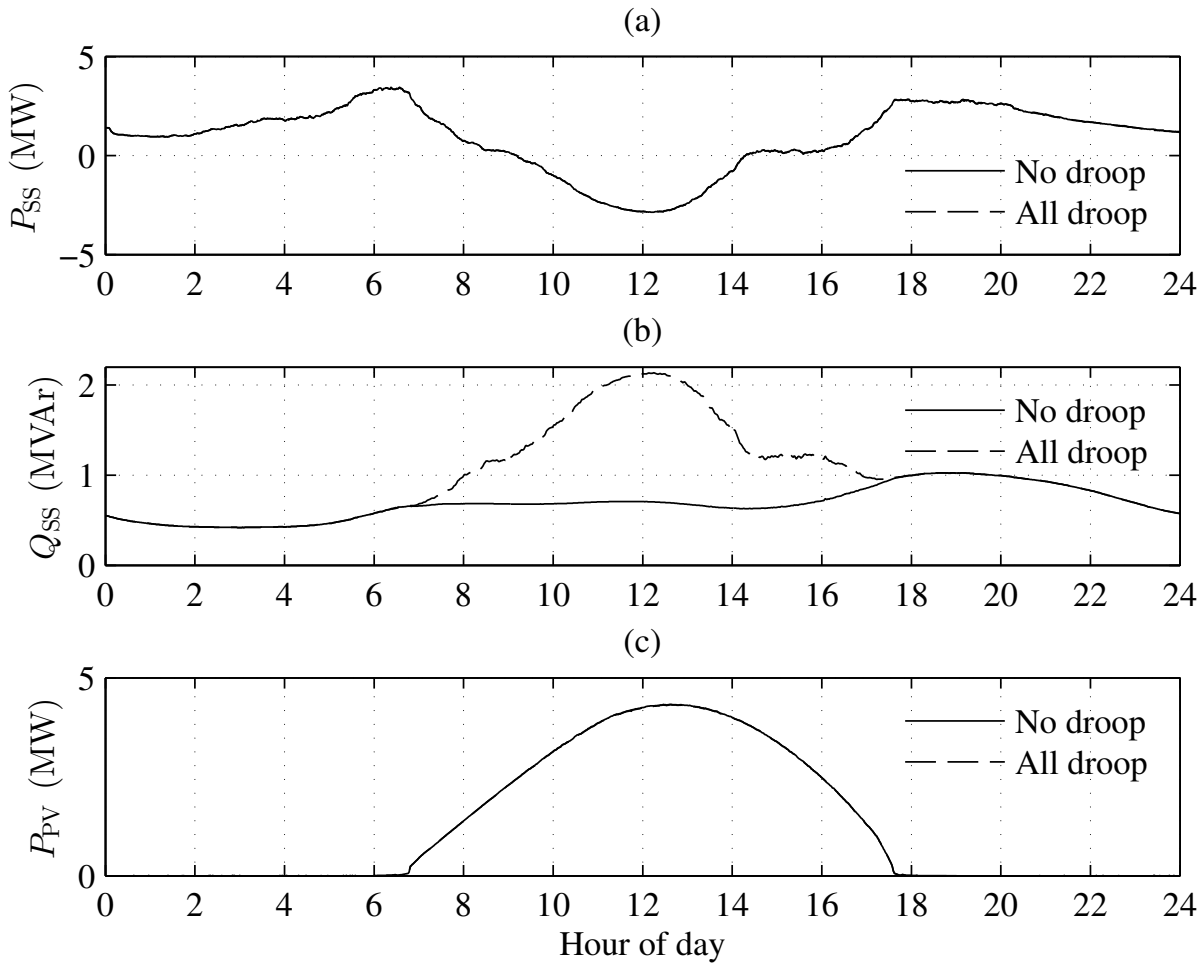

Figure 3.7 50% PV penetration in ABDTF: (a) Real power at the substation; (b) Reactive power at the substation; (c) Total PV real power generation.

conditions, and how all voltages remain below their upper limit. It can be observed that overvoltages have been mitigated in all controlled cases, but as D decreases, reactive power absorption increases, which also increases the reactive energy at the substation and the total system loss.

3.4.1.2 Taxonomy feeders

In the uncontrolled case, the voltage violation ratio (VVR) is always nonzero, as can be observed from Tables 3.3, 3.4 and 3.5 of Appendix B. On the other hand, the proposed distributed control scheme mitigates overvoltages successfully in all cases (with

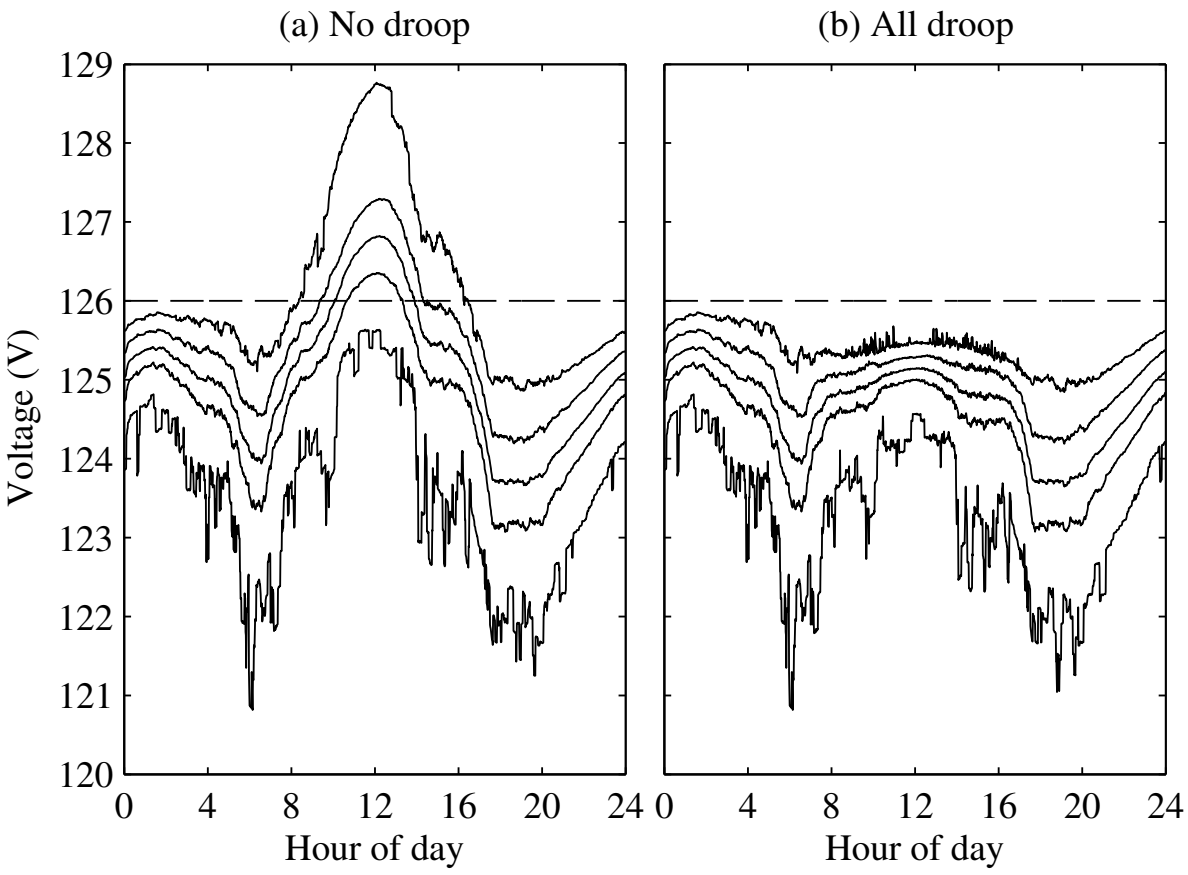

Figure 3.8 Statistics of voltages at meters of residential loads for 50% PV penetration in ABDTF ($V^a = 114$ V, $V^d = 126$ V, $D = 10$ V). The five traces correspond to the minimum, mean value minus one standard deviation, mean value, mean value plus one standard deviation, and maximum voltage.

the exception of a few cases where $D = 10$ V). Fig. 3.9 depicts the maximum voltage magnitudes that appear at the meters of all residential consumers for a selected subset of PNNL taxonomy feeders (one from each region). Fig. 3.10 illustrates the change in statistical distribution of voltages at the meters of the residential loads throughout the day in feeder R5-3500-1. Similar patterns are observed in all feeders. Generally, the estimated loss in PV energy production due to the reactive power control action is on the order of 1–2% (during this light-load day) as shown in Fig. 3.11 for the same five feeders as previously. Fig. 3.12 depicts the change in reactive energy consumption at the substation.

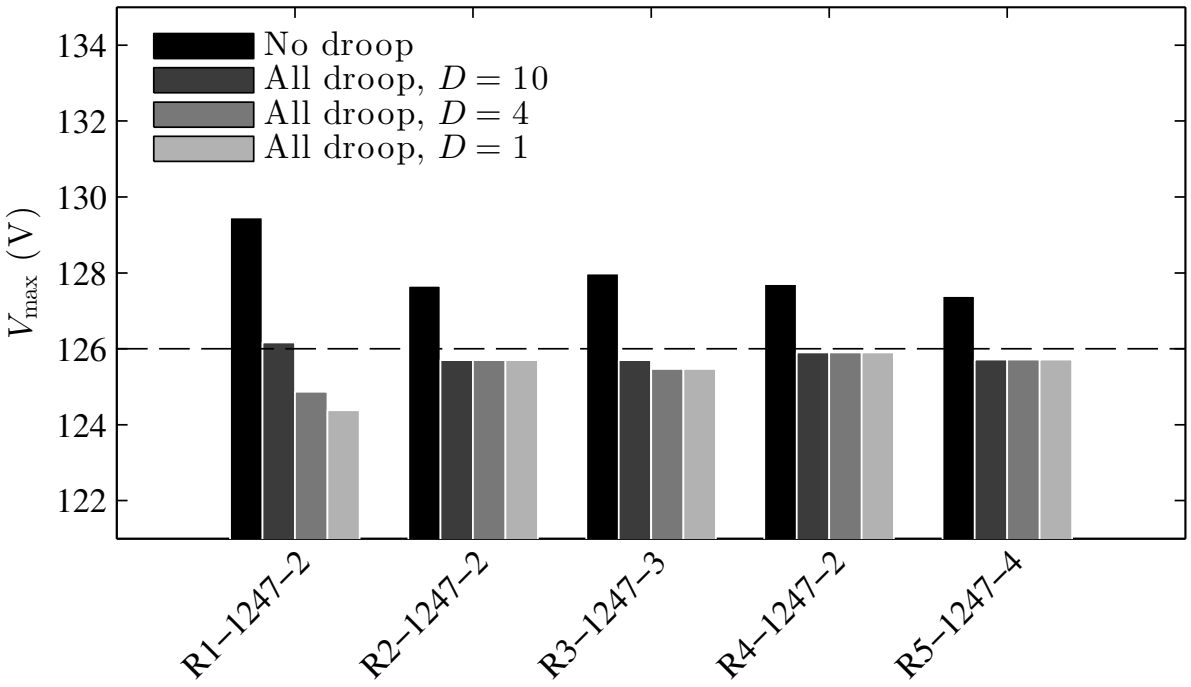

Figure 3.9 Maximum voltage in PNNL taxonomy feeders for 50% penetration level.

More comprehensive simulation results for all studies conducted on the 22 PNNL taxonomy feeders are given in Tables 3.3, 3.4 and 3.5 in Appendix B. It is noted that decreasing the deadband width D is beneficial with respect to eliminating voltage rises. This could also improve the overall dynamic system stability, due to the corresponding reduction in the slope of the droop characteristic. However, it comes at the expense of higher inverter and distribution feeder energy loss, and substantially higher reactive power demand at the substation.

3.4.2 Cloudy Sky

In the previous subsection cloud effect has been ignored, for a relatively temperate day with a sunny sky, and all PV panels were assumed to receive the same amount of solar irradiance. However, the output of a PV system in a cloudy day can be quite intermittent and it causes voltage and power fluctuations in the distribution systems. This subsection contains the effect of cloud transients on distribution system performance using the

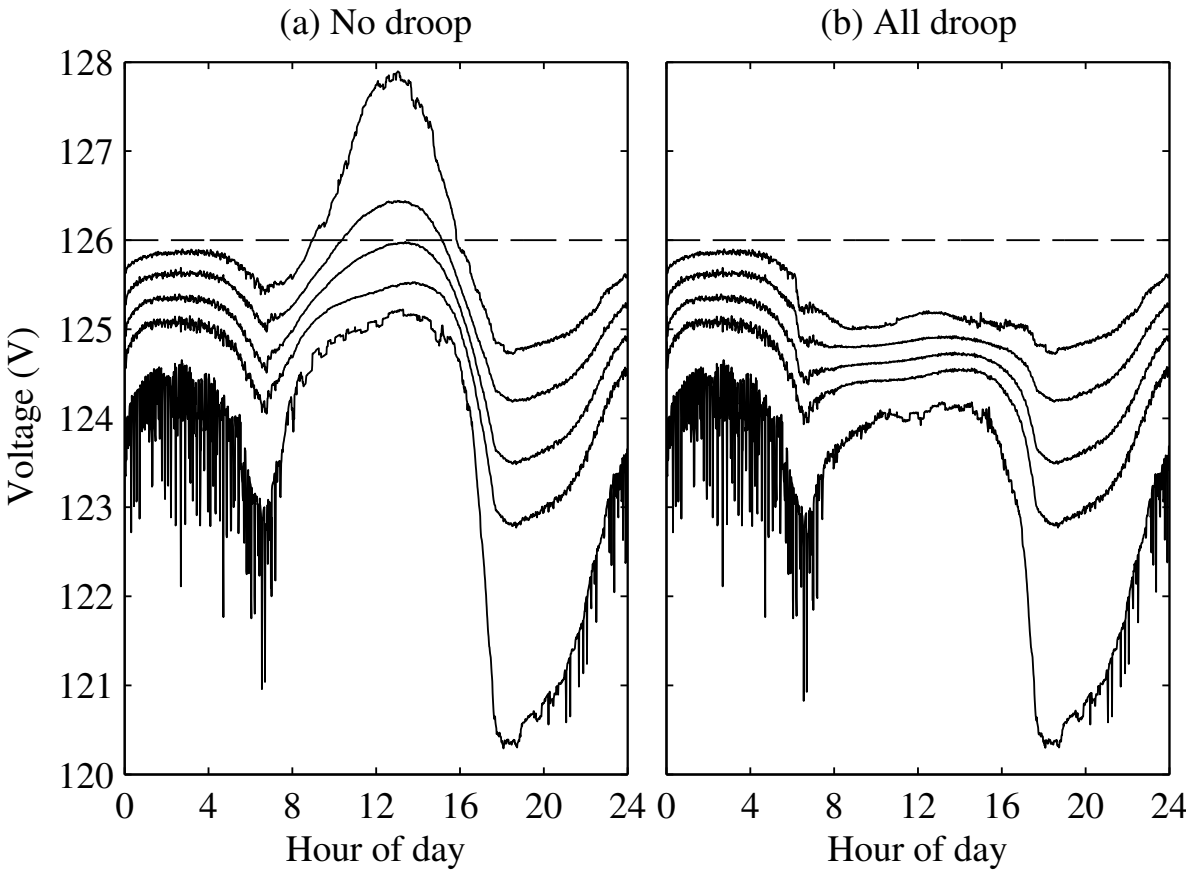

Figure 3.10 Statistics of voltages at meters of residential loads for 50% PV penetration in PNNL feeder R5-3500-1 ($V^a = 114$ V, $V^d = 126$ V, $D = 10$ V).

proposed distributed Volt/VAr controller. In this case, PV panels are not receiving the same amount of solar irradiance. Because during cloudy days, using the same solar irradiance time series for calculating real power of hundreds of PV systems scattered over a large area can lead to significant error. In order to model this condition with high fidelity, fractal cloud model, proposed in [71], are used to model a realistic cloud pattern that moves over the ABDTF feeder (explained in Subsection 3.4.1.1). To achieve this, the original solar source code of GridLAB-D was modified to represent this model[9]. In the modified codes, PV panels of houses connected to the same distribution transformers are receiving the same amount of solar irradiance time series. The obtained cloud shadow

[9]In the original source code of GridLAB-D, house and solar panel models are coded to look for a single climate object.

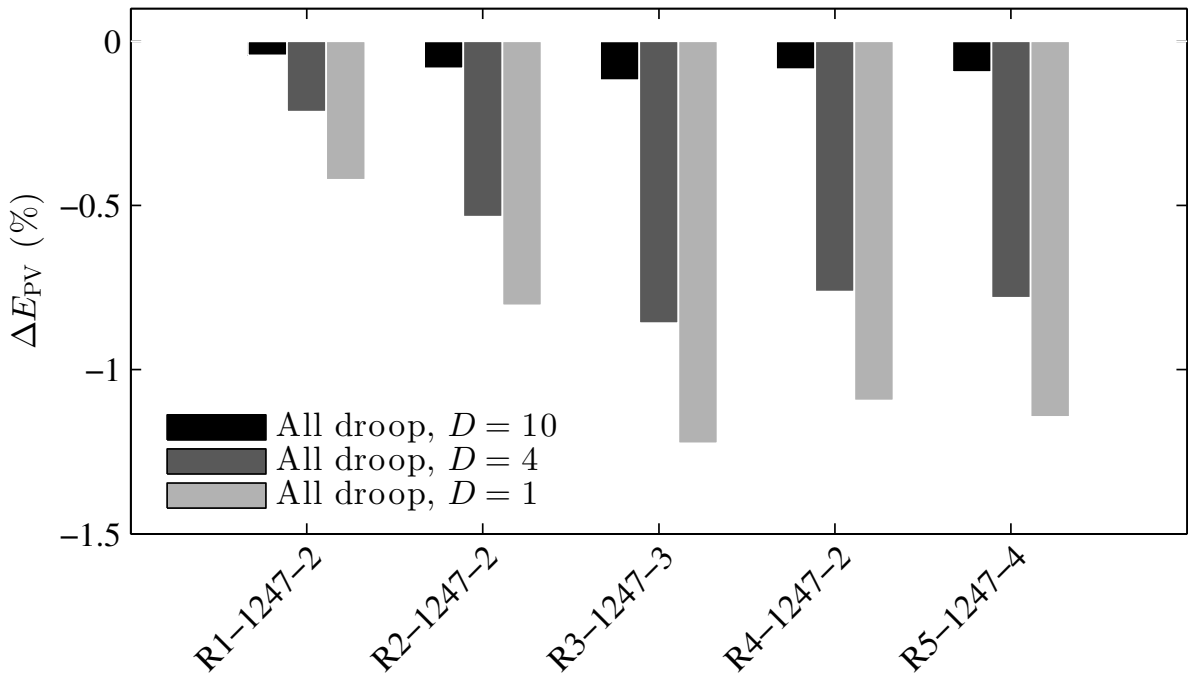

Figure 3.11 Relative change of PV energy in PNNL taxonomy feeders for 50% penetration level.

pattern from the model in [71], is shown in Fig. 3.13 (bottom), and a magnified portion of this (indicated by a small box around 14:45) is displayed in Fig. 3.14. The figures are in gray scale; darker pixels correspond to increased shading.

Power and statistics of voltages are shown in Figs. 3.15 and 3.16. As can be observed in Fig. 3.15(a), the real power flow at the substation is reversed most of the time during one hour simulation. Fig. 3.15(b), depicts total reactive power at the substation. The plot in the controlled case reflects the level of reactive power absorbed from the PV inverters to mitigate voltage rise. Fig. 3.15(c) presents the total real power generated from the PV units. As you can see cumulus clouds caused significant fluctuations in PV outputs. Fig. 3.16 depicts the statistical distribution of voltages at the household meters. Fig. 3.16(a) illustrates that without the droop control the maximum voltages significantly exceed the upper limit for a substantial number of residential customers, with a significant amount of fluctuations. Fig. 3.16(b) shows how the proposed controllers

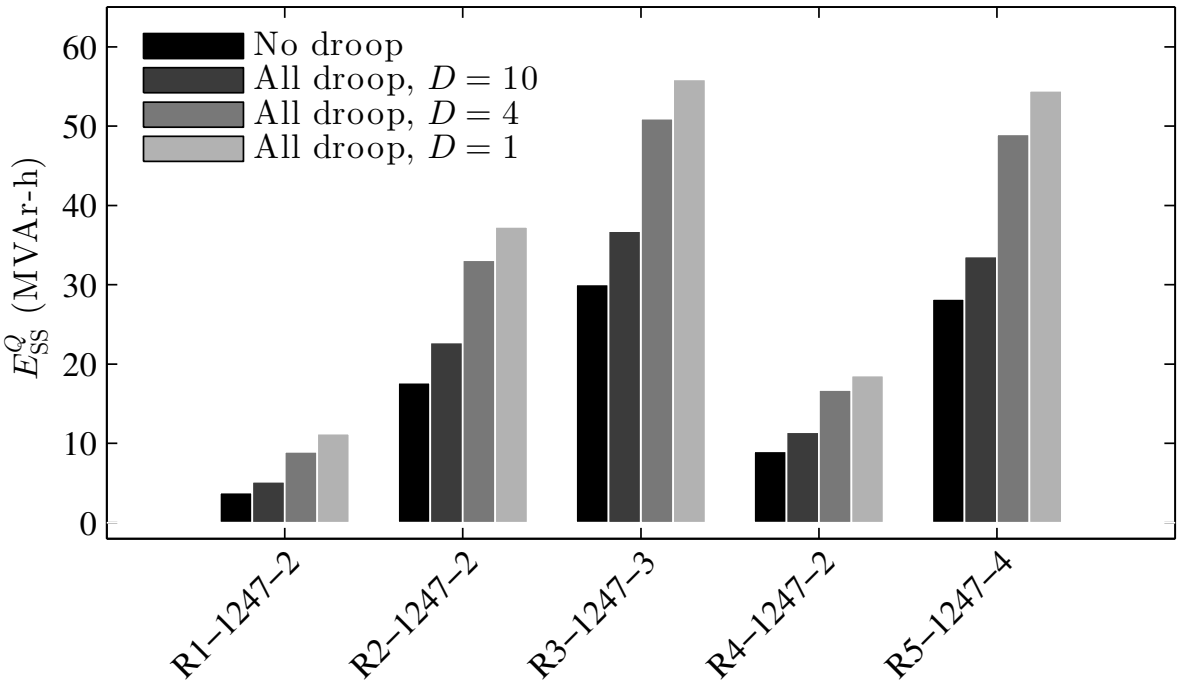

Figure 3.12 Reactive energy at the substation in PNNL taxonomy feeders for 50% penetration level.

can offset voltage rise conditions with a lot of fluctuations, and how all voltages remain below their upper limit.

3.5 Conclusion

We studied the mitigation of voltage rise via reactive power absorption from distributed PV inverters. Analyses were conducted with detailed computer simulations of an array of real and realistic feeders representative of all US regions for several PV penetration levels, as high as 50%. Also, the effect of cloud transients on distribution system performance using the proposed distributed Volt/VAr controller was studies. The results indicate that voltages can be successfully controlled within normal bounds in all cases that were analyzed.

One potential technical issue of high significance is the substantial amount of extra reactive power that is absorbed by the feeder at the substation. This reactive power would

have to be compensated, perhaps using capacitor banks at the substation, otherwise problems related to transmission system voltage stability might arise. However, fast cloud transients and the reaction of the distributed Volt/VAr PV controllers might render capacitor bank-based compensation unsuitable for this purpose. Furthermore, it would be interesting to study if and how the proposed control scheme could be integrated into more conventional Volt/VAr controls that use capacitor banks and load tap changers.

Appendix A: Example System Parameters

The two-bus system has the following parameters: The voltage of bus 1 is fixed at $V_1 = 129$ V. The load consumes $P_l = 3$ kW and $Q_l = 1$ kVAr. The PV inverter is rated at $S^{\max} = 1.5$ kVA, and is assumed to be lossless. Its real power generation is initially zero, and is stepped to $P^{\text{inv}} = 1$ kW during period 6. The impedance of the line is $0.076 + j0.268\ \Omega$. The droop function parameters are $V^a = 114$ V, $V^d = 126$ V, and $D = 10$ V.

The three-bus system is similar to the two-bus system, with the following differences: The loads consume $P_{l2} = P_{l3} = 1.5$ kW and $Q_{l2} = Q_{l3} = 0.5$ kVAr. The line impedance between bus 1 and bus 2 is $0.076 + j0.268\ \Omega$, and the impedance between bus 2 and bus 3 is $0.0076 + j0.0268\ \Omega$.

Appendix B: Comprehensive Simulation Results for PNNL Taxonomy Feeders

Tables 3.3, 3.4 and 3.5 contain a comprehensive set of simulation results for studies conducted on 22 PNNL taxonomy feeders. The PV inverters are operating with various droop function parameters ($V^a = 114$ V, $V^d = 126$ V, variable D) under a 50% penetration level.

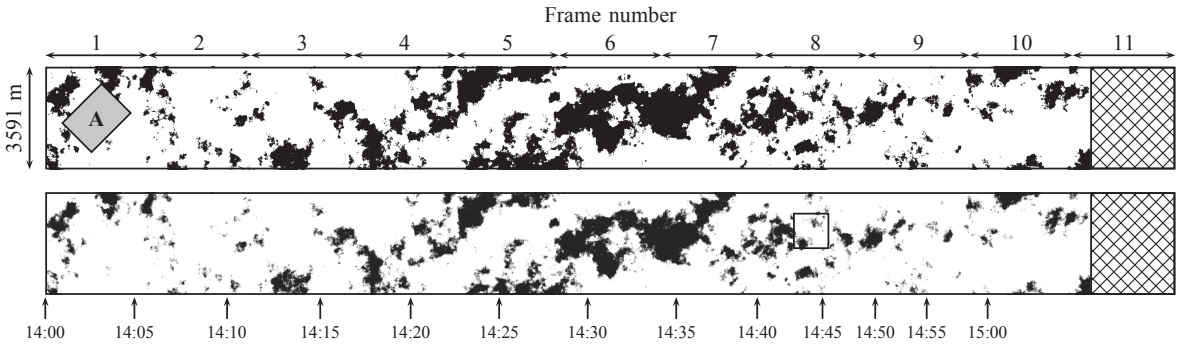

Figure 3.13 (Top) Generated binary cloud shadow pattern for time period between 2:00 and 3:00 PM. The wind direction is SW. A is the study area. (Bottom) Final cloud shadow pattern, using a multi-layer rendering technique [71].

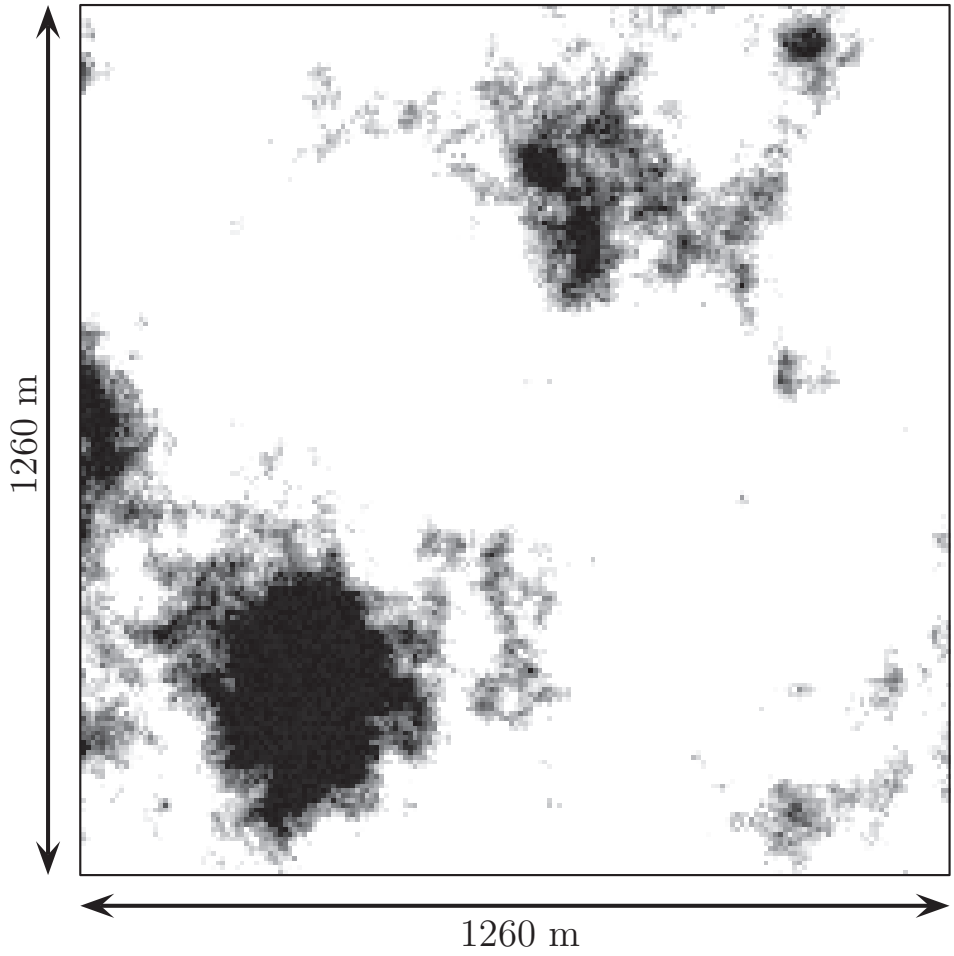

Figure 3.14 Magnified cloud shadow pattern [71].

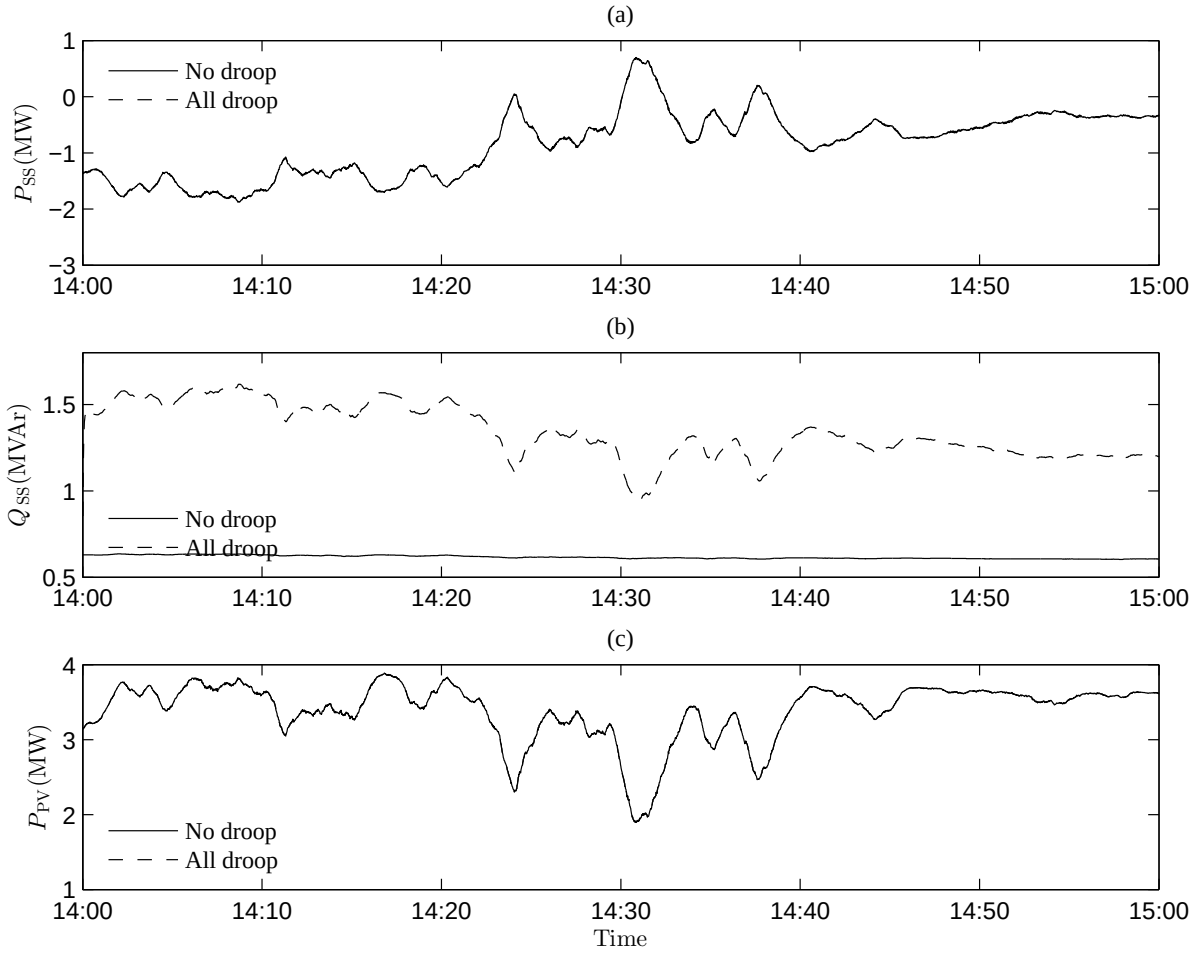

Figure 3.15 50% PV penetration in ABDTF on a cloudy sky: (a) Real power at the substation; (b) Reactive power at the substation; (c) Total PV real power generation.

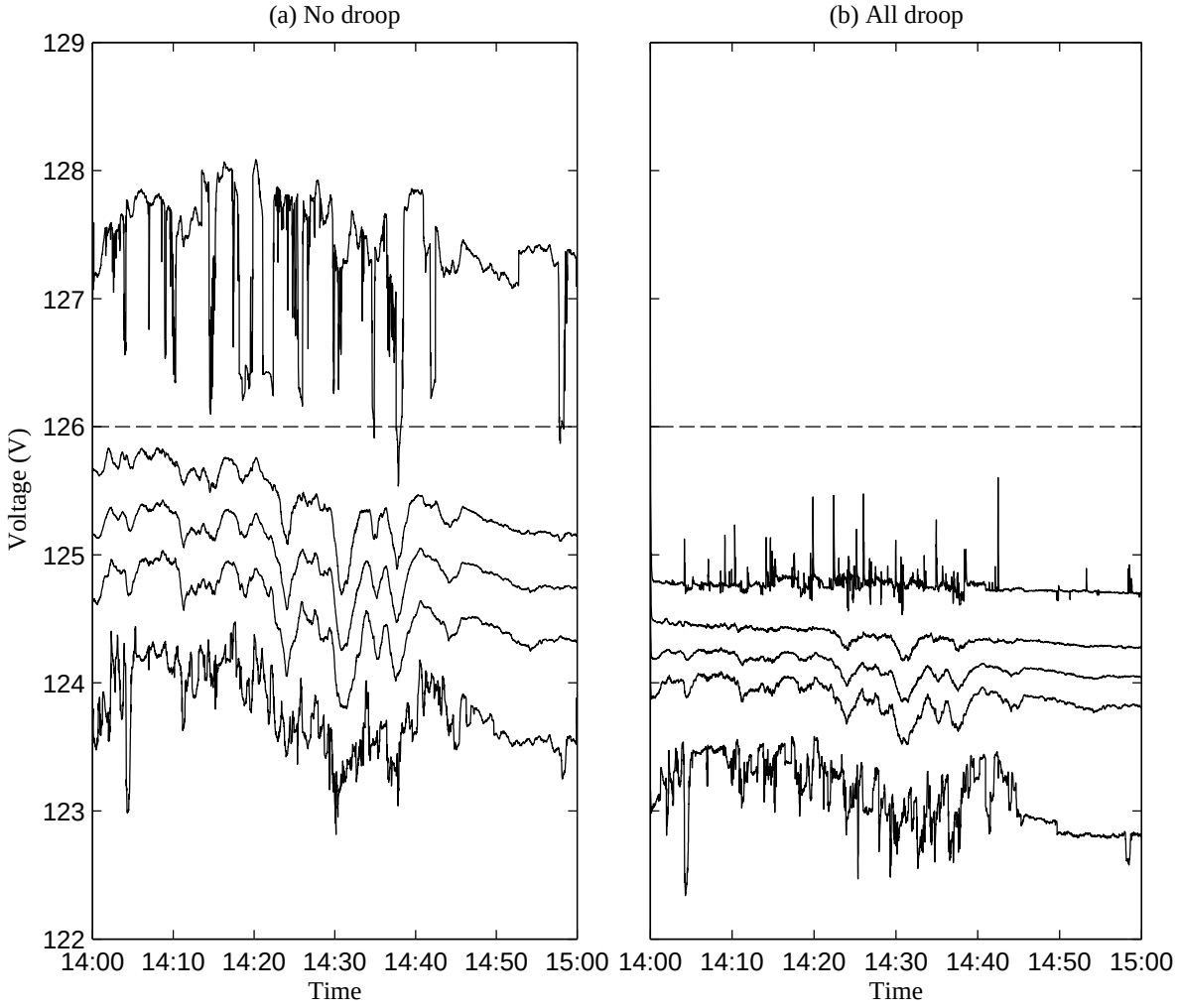

Figure 3.16 Statistics of voltages at meters of residential loads for 50% PV penetration in ABDTF on a cloudy sky ($V^a = 114$ V, $V^d = 126$ V, $D = 8$ V). The five traces correspond to the minimum, mean value minus one standard deviation, mean value, mean value plus one standard deviation, and maximum voltage.

Table 3.3 PNNL Taxonomy Feeders' Metrics for 50% Penetration Level

D (V)	VVR (%)	$V_{\max}$ (V)	$V_{\min}$ (V)	ΔE_{load} (MWh)	ΔE_{loss} (MWh)	ΔE_{PV} (MWh)	ΔE_{SS} (MWh)	ΔE^{Q}_{SS} (MVAr-h)	ΔE^{Q}_{PV} (MVAr-h)
R1-1247-1 with 1594 houses and 777 PV systems:									
N/A	43.91	129.52	114.33	63.056*	1.849*	46.698*	18.208*	22.471*	0.000*
10.00	0.19	126.92	114.30	-0.073	0.045	-0.010	-0.019	3.271	-3.175
4.00	0.00	125.99	114.30	-0.288	0.168	-0.105	-0.014	13.299	-12.919
1.00	0.00	125.99	114.27	-0.412	0.250	-0.183	0.022	18.193	-17.627
R1-1247-2 with 544 houses and 286 PV systems:									
N/A	39.34	129.46	114.82	22.867*	0.840*	17.316*	6.392*	3.803*	0.000*
10.00	0.18	126.17	114.82	-0.020	0.025	-0.007	0.012	1.353	-1.318
4.00	0.00	124.87	114.80	-0.081	0.081	-0.037	0.037	5.145	-5.021
1.00	0.00	124.38	114.26	-0.117	0.122	-0.073	0.078	7.435	-7.253
R1-1247-3 with 22 houses and 12 PV systems:									
N/A	100.00	126.20	123.42	10.334*	0.052*	0.730*	9.656*	0.541*	0.000*
10.00	0.00	125.73	123.42	-0.007	0.002	-0.003	-0.002	0.319	-0.319
4.00	0.00	125.73	122.34	-0.015	0.008	-0.014	0.006	0.731	-0.729
1.00	0.00	125.73	121.94	-0.018	0.010	-0.017	0.009	0.828	-0.824
R1-1247-4 with 652 houses and 339 PV systems:									
N/A	56.44	130.04	116.35	45.544*	0.680*	21.367*	24.857*	19.541*	0.000*
10.00	0.61	126.67	116.35	-0.067	0.053	-0.014	-0.000	3.008	-2.968
4.00	0.00	124.88	116.35	-0.212	0.176	-0.090	0.054	9.215	-9.071
1.00	0.00	124.88	116.25	-0.276	0.249	-0.149	0.122	12.033	-11.816
R1-2500-1 with 40 houses and 21 PV systems:									
N/A	2.50	126.14	122.39	19.497*	0.314*	1.336*	18.475*	-10.353*	0.000*
10.00	0.00	125.88	122.38	-0.001	-0.000	-0.002	0.000	0.146	-0.145
4.00	0.00	125.88	122.34	-0.004	-0.002	-0.018	0.011	1.020	-1.022
1.00	0.00	125.88	121.96	-0.006	-0.001	-0.025	0.017	1.286	-1.288
R2-1247-1 with 176 houses and 87 PV systems:									
N/A	15.34	126.57	123.96	49.802*	0.593*	6.936*	43.459*	5.211*	0.000*
10.00	0.00	125.99	123.96	-0.043	0.005	-0.023	-0.015	2.178	-2.171
4.00	0.00	125.99	122.61	-0.140	0.029	-0.132	0.022	6.811	-6.760
1.00	0.00	125.99	121.94	-0.162	0.039	-0.164	0.041	7.897	-7.829
R2-1247-2 with 836 houses and 437 PV systems:									
N/A	82.66	127.66	120.38	40.733*	0.932*	33.674*	7.991*	17.666*	0.000*
10.00	0.00	125.70	120.38	-0.090	0.043	-0.028	-0.019	5.071	-5.023
4.00	0.00	125.70	119.94	-0.284	0.152	-0.180	0.048	15.443	-15.219
1.00	0.00	125.70	118.91	-0.360	0.215	-0.271	0.126	19.640	-19.299
R2-1247-3 with 1506 houses and 756 PV systems:									
N/A	24.50	128.86	114.11	60.470*	1.684*	49.826*	12.328*	25.087*	0.000*
10.00	0.07	126.70	114.09	-0.029	0.005	-0.004	-0.020	1.306	-1.272
4.00	0.00	125.91	114.10	-0.204	0.040	-0.051	-0.114	7.776	-7.661
1.00	0.00	125.91	114.14	-0.331	0.073	-0.102	-0.157	12.032	-11.874

* These values represent energies for the base case.

Table 3.4 PNNL Taxonomy Feeders' Metrics for 50% Penetration Level

D (V)	VVR (%)	$V_{\max}$ (V)	$V_{\min}$ (V)	ΔE_{load} (MWh)	ΔE_{loss} (MWh)	ΔE_{PV} (MWh)	ΔE_{SS} (MWh)	ΔE_{SS}^{Q} (MVAr-h)	ΔE_{PV}^{Q} (MVAr-h)
R2-2500-1 with 910 houses and 465 PV systems:									
N/A	43.85	127.11	121.95	142.723*	1.348*	38.057*	106.015*	24.249*	0.000*
10.00	0.00	125.98	121.81	-0.203	0.056	-0.072	-0.074	9.632	-9.582
4.00	0.00	125.98	120.99	-0.627	0.236	-0.500	0.109	29.981	-29.702
1.00	0.00	125.98	120.52	-0.759	0.316	-0.664	0.222	35.873	-35.482
R2-3500-1 with 90 houses and 44 PV systems:									
N/A	13.33	126.13	123.67	94.617*	0.775*	3.166*	92.225*	0.612*	0.000*
10.00	0.00	125.97	123.66	-0.014	0.000	-0.014	-0.000	0.795	-0.788
4.00	0.00	125.93	123.14	-0.092	0.010	-0.085	0.003	3.846	-3.818
1.00	0.00	125.93	122.89	-0.106	0.014	-0.101	0.009	4.393	-4.359
R3-1247-1 with 457 houses and 232 PV systems:									
N/A	5.25	126.26	123.81	62.946*	1.258*	12.511*	51.693*	13.858*	0.000*
10.00	0.00	125.94	123.76	-0.071	0.008	-0.031	-0.033	3.567	-3.558
4.00	0.00	125.94	122.66	-0.248	0.054	-0.243	0.049	12.499	-12.416
1.00	0.00	125.94	122.14	-0.285	0.072	-0.306	0.093	14.600	-14.486
R3-1247-3 with 1326 houses and 725 PV systems:									
N/A	64.40	127.98	120.51	50.483*	2.748*	33.887*	19.345*	30.050*	0.000*
10.00	0.00	125.70	120.50	-0.080	0.046	-0.040	0.007	6.724	-6.699
4.00	0.00	125.47	119.61	-0.263	0.182	-0.291	0.211	20.897	-20.742
1.00	0.00	125.47	118.96	-0.326	0.259	-0.415	0.348	25.861	-25.619
R4-1247-1 with 523 houses and 239 PV systems:									
N/A	14.72	126.99	120.05	32.487*	1.042*	17.801*	15.729*	18.346*	0.000*
10.00	0.00	125.73	120.06	-0.047	0.009	-0.017	-0.020	3.066	-3.062
4.00	0.00	125.56	119.28	-0.174	0.063	-0.183	0.072	11.869	-11.793
1.00	0.00	125.56	119.25	-0.217	0.090	-0.255	0.129	14.651	-14.528
R4-1247-2 with 370 houses and 212 PV systems:									
N/A	87.03	127.70	120.45	14.092*	0.494*	13.766*	0.820*	8.988*	0.000*
10.00	0.00	125.90	120.43	-0.028	0.007	-0.012	-0.009	2.425	-2.423
4.00	0.00	125.90	118.56	-0.095	0.034	-0.105	0.045	7.722	-7.697
1.00	0.00	125.90	117.68	-0.118	0.049	-0.151	0.081	9.577	-9.533
R4-2500-1 with 168 houses and 72 PV systems:									
N/A	16.07	127.39	118.87	5.916*	0.225*	4.800*	1.341*	4.054*	0.000*
10.00	0.00	125.96	118.88	-0.007	0.003	-0.004	0.000	0.583	-0.581
4.00	0.00	125.96	118.88	-0.027	0.010	-0.023	0.006	1.911	-1.904
1.00	0.00	125.96	118.00	-0.037	0.014	-0.035	0.012	2.491	-2.480

* These values represent energies for the base case.

Table 3.5 PNNL Taxonomy Feeders' Metrics for 50% Penetration Level

D (V)	VVR (%)	$V_{\max}$ (V)	$V_{\min}$ (V)	ΔE_{load} (MWh)	ΔE_{loss} (MWh)	ΔE_{PV} (MWh)	ΔE_{SS} (MWh)	ΔE_{SS}^{Q} (MVAr-h)	ΔE_{PV}^{Q} (MVAr-h)
R5-1247-1 with 1002 houses and 536 PV systems:									
N/A	9.08	126.86	120.07	77.910*	1.011*	38.482*	40.439*	24.891*	0.000*
10.00	0.00	125.31	120.07	-0.057	0.011	-0.007	-0.039	2.375	-2.359
4.00	0.00	125.31	120.08	-0.399	0.103	-0.213	-0.083	17.779	-17.597
1.00	0.00	125.31	118.99	-0.549	0.160	-0.346	-0.044	23.733	-23.431
R5-1247-2 with 306 houses and 172 PV systems:									
N/A	6.21	128.27	115.67	40.443*	0.641*	11.976*	29.108*	19.392*	0.000*
10.00	0.33	126.43	115.67	-0.019	0.010	-0.004	-0.005	0.797	-0.793
4.00	0.00	125.66	115.56	-0.162	0.102	-0.095	0.035	6.709	-6.659
1.00	0.00	125.66	115.61	-0.217	0.149	-0.147	0.080	8.871	-8.786
R5-1247-3 with 2024 houses and 1065 PV systems:									
N/A	46.54	134.31	114.23	68.724*	4.185*	73.835*	-0.925*	13.655*	0.000*
10.00	10.13	127.91	114.19	-0.244	0.084	-0.039	-0.121	7.093	-6.392
4.00	0.00	125.98	114.23	-0.451	0.167	-0.064	-0.220	11.651	-10.520
1.00	0.00	125.90	114.23	-0.559	0.258	-0.115	-0.185	15.270	-13.790
R5-1247-4 with 926 houses and 493 PV systems:									
N/A	39.63	127.39	121.32	60.587*	1.271*	36.767*	25.092*	28.205*	0.000*
10.00	0.00	125.71	121.27	-0.096	0.038	-0.034	-0.024	5.349	-5.344
4.00	0.00	125.71	120.70	-0.385	0.188	-0.287	0.090	20.778	-20.696
1.00	0.00	125.71	119.73	-0.485	0.269	-0.421	0.204	26.263	-26.115
R5-1247-5 with 1539 houses and 802 PV systems:									
N/A	35.67	128.78	117.90	70.804*	2.096*	59.586*	13.313*	37.419*	0.000*
10.00	0.06	126.04	118.02	-0.127	0.079	-0.026	-0.023	4.857	-4.765
4.00	0.00	125.79	117.57	-0.489	0.263	-0.177	-0.049	19.254	-18.837
1.00	0.00	125.79	117.78	-0.671	0.382	-0.292	0.003	25.898	-25.245
R5-2500-1 with 2146 houses and 1095 PV systems:									
N/A	30.75	130.40	115.57	96.909*	1.987*	88.829*	10.067*	51.493*	0.000*
10.00	0.05	126.98	115.57	-0.150	0.092	-0.044	-0.014	9.954	-9.910
4.00	0.00	125.46	115.21	-0.633	0.393	-0.489	0.249	41.314	-41.122
1.00	0.00	125.42	114.51	-0.824	0.565	-0.761	0.501	53.278	-52.951
R5-3500-1 with 2192 houses and 1155 PV systems:									
N/A	38.55	127.90	120.29	98.390*	1.919*	86.029*	14.281*	50.383*	0.000*
10.00	0.00	125.90	120.30	-0.216	0.150	-0.110	0.044	15.202	-15.174
4.00	0.00	125.90	118.72	-0.694	0.416	-0.698	0.419	49.428	-49.366
1.00	0.00	125.90	117.80	-0.864	0.563	-0.988	0.687	61.213	-61.081

* These values represent energies for the base case.

4. Local Reactive Power Compensation by Rooftop PV Inverters

A paper to be submitted in the *IEEE Transactions on Power Delivery*.

Pedram Jahangiri [1], Dionysios C. Aliprantis, and Lyndon Cook

Abstract

This paper studies the behavior of distribution feeders with high penetration level of rooftop photovoltaics (PV), in the case where PV inverters compensate the reactive power consumption of local households loads. In this context, some important theoretical aspects of control design are investigated. Case studies involving simulations of realistic distribution feeders with hundreds of households and their appliances modeled in high detail are performed to study the distribution system impacts of the proposed controller. It is shown that this control typically leads to a reduction of real power losses, and helps to decrease congestion at the transmission side.

4.1 Introduction

THE INSTALLED capacity of embedded rooftop photovoltaic (PV) generation in residential distribution systems is rising rapidly worldwide [7], driven by reductions in costs, increases in electricity prices, and higher sensitivity about sustainability.

[1] Primary researcher and author.

Modern PV inverters have the capability to supply or absorb reactive power, independently of their production of real power, at essentially no extra cost. This functionality can be exploited in a number of ways, for instance, for reducing the voltage rise phenomenon due to the reverse power flow in feeders [29, 72]. In this paper, we study the case where PV inverters are operated as local VAr compensators (LVArC), that is, when they are providing the reactive power consumed by local loads as measured at their point of common coupling (PCC).

In general, VAr compensation reduces transmission loss, maximizes power transmission capability, enhances stability, and helps support the supply voltage [69, 73–76]. In distribution systems, reactive power is typically supplied from capacitor banks, although power electronic equipment can be used as well [77, 78]. PV systems that are capable of providing reactive power support to the grid are now commercially available [25, 26].

In the approach considered herein, the supply of reactive power from the PV inverters is adjusted dynamically based on local measurements. The control objective is to make each customer (e.g., house) appear as a unity power factor load in the steady state, to the extent that this is possible given the limitations of the inverter. This is achieved using a simple yet effective proportional-integral (PI) control, but also requires the presence of an advanced (or "smart") utility meter with an appropriate communication interface, e.g., via ZigBee [79–82]. The meter measures the reactive power consumption at the PCC of each house with the utility, then transmits this signal to the power electronics periodically, e.g., every 1 s. The proposed system does not require communication or cooperation with other PV inverters [58, 64]. Also, since the PV inverters are not actively regulating the voltage level, safety concerns are alleviated, and the system is in compliance with current interconnection codes and standards, such as UL 1741 [23] and IEEE Std. 1547 [24].

The literature contains numerous examples of inverter-based reactive power support for achieving various objectives. One approach is to formulate a constrained optimization

problem, where the objectives can be the minimization of loss and/or the maximization of the voltage profile flatness along the feeder [83–86]. The solution of this problem requires knowledge of a great amount of data related to the feeder configuration (e.g., cable parameters) and its dynamic state (e.g., available inverters, voltages, real and reactive powers, etc.). Data is transmitted to a central controller, where the problem is solved, and then commanded set-points are communicated back to the controllers of the inverters. In theory, these schemes can find globally optimal solutions; however, they are not practical to implement. The alternate approach is to calculate the dispatch of the reactive power of inverters in a distributed fashion [33,87–89]. These techniques are based on local information and limited communication with surrounding nodes, they are less computationally demanding, they impose reduced communication overhead, and they have been shown to be robust, even though convergence rate can be slow. Nevertheless, such control strategies typically consider the voltage regulation problem only. Hence, they can lead to unacceptably low power factor at the substation, and increased losses in the distribution and transmission grid.

The salient contributions of this work can be summarized as follows: 1) A control scheme that permits residential rooftop PV inverters to compensate their local reactive power consumption is proposed. 2) The control is validated via high-fidelity time-series simulations of several realistic distribution feeders with hundreds of households and their appliances modeled in detail. The simulations are run using GridLAB-D [31], which is an open-source software platform developed by the U.S. Department of Energy at the Pacific Northwest National Laboratory (PNNL) for the simulation of electric power distribution systems. GridLAB-D has a comprehensive library of precise load models, including their dependence on voltage levels. The original inverter source code of GridLAB-D was modified to represent the proposed control. The reactive power capability of the inverter is modeled accurately as dynamically dependent on the real power generation, and inverter losses are accounted for as well. 3) The dynamic interactions between

PV inverters operating in tandem (but not necessarily in a synchronized manner) are investigated. Previous work has pointed out that this may arise from inappropriate choice of controller parameters [32, 33]. Here, system stability is established using a novel distribution system analysis framework.

The remainder of this paper is organized as follows: Section 4.2 sets forth the proposed controller and discusses system stability. Illustrative findings from computer simulations on several realistic feeders are reported in Section 4.3. Concluding remarks are provided in Section 4.4.

4.2 System Modeling and Control Strategy

4.2.1 Reactive Power Compensation by Power Electronics

Fig. 4.1 shows the proposed modification to a PV inverter with maximum power point tracking (MPPT) functionality. The MPPT algorithm determines the real power output of the inverter at each period n, $P_n^{\text{inv}} = \hat{P}_n - P_n^{\text{inv, loss}}$. The reactive power output, $Q_n^{\text{inv}} \approx \hat{Q}_n$, is determined by a PI controller and a limiter block. Other functions of the inverter, such as the phase-locked loop for tracking the terminal voltage and anti-islanding detection schemes, are not shown here. The generation of an additional reactive power component is relatively simple to implement (for example, using qd reference frame theory), and amounts to injecting the appropriate current component ninety degrees out of phase with the voltage.

The reactive power compensating controller of inverter j attempts to bring the measured PCC reactive power to zero, and operates based on the following discrete-time equations

$$E_{j,n}^{Q} = \begin{cases} \max\left(\min\left(E_j^{Q,\max}, E_{j,n-1}^{Q} + Q_{j,n-1}^{m} M\Delta t\right),\ -E_j^{Q,\max}\right) & \text{if } n = kM + j, k \in \mathbb{N} \\ E_{j,n-1}^{Q} & \text{otherwise} \end{cases} \tag{4.1}$$

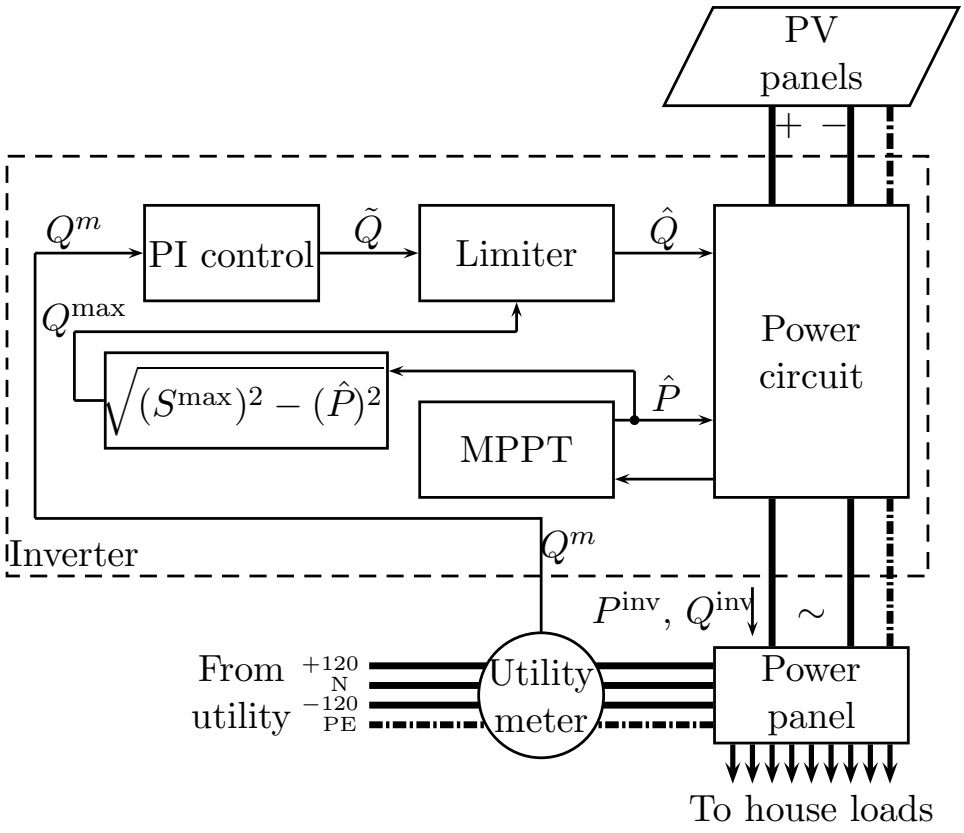

Figure 4.1 Block diagram of the proposed local VAr compensator scheme.

and

$$\tilde{Q}_{j,n} = \begin{cases} G_j^I E_{j,n-1}^Q + G_j^P Q_{j,n-1}^m & \text{if } n = kM + j, k \in \mathbb{N} \\ \tilde{Q}_{j,n-1} & \text{otherwise} \end{cases} \tag{4.2}$$

where $E_{j,n}^Q$ stands for "reactive energy," $E_j^{Q,\max} > 0$ is an anti-windup limit, and $\tilde{Q}_{j,n}$ is the reactive power command for controller j at time slot n. The parameters G_j^I and G_j^P are PI control gains. It is assumed that each second is subdivided into an integer number M of intervals of duration Δt seconds, and that each inverter acts as soon as the reactive power measurement $Q_{j,n}^m$ is received from the smart meter, which happens periodically every 1 s. (Hence, $M\Delta t = 1$ s.) This formulation allows the analysis of multiple controllers acting independently of each other, not necessarily in a synchronized manner, since it is not realistic to expect that such a synchronization scheme would be

in place.

The maximum reactive power capability at period n is computed based on the real power generation and the apparent power rating of the inverter $S_j^{\max}$, by

$$Q_{j,n}^{\max} = [(S_j^{\max})^2 - (\hat{P}_{j,n})^2]^{1/2}. \tag{4.3}$$

Hence, the commanded value of reactive power $\hat{Q}_n$ is

$$\hat{Q}_{j,n} = \begin{cases} \tilde{Q}_{j,n} & \text{if } |\tilde{Q}_{j,n}| \leq Q_{j,n}^{\max} \\ \text{sgn}(\tilde{Q}_{j,n}) \cdot Q_{j,n}^{\max} & \text{otherwise}\,. \end{cases} \tag{4.4}$$

The power loss of the inverter is modeled as

$$P_{j,n}^{\text{inv, loss}} = \left(ae^{-b\hat{P}_{j,n}} + c\right) \cdot \sqrt{(\hat{P}_{j,n})^2 + (\hat{Q}_{j,n})^2} \tag{4.5}$$

where $a = 0.04$, $b = 0.01$, and $c = 0.018$. This functional representation yields a realistic loss model [90, 91].

4.2.2 Load Modeling

The loads at each bus are modeled using the ZIP model [92]. A wide variety of ZIP load parameters obtained from laboratory measurements can be found in [93]. The real and reactive power loads at house i are modeled as

$$P_{i,n}^l = P_i^l(V_{i,n}) = a_i^p V_{i,n}^2 + b_i^p V_{i,n} + c_i^p \tag{4.6}$$

$$Q_{i,n}^l = Q_i^l(V_{i,n}) = a_i^q V_{i,n}^2 + b_i^q V_{i,n} + c_i^q \tag{4.7}$$

where the constants a_i^p, b_i^p, c_i^p, a_i^q, b_i^q, c_i^q are representative of the total load at house i.

4.2.3 Stability Analysis of Distribution Feeders with Proposed Control

A general framework for stability analysis of distribution systems with LVArC inverters is established in this section. This is based on a sequence of quasi steady-state

operating points. It should be noted that recent work on microgrids has analyzed the interactions of droop controllers (during microgrid islanded operation) [94–96], which have been shown to cause instability under certain conditions. Also, research has shown that resonances in line currents can occur due to inverter LCL filter interactions at various frequencies, typically above 300 Hz [97–101]. Here, such issues are not of concern.

Consider the general case of an N-bus distribution feeder system with a constant-voltage slack bus representing the substation, and $N-1$ load buses with LVArC PV inverters, i.e., $N-1$ PQ buses. The loads are modeled using the ZIP model described in subsection 4.2.2. For simplicity, let this be a single-phase system.

Assume that the limiter and anti-windup blocks are not activated, i.e., $\hat{Q} = \tilde{Q}$, and that the reactive power output of the inverter is equal to the commanded value, i.e., $Q^{\text{inv}} = \hat{Q}$. The asynchronous behavior of the $N-1$ controllers is modeled by staggering them evenly within one second. Hence $M = N-1$ and $\Delta t = (N-1)^{-1}$ s. This dynamic system has $2(N-1)$ states representing the measured reactive energy and power output of each inverter during period n, contained in a column vector $X_n = [E_n^Q; \hat{Q}_n]$, where $E_n^Q = [E_{2,n}^Q \; E_{3,n}^Q \; \cdots \; E_{N,n}^Q]^T$ and $\hat{Q}_n = [\hat{Q}_{2,n} \; \hat{Q}_{3,n} \; \cdots \; \hat{Q}_{N,n}]^T$.

The dynamic system model is

$$X_n = f(X_{n-1}, n) = \begin{bmatrix} E_{n-1}^Q + C_n Q_{n-1}^m M \Delta t \\ C_n(G^I E_{n-1}^Q + G^P Q_{n-1}^m) + (\mathbb{I} - C_n)\hat{Q}_{n-1} \end{bmatrix} \tag{4.8}$$

where $\mathbb{I}$ is an $(N-1) \times (N-1)$ identity matrix, the vector of measured reactive powers is $Q_n^m = [Q_{2,n}^m \; \cdots \; Q_{N,n}^m]^T$, and the vector of reactive power demands (assumed to be constant in this analysis) is defined as $Q_n^l = [Q_{2,n}^l \; \cdots \; Q_{N,n}^l]^T$. Note that $Q_n^m = Q_n^l - \hat{Q}_n$. Also, G^I, G^P, and C_n are diagonal matrices, $G^I = \text{diag}([G_2^I \cdots G_N^I])$, $G^P = \text{diag}([G_2^P \cdots G_N^P])$, and $C_n = \text{diag}([c_{2,n} \cdots c_{N,n}])$, respectively, where $c_{j,n} = 1$, for $n = kM + j - 1, k \in \mathbb{N}$, and zero otherwise. Therefore, $C_n = \text{diag}([0 \cdots 0 \; 1 \; 0 \cdots 0])$ is a matrix where all diagonal elements are zero except one, corresponding to the inverter that is activated in the n^{th} time slot.

The stationary states (fixed points) $[\bar{E}^Q; \bar{Q}]$ satisfy the nonlinear equation:

$$\bar{X} = \begin{bmatrix} \bar{E}^Q \\ \bar{Q} \end{bmatrix} = f(\bar{E}^Q, \bar{Q}) = \begin{bmatrix} {G^I}^{-1} Q^l \\ Q^l \end{bmatrix} . \tag{4.9}$$

The stability of this nonlinear periodic time-variant discrete-time system in the vicinity of its stationary states can be determined using the following result [102]:

> *Theorem:* For the periodic time-variant discrete-time system $X_n = \phi(X_{n-1}, n)$, suppose $\phi : \mathbb{U} \times \mathbb{Z}_+ \to \mathbb{U}$, $\mathbb{U} \subseteq \mathbb{R}^m$, is continuously differentiable in some neighborhood of a fixed point $\bar{X} \in \mathbb{U}$. Let $J(n) = [\partial\phi(X, n)/\partial X]_{X=\bar{X}}$ be the Jacobian matrix of ϕ, evaluated at $\bar{X}$. Also, $\phi(X_n, n) = \phi(X_n, n+M)$, where M is the period of the system, and $\bar{J} = \prod_{n=M}^{1} J(n)$. Then:
>
> - $\bar{X}$ is asymptotically stable if all eigenvalues of $\bar{J}$ have magnitude less than 1.
> - $\bar{X}$ is unstable if at least one eigenvalue of $\bar{J}$ has magnitude greater than 1.

Here, the Jacobian matrix of (4.8) becomes

$$\begin{aligned} J(n) = \left[\frac{\partial f(X,n)}{\partial X}\right]_{X=\bar{X}} &= \begin{bmatrix} \frac{\partial f_1}{\partial E^Q} & \frac{\partial f_1}{\partial \hat{Q}} \\ \frac{\partial f_2}{\partial E^Q} & \frac{\partial f_2}{\partial \hat{Q}} \end{bmatrix}_{X=\bar{X}} \\ &= \begin{bmatrix} \mathbb{I} & C_n \left(\left[\frac{\partial Q^l}{\partial V}\right] \left[\frac{\partial V}{\partial \hat{Q}}\right] - \mathbb{I} \right) M\Delta t \\ C_n G^I & C_n G^P \left(\left[\frac{\partial Q^l}{\partial V}\right] \left[\frac{\partial V}{\partial \hat{Q}}\right] - \mathbb{I} \right) + \mathbb{I} - C_n \end{bmatrix}_{X=\bar{X}} \end{aligned} \tag{4.10}$$

where $[\partial Q^l/\partial V]$ is a diagonal matrix,

$$\left[\frac{\partial Q^l}{\partial V}\right] = \begin{bmatrix} \frac{\partial Q^l_2}{\partial V_2} & & 0 \\ & \ddots & \\ 0 & & \frac{\partial Q^l_N}{\partial V_N} \end{bmatrix} . \tag{4.11}$$

The diagonal elements can be obtained from (4.7), $\partial Q_i^l/\partial V_i = 2a_i^q V_i + b_i^q$. The matrix $[\partial V/\partial \hat{Q}]$ contains the partial derivatives

$$\left[\frac{\partial V}{\partial \hat{Q}}\right] = \begin{bmatrix} \frac{\partial V_2}{\partial \hat{Q}_2} & \frac{\partial V_2}{\partial \hat{Q}_3} & \cdots & \frac{\partial V_2}{\partial \hat{Q}_N} \\ \frac{\partial V_3}{\partial \hat{Q}_2} & \frac{\partial V_3}{\partial \hat{Q}_3} & \cdots & \frac{\partial V_3}{\partial \hat{Q}_N} \\ \vdots & \vdots & & \vdots \\ \frac{\partial V_N}{\partial \hat{Q}_2} & \frac{\partial V_N}{\partial \hat{Q}_3} & \cdots & \frac{\partial V_N}{\partial \hat{Q}_N} \end{bmatrix}. \tag{4.12}$$

To calculate $[\partial V/\partial \hat{Q}]$, we first write the power flow equations as implicit functions of the reactive power injections by the PV inverters $\hat{Q}$:

$$P(\delta(\hat{Q}), V(\hat{Q})) - (P^{\text{inv}} - P^l(V(\hat{Q}))) = 0 \tag{4.13}$$

$$Q(\delta(\hat{Q}), V(\hat{Q})) - (\hat{Q} - Q^l(V(\hat{Q}))) = 0\,. \tag{4.14}$$

Here, the vector functions $P = [P_2\ P_3\ \cdots\ P_N]^T$ and $Q = [Q_2\ Q_3\ \cdots\ Q_N]^T$ represent real and reactive power injections, respectively, and P^{inv} is a constant vector. The net power injections at each load bus $i = 2, 3, \ldots, N$, are

$$P_i = \sum_{j=1}^{N} V_i V_j |Y_{i,j}| \cos(\delta_j - \delta_i + \theta_{i,j}) \tag{4.15}$$

$$Q_i = -\sum_{j=1}^{N} V_i V_j |Y_{i,j}| \sin(\delta_j - \delta_i + \theta_{i,j}) \tag{4.16}$$

where the elements of the nodal admittance matrix of the system are denoted by $Y_{i,j} = |Y_{i,j}|\underline{/\theta_{i,j}}$. Hence, from (4.13)–(4.14), we obtain:

$$\left[\frac{\partial P}{\partial \delta}\right]\left[\frac{\partial \delta}{\partial \hat{Q}}\right] + \left[\frac{\partial P}{\partial V}\right]\left[\frac{\partial V}{\partial \hat{Q}}\right] + \left[\frac{\partial P^l}{\partial V}\right]\left[\frac{\partial V}{\partial \hat{Q}}\right] = 0 \tag{4.17}$$

$$\left[\frac{\partial Q}{\partial \delta}\right]\left[\frac{\partial \delta}{\partial \hat{Q}}\right] + \left[\frac{\partial Q}{\partial V}\right]\left[\frac{\partial V}{\partial \hat{Q}}\right] + \left[\frac{\partial Q^l}{\partial V}\right]\left[\frac{\partial V}{\partial \hat{Q}}\right] = \mathbb{I}\,. \tag{4.18}$$

The diagonal matrix $[\partial P_l/\partial V]$ is similar to $[\partial Q_l/\partial V]$,

$$\left[\frac{\partial P^l}{\partial V}\right] = \begin{bmatrix} \frac{\partial P_2^l}{\partial V_2} & & 0 \\ & \ddots & \\ 0 & & \frac{\partial P_N^l}{\partial V_N} \end{bmatrix}. \tag{4.19}$$

Its diagonal elements can be obtained from (4.6): $\partial P_i^l/\partial V_i = 2a_i^p V_i + b_i^p$. Manipulation of (4.17)–(4.18) yields

$$\left[\frac{\partial V}{\partial \hat{Q}}\right] = \left\{\left[\frac{\partial Q}{\partial V}\right] + \left[\frac{\partial Q^l}{\partial V}\right] - \left[\frac{\partial Q}{\partial \delta}\right]\left[\frac{\partial P}{\partial \delta}\right]^{-1}\left(\left[\frac{\partial P}{\partial V}\right] + \left[\frac{\partial P^l}{\partial V}\right]\right)\right\}^{-1}. \tag{4.20}$$

In addition to $[\partial P^l/\partial V]$ and $[\partial Q^l/\partial V]$, this expression contains four submatrices of the Jacobian of the power flow problem (not to be confused with the Jacobian of the dynamic system function f), which have well-known expressions that can be computed from (4.13)–(4.14) or found in a power systems textbook.

The Jacobian $J(n)$ in (4.10) can be further approximated by noting that the magnitude of the elements of the matrix $[\partial V/\partial \hat{Q}]$ is typically on the order of 0.5–2.5 V/kVAr.[2] (This is the impact of injected reactive power on local voltage.) Moreover, $[\partial Q^l/\partial V]$ is a diagonal matrix with elements in the range 5–15 VAr/V. Therefore, the term $([\partial Q^l/\partial V][\partial V/\partial \hat{Q}] - \mathbb{I})$ in (4.10) is approximately equal to $-\mathbb{I}$. Hence,

$$J(n) \approx \begin{bmatrix} \mathbb{I} & -C_n M \Delta t \\ C_n G^I & -C_n G^P + \mathbb{I} - C_n \end{bmatrix}. \tag{4.21}$$

It can be readily shown that

$$\bar{J} = \prod_{n=N-1}^{1} J(n) \approx \begin{bmatrix} \mathbb{I} & -\mathbb{I} \\ G^I & -G^P \end{bmatrix}. \tag{4.22}$$

It follows that the eigenvalues (λ) of $\bar{J}$ satisfy

$$\det(\bar{J} - \lambda \mathbb{I}_2) \approx \det \begin{bmatrix} \mathbb{I} - \lambda\mathbb{I} & -\mathbb{I} \\ G^I & -G^P - \lambda\mathbb{I} \end{bmatrix} = 0 \tag{4.23}$$

where $\mathbb{I}_2$ is a $2(N-1) \times 2(N-1)$ identity matrix. The determinant is evaluated using

[2] This has been confirmed for numerous small and large test systems.

a well known matrix property[3] [103]:

$$\det(\bar{J} - \lambda \mathbb{I}_2) \approx \det\left(\lambda^2 \mathbb{I} + \lambda(G^P - \mathbb{I}) + (G^I - G^P)\right)$$
$$= \prod_{i=2}^{N} \left(\lambda^2 + \lambda(G_i^P - 1) + (G_i^I - G_i^P)\right) = 0\,. \tag{4.24}$$

Hence, for $i = 2, 3, \ldots, N$,

$$\lambda_i^{\alpha,\beta} \approx \frac{-(G_i^P - 1) \pm \sqrt{(G_i^P - 1)^2 - 4(G_i^I - G_i^P)}}{2}\,. \tag{4.25}$$

In order to ensure the stability of the system, all eigenvalues should have magnitude less than 1. It can be concluded that stable sets of gains for each controller separately lead to a stable distribution system with multiple LVArC controllers acting asynchronously. For the case studies in the next section, the PI gains are $G^I = 0.3$ and $G^P = 0.1$ for all inverters.

It is also interesting to briefly discuss stability in the other extreme case when all controllers act simultaneously every 1 s. Now, the Jacobian is time-invariant and approximately equal to the matrix in (4.22). Hence, the same set of eigenvalues is obtained.

4.3 Case Studies

This section contains a distillation of extensive simulation-based analyses on a wide range of PNNL taxonomy feeders that were modeled and populated with PV systems in very high detail. In the simulations, the controllers are not staggered but they all act simultaneously, because GridLAB-D does not support time steps less than 1 s. As was shown in Section 4.2.3, system stability should not be influenced by this.

The incident solar radiation on a tilted PV array is calculated using classical formulas [67], implemented in GridLAB-D. The calculation involves various types of irradiance

[3] Let $M = \begin{bmatrix} A & B \\ C & D \end{bmatrix}$, where A, B, C, D are square matrices and C, D commute (i.e., $CD = DC$). Then $\det \begin{bmatrix} A & B \\ C & D \end{bmatrix} = \det(AD - BC)$.

adjusted for time of day, the site latitude, and the orientation and tilt angle of the PV panels.

In the simulations, PV panels are virtually installed on residential rooftops according to a PV penetration level parameter, which is defined as:

$$\text{penetration level} = \frac{\text{residential customers with PV systems}}{\text{total number of residential customers in the feeder}} \tag{4.26}$$

The houses are assumed to have two types of orientation, namely, north-south and east-west. The orientation of houses with PV systems is split in a 3:1 ratio, signifying that there is higher probability that PV panels will be installed on a south-facing rather than on a west-facing roof in the northern hemisphere. The roof angle is uniformly selected from a set with pitch equal to $x/12$, where $x = \{0, 3, 4, \ldots, 12\}$. If the roof is flat ($x = 0$), the solar panels are assumed to be facing south and tilted to a degree equal to the site latitude; otherwise, solar panels are assumed to be installed parallel to the roof.

The southern or western part of the roof area is set equal to

$$\text{south- or west-facing roof area} = (0.5) \cdot (\text{floor area}) / \cos(\text{roof angle})\,. \tag{4.27}$$

Then the total panel area is randomly generated according to a uniform distribution within 50% to 90% of the south- or west-facing roof area. For a given PV panel area value, the nominal apparent power rating of the inverter should satisfy:

$$\begin{aligned} S_j^{\max} &\geq (\text{CF}) \cdot (\text{panel efficiency}) \cdot (\text{rated insolation}) \cdot (\text{area}) \\ &= (1.15) \cdot (0.15) \cdot (1000\ (\text{W/m}^2)) \cdot (\text{area}\ (\text{m}^2))\,, \end{aligned} \tag{4.28}$$

where CF represents a corrective factor, since in certain cases the rated insolation can be exceeded. $S_j^{\max}$ is selected from a list that has been compiled from commercially available inverters (up to 30 kVA) [68], as the next higher value in the list. In other words, the most economical inverter that can handle the rated real power for any given PV installation is still being selected, so that additional investment costs for providing

reactive power support are not incurred to the customer. The anti-windup limit in (4.1) is set to $E_j^{Q,\max} = (1.5/G_j^I) \cdot S_j^{\max}$.

Meteorological data are obtained from the National Renewable Energy Laboratory Measurement and Instrumentation Data Center (MIDC) database [70], which contains records of solar irradiance and air temperature recorded at 1-minute intervals from several stations. A hot day (peak day) with a clear sky is selected from the Loyola Marymount University, University Hall, Los Angeles, CA site, for all feeders.

In the studies described below, the "No Control" case represents a base scenario where none of the inverters have the local VAr compensator, whereas in the "LVArC" case all inverters have the proposed control.

4.3.1 Distribution Feeders

This section provides details about the distribution feeders that are used for the case studies. All feeders are connected to a high-voltage bus through a substation transformer with an impedance of $0.009 + j0.06$ pu. The voltage regulator is activated and the output node of the regulator's voltage is controlled. Tap changes are performed based on default values of band center and width in taxonomy feeders. The voltage at the transmission side of the substation transformer for all feeders is assumed to be constant and equal to 1.02 pu.

4.3.1.1 PNNL taxonomy feeders

The so-called "taxonomy feeders" are prototypical feeders developed by researchers at PNNL. They represent the fundamental characteristics of radial distribution feeders found in the U.S., based on 575 distribution feeders from 151 separate substations from different utilities across the U.S. Each prototypical feeder is characterized as belonging to one of five U.S. climate regions[4], by primary distribution voltage level, and other

[4]Region 1 is the west coast, region 2 is the north-central and eastern U.S., region 3 is the non-coastal southwest U.S., region 4 is the non-coastal southeast and central U.S., and region 5 is the southeast.

features [40]. For example, the PNNL feeder named R1-1247-1 is in climate region 1, and has 12.47 kV line-to-line rms nominal primary distribution voltage[5]. The models of the taxonomy feeders are provided as part of the GridLAB-D software package. Simulation studies were performed on 20 taxonomy feeders that contain houses. The feeders have been modeled with high fidelity from the substation down to the individual customer meters, including detailed end-use load representations (heating, ventilation, and air-conditioning, and various other constant impedance, current, and power loads). The houses of each feeder are equipped with rooftop PV systems (with embedded LVArC control) at 50% penetration level.

4.3.1.2 Agent-based distribution test feeder

A so-called "agent-based distribution test feeder" (ABDTF) has been developed by the authors [69], based on an actual feeder of an electric utility in Iowa, with detailed specifications for feeder equipment (such as fuses, switches, overhead and underground conductors, and service transformers) as well as for residential and/or commercial customers, including the floor areas of the houses.[6] The peak power of the feeder at the substation is reported by the utility to be approximately 14 MVA, and the primary distribution voltage is 13.2 kV. The end-use loads of the households include conventional thermostatically controlled air-conditioning, water heaters, TV sets, fans, lights, ovens, and other common electric devices. This feeder has 1372 houses.

4.3.2 Metrics for Evaluation

In this section, the metrics that will be used to evaluate the performance of the LVArC controller are described. The metrics are observed over a span of 24 hours, at a

[5]All voltages in the paper are provided as rms values.

[6]In its original implementation, the feeder was equipped with an array of intelligent "agents," such as price-responsive air-conditioning units and plug-in electric vehicles, hence the name of the feeder. However, this type of functionality has now been disabled, and the feeder only contains conventional non-price-responsive load.

time interval of 1 s.

The first set of metrics is related to voltage. These metrics are the average, maximum and minimum voltage magnitudes (V_{mean}, V_{max}, V_{min}) that appear at the meters of all residential consumers, over a span of 24 hours. Also, $\bar{V}_{\text{mean}}$ is defined as the time average of the spacial average V_{mean} over the 24 hours.

The second set of metrics is related to energy. These are the energy consumed by all loads (E_{load}), the energy loss of the feeder (E_{loss}), the energy generated by all PV systems (E_{PV}), and the energy measured at the low-voltage side of the substation transformer (E_{SS}). Also, by integrating reactive power, "reactive energy" metrics can be defined, measured in MVAr-h. These are the reactive energy measured at the substation (E^{Q}_{SS}) and the reactive energy generated by all PV systems (E^{Q}_{PV}).

Differences between the case where PV inverters are supplying reactive power ("LVArC") and the base ("No Control") case are denoted by "ΔE". In general, we expect to obtain negative value for ΔE_{loss}, which represents reduced real energy losses throughout the distribution feeder. This is because reactive energy of loads is compensated locally. Also, since reactive energy demand is reduced at the substation, ΔE^{Q}_{SS} will be negative. ΔE_{PV} should be negative as well, because of extra inverter losses due to the reactive power current component. Generally the voltages are increased in the "LVArC" case (because of reactive power injection at each node), they usually result to higher power consumption (from voltage-dependent loads) thus yielding positive values of ΔE_{load}. The substation energy difference is given by

$$\Delta E_{\text{SS}} = \Delta E_{\text{load}} + \Delta E_{\text{loss}} - \Delta E_{\text{PV}} \,. \tag{4.29}$$

4.3.3 Simulation Results

Simulation results for studies conducted on PNNL taxonomy feeders and ABDTF are given in Table 4.1, Table 4.2 and Table 4.3. As can be observed, energy losses have been decreased in all cases by 0.1–9.5% and on average by 3% (negative ΔE_{loss}, as expected).

In all feeders, "reactive energy" demand has been decreased significantly (14–86%) in the controlled cases (negative $\Delta E^{Q}_{\mathrm{SS}}$). This would lead to further loss reduction in the substation transformer and the bulk transmission system, which are not modeled here. Although energy losses were decreased in all "LVArC" cases, the real energy demand at the substation in some cases increased (positive E_{SS}); this is due to a slight decrease in real energy production from the PV units (negative ΔE_{PV}) and an increase in energy consumed by voltage dependent loads (positive ΔE_{load}) according to (4.29). Also, it can be observed from the V_{max} and V_{min} columns that the voltages in the controlled cases are in compliance with the ANSI Standard C84.1[7] [18] in all feeders.

Fig. 4.2 illustrates power waveforms for one arbitrarily selected house.[8] The large pulses in Fig. 4.2(a) are due to the turning on and off of the A/C and water heater. In this house, the power rating of the A/C unit is approximately 3 kVA (2.9 kW and 0.7 kVAr), and the heating element capacity of the water heater is 5.5 kW. Since the water heater does not consume reactive power, the large pulses (around 5.5 kW) in Fig. 4.2(a) that do not coincide with pulses in Fig. 4.2(c) are identified as caused by the water heater. The other large pulses in Fig. 4.2(a) are due to periodic A/C action. The small jumps are caused by other appliances turning on and off. Fig. 4.2(d) shows how the LVArC controller of the PV inverter attempts to bring the measured PCC reactive power to zero. It can be observed that when real power generation is highest (around noon), the reactive power load cannot be compensated fully because the maximum reactive power capability is limited ($S_j^{\mathrm{max}} = 2.4$ kVA). Fig. 4.3 shows a magnified version (around 17:55-17:56) of Figs. 4.2(c), 4.2(d) and 4.2(e), when the controller compensates reactive power

[7] The voltage at the PCC of residential loads should remain within five percent (114–126 V) from its nominal value (120 V).

[8] In GridLAB-D, the electric water heater and air-conditioner (A/C) are modeled as thermostatically controlled loads using appropriate physics-based models. Additionally, time-variant ZIP models are used for other appliances (lighting, TV, fans, and plug loads). The real and reactive power of the A/C depends on the outside air temperature (changing from 70° F to 90° F here), the inside air temperature, equipment and house parameters, terminal voltage, and occupant-controlled set point (here, this varies from 70° F to 75° F during the day). The houses have different realistic set points for A/C systems. Some houses do not have an electric water heater.

load. (These waveforms are captured on a second-by-second basis.)

Fig. 4.4 shows the real power losses on the various types of feeder components (overhead lines, underground cables, service transformers, service lines) in feeder R1-1247-1. As can be observed, real power losses have decreased in the controlled cases. Figs. 4.5(a)–(c) depict the total apparent, real and reactive power load at the substation of feeder R1-1247-1. Figs. 4.5(d) and 4.5(e) present the total real and reactive power generated from the PV units in the same feeder.

4.4 Conclusion

This study investigated the implementation of a local reactive power compensating control for rooftop PV inverters, which would work seamlessly with an advanced meter. Additionally, in the context of a distribution feeder with many such inverters, system stability was established using an appropriate distribution system analysis framework. The controller was extensively tested with case studies using detailed computer simulations.

A major finding is that the proposed controller can reduce real energy losses in the feeder and reactive energy demand at the substation. The obtained operating point might not be the globally-optimal loss-minimizing point that could perhaps be calculated by rigorous feeder-level optimization. However, the reduction in loss is substantial, and is achieved with a relatively simple system that requires no communication between inverters or advanced computing capabilities. It was also shown that feeder-level voltage stability will be guaranteed by using individually well-tuned controllers, which should alleviate power quality concerns by utilities.

In future work, it would be interesting to integrate the LVArC controller with Volt/VAr controls and conservation voltage reduction, for reducing the induced voltage rise due to local reactive power injection, and thus conserving energy. To this end, the PV inverter could be a multi-functional device with several operational modes.

Table 4.1 PNNL Taxonomy Feeders' Metrics for 50% Penetration Level

Ctrl	$\bar{V}_{\text{mean}}$ (V)	$V_{\max}$ (V)	$V_{\min}$ (V)	ΔE_{load} (MWh)	ΔE_{loss} (MWh)	ΔE_{PV} (MWh)	ΔE_{SS} (MWh)	ΔE^{Q}_{SS} (MVAr-h)	ΔE^{Q}_{PV} (MVAr-h)
R1-1247-1 with 1594 houses and 805 PV systems:									
a**	122.0	125.3	114.6	59.058*	1.472*	21.866*	38.664*	20.014*	0.000*
b	122.4	126.0	115.3	0.024	−0.081	−0.009	−0.048	−15.226	15.030
R1-1247-2 with 544 houses and 270 PV systems:									
a**	122.3	124.8	115.8	21.749*	0.689*	7.113*	15.325*	10.916*	0.000*
b	122.5	125.2	116.5	0.001	−0.040	−0.003	−0.037	−5.124	5.089
R1-1247-3 with 22 houses and 10 PV systems:									
a**	123.8	124.3	121.5	9.248*	0.045*	0.253*	9.041*	0.658*	0.000*
b	123.8	124.3	121.6	0.000	−0.001	−0.000	−0.000	−0.182	0.182
R1-1247-4 with 652 houses and 338 PV systems:									
a**	121.1	126.0	114.3	41.523*	0.500*	10.065*	31.958*	17.585*	0.000*
b	121.2	125.9	114.1	−0.011	−0.037	−0.003	−0.045	−4.257	4.238
R1-2500-1 with 40 houses and 19 PV systems:									
a**	123.1	124.0	120.4	15.320*	0.130*	0.437*	15.012*	1.309*	0.000*
b	123.0	124.1	120.5	−0.001	−0.001	−0.000	−0.001	−0.317	0.316
R2-1247-1 with 176 houses and 89 PV systems:									
a**	124.2	125.0	121.5	43.841*	0.515*	3.128*	41.229*	5.375*	0.000*
b	124.3	125.1	121.5	0.005	−0.002	−0.001	0.004	−1.876	1.873
R2-1247-2 with 836 houses and 432 PV systems:									
a**	123.2	125.7	118.7	37.989*	0.799*	15.843*	22.944*	15.677*	0.000*
b	123.2	125.6	119.1	0.007	−0.030	−0.003	−0.019	−5.876	5.835

* These values represent energies for the base case.
** a: No control. b: LVArC control.

Table 4.2 PNNL Taxonomy Feeders' Metrics for 50% Penetration Level

Ctrl	$\bar{V}_{\text{mean}}$ (V)	$V_{\max}$ (V)	$V_{\min}$ (V)	ΔE_{load} (MWh)	ΔE_{loss} (MWh)	ΔE_{PV} (MWh)	ΔE_{SS} (MWh)	ΔE^{Q}_{SS} (MVAr-h)	ΔE^{Q}_{PV} (MVAr-h)
R2-1247-3 with 1506 houses and 780 PV systems:									
a**	122.9	125.1	114.0	57.997*	1.461*	23.568*	35.891*	22.625*	0.000*
b	123.2	125.9	114.5	0.020	−0.059	−0.009	−0.030	−14.891	14.804
R2-2500-1 with 910 houses and 497 PV systems:									
a**	123.9	125.2	120.7	119.806*	1.201*	18.352*	102.655*	22.693*	0.000*
b	124.0	125.5	120.8	0.020	−0.029	−0.006	−0.003	−10.336	10.312
R2-3500-1 with 90 houses and 47 PV systems:									
a**	124.2	124.9	121.2	75.956*	0.836*	1.590*	75.202*	1.096*	0.000*
b	124.2	124.9	121.3	0.004	−0.001	−0.001	0.003	−0.947	0.946
R3-1247-1 with 457 houses and 228 PV systems:									
a**	123.8	124.6	120.8	53.259*	1.326*	6.141*	48.444*	13.614*	0.000*
b	123.9	124.6	120.8	0.015	−0.011	−0.003	0.007	−4.170	4.159
R3-1247-3 with 1326 houses and 696 PV systems:									
a**	122.8	125.3	117.1	45.613*	2.569*	14.405*	33.777*	27.888*	0.000*
b	122.5	125.0	117.5	−0.019	−0.046	−0.005	−0.060	−7.723	7.651
R4-1247-1 with 523 houses and 254 PV systems:									
a**	123.9	125.0	119.2	28.839*	1.031*	8.747*	21.123*	16.472*	0.000*
b	124.0	125.1	119.4	0.006	−0.012	−0.002	−0.005	−3.399	3.386
R4-1247-2 with 370 houses and 201 PV systems:									
a**	124.2	125.4	120.5	12.263*	0.439*	6.293*	6.410*	8.061*	0.000*
b	124.4	125.8	120.5	0.002	−0.008	−0.002	−0.003	−3.927	3.918

* These values represent energies for the base case.
** a: No control. b: LVArC control.

Table 4.3 PNNL Taxonomy Feeders and ABDTF's Metrics for 50% Penetration Level

Ctrl	$\bar{V}_{\text{mean}}$ (V)	$V_{\max}$ (V)	$V_{\min}$ (V)	ΔE_{load} (MWh)	ΔE_{loss} (MWh)	ΔE_{PV} (MWh)	ΔE_{SS} (MWh)	ΔE^{Q}_{SS} (MVAr-h)	ΔE^{Q}_{PV} (MVAr-h)
R4-2500-1 with 168 houses and 81 PV systems:									
a**	122.7	125.3	117.5	5.304*	0.201*	2.447*	3.058*	3.686*	0.000*
b	122.6	126.2	118.6	−0.000	−0.004	−0.001	−0.003	−1.538	1.533
R5-1247-1 with 1002 houses and 509 PV systems:									
a**	123.6	125.0	119.7	67.164*	1.006*	17.126*	51.043*	22.775*	0.000*
b	123.8	125.5	120.1	0.031	−0.042	−0.006	−0.004	−10.300	10.253
R5-1247-2 with 306 houses and 162 PV systems:									
a**	123.0	125.1	115.2	32.137*	0.647*	5.061*	27.724*	15.178*	0.000*
b	123.1	125.5	115.3	0.008	−0.021	−0.001	−0.012	−2.086	2.077
R5-1247-4 with 926 houses and 466 PV systems:									
a**	123.9	125.3	119.2	53.208*	1.220*	16.209*	38.219*	24.501*	0.000*
b	124.0	125.6	119.4	0.007	−0.034	−0.004	−0.023	−6.218	6.198
R5-1247-5 with 1539 houses and 759 PV systems:									
a**	120.3	123.4	115.0	62.878*	1.795*	24.799*	39.875*	33.015*	0.000*
b	120.9	124.8	115.6	0.075	−0.169	−0.009	−0.085	−15.356	15.156
R5-3500-1 with 2192 houses and 1103 PV systems:									
a**	122.7	124.6	120.5	85.561*	1.314*	36.520*	50.355*	30.212*	0.000*
b	122.7	124.6	120.6	0.005	−0.033	−0.009	−0.019	−14.448	14.438
ABDTF with 1372 houses and 691 PV systems:									
a**	121.5	124.3	118.5	46.077*	0.853*	30.895*	16.036*	21.383*	0.000*
b	121.6	124.8	118.7	0.009	−0.044	−0.005	−0.030	−10.045	9.983

* These values represent energies for the base case.
** a: No control. b: LVArC control.

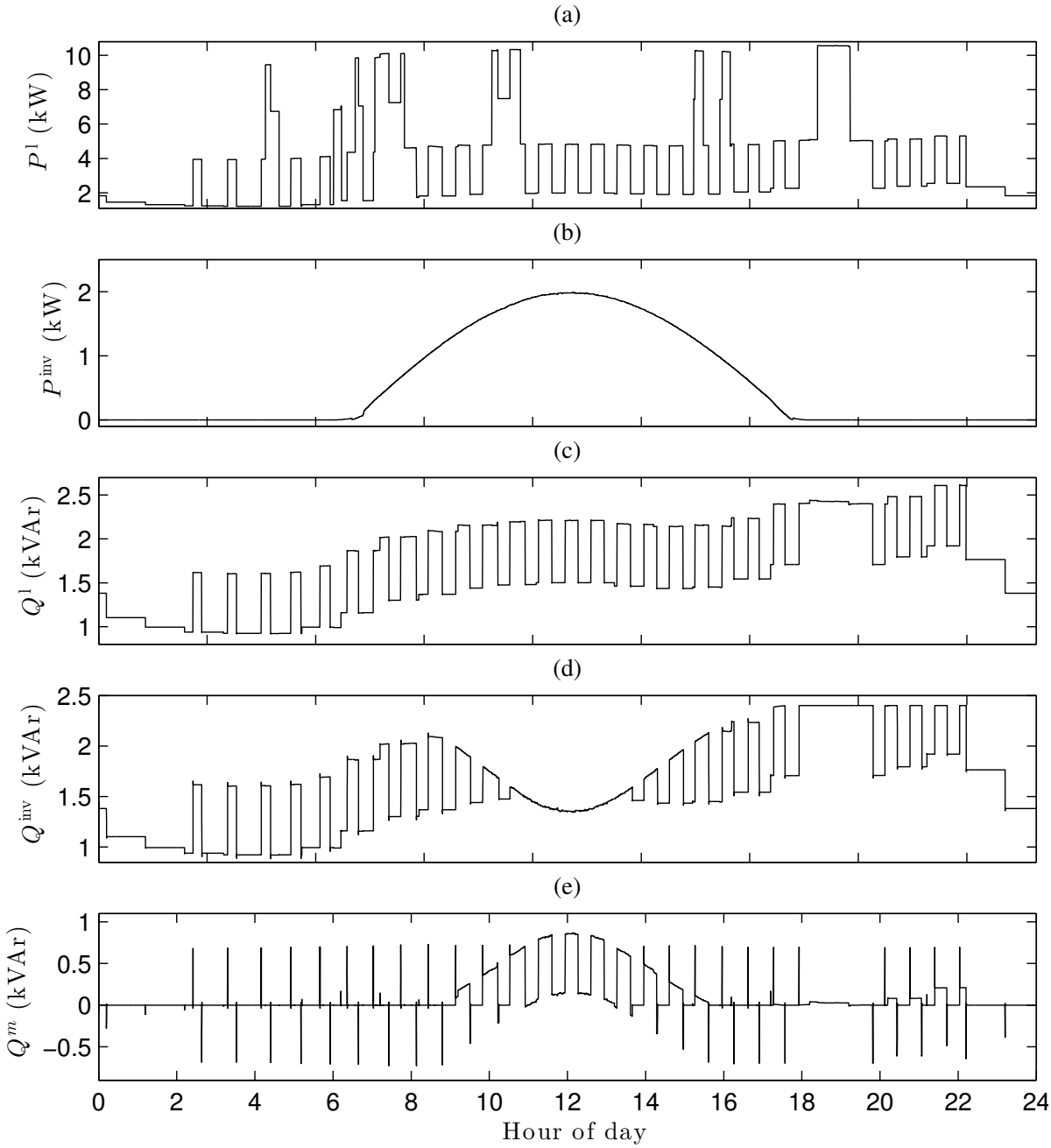

Figure 4.2 Power waveforms for one arbitrarily selected house: (a) Real power consumption of the house, (b) Real power generation from PV unit, (c) Reactive power consumption of the house, (d) Reactive power generation from PV unit, (e) Reactive power measured by the utility meter.

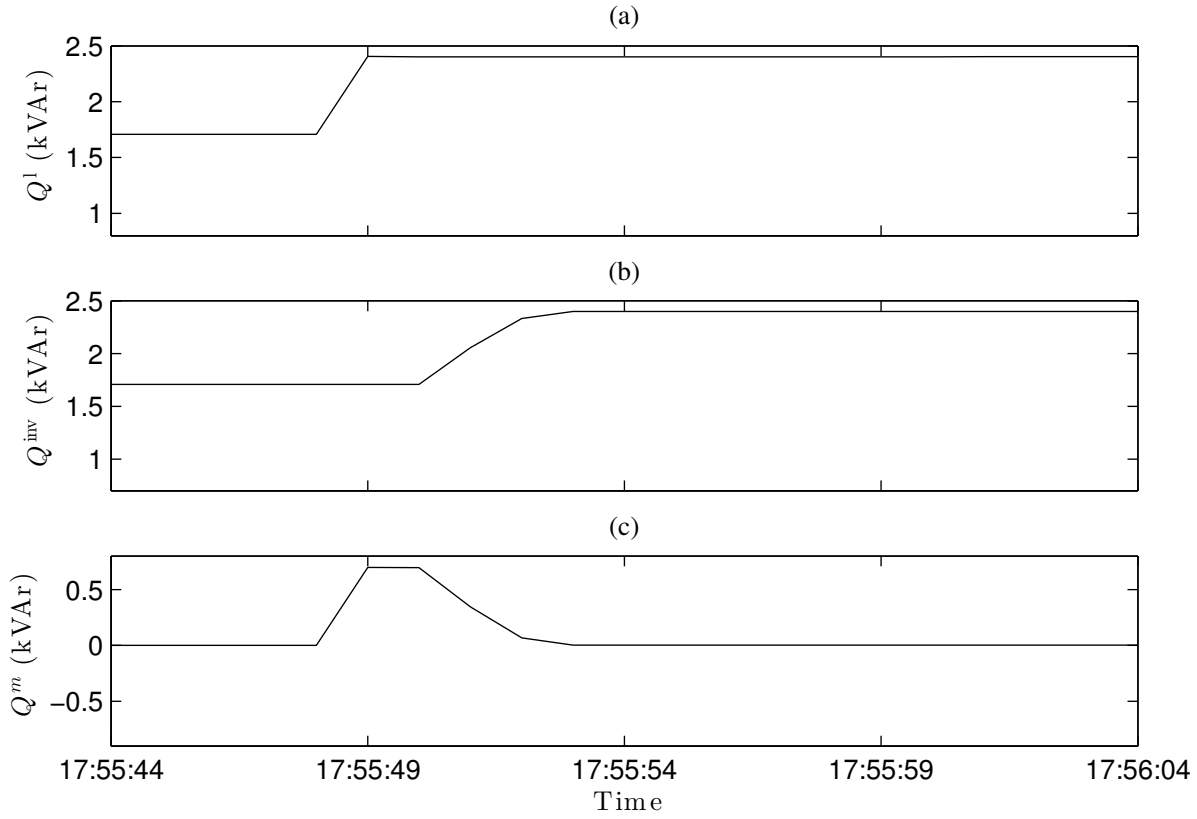

Figure 4.3 Magnified view of power waveforms for the arbitrarily selected house: (a) Reactive power consumption of the house, (b) Reactive power generation from PV unit, (c) Reactive power measured by the utility meter.

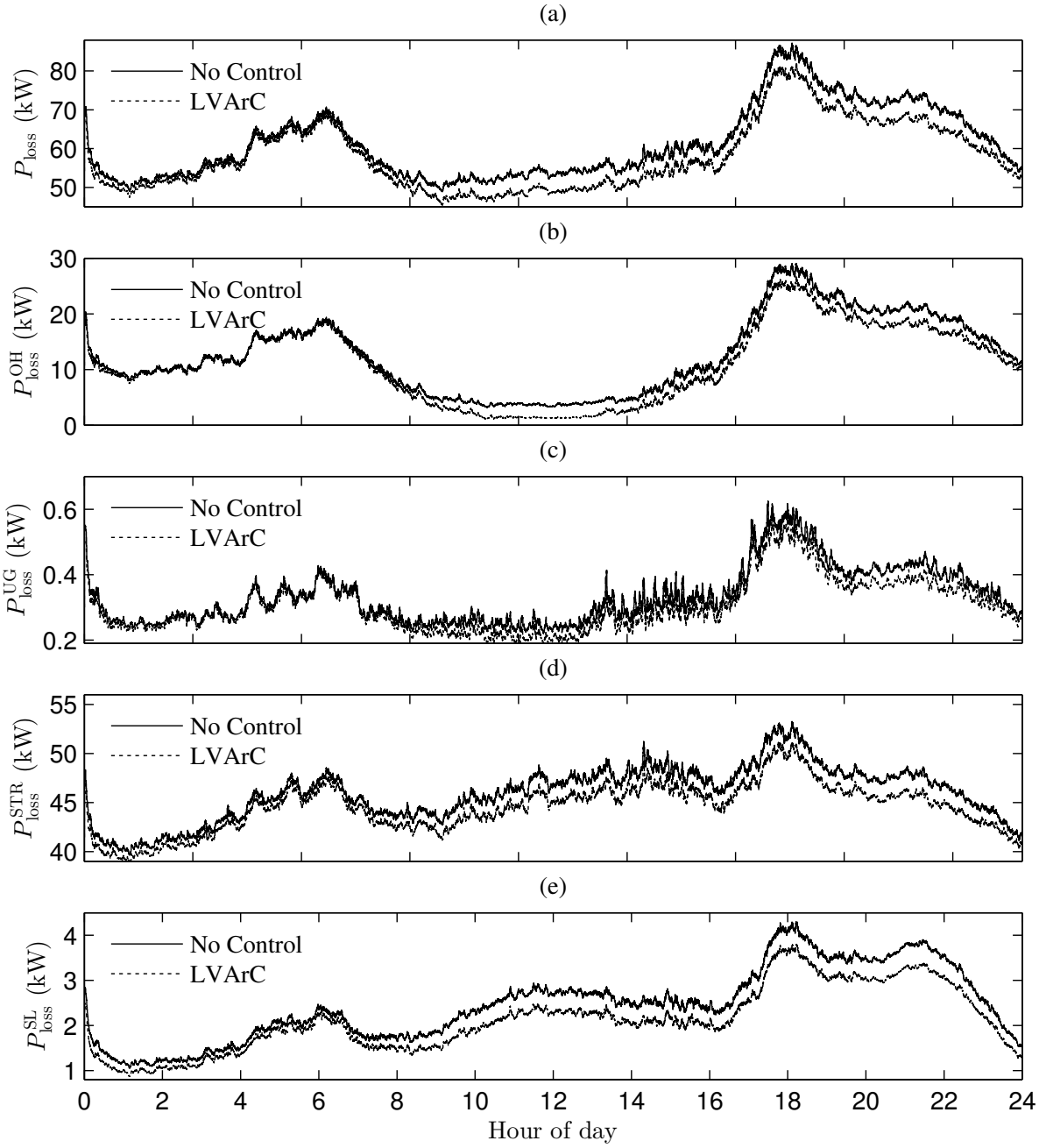

Figure 4.4 Real power loss metrics for 50% PV penetration in R1-1247-1: (a) Total loss, (b) Loss in overhead lines, (c) Loss in underground cables, (d) Loss in service transformers, (e) Loss in service lines (120 V).

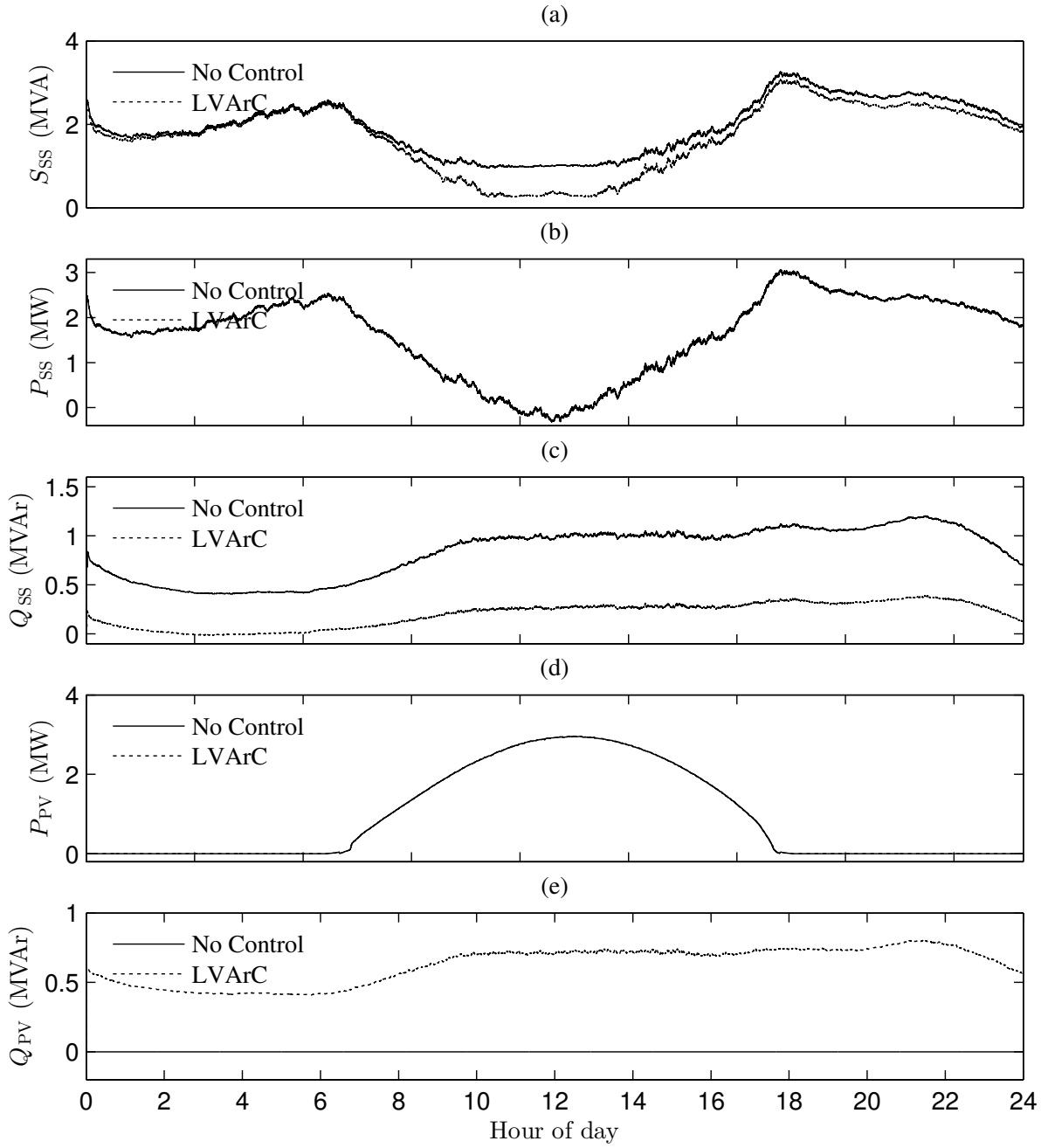

Figure 4.5 Power metrics for 50% PV penetration in R1-1247-1: (a) Apparent power at the substation, (b) Real power at the substation, (c) Reactive power at the substation, (d) Real power generation from all PV units, (e) Reactive power generation from all PV units.

5. CONCLUSIONS AND FUTURE WORK

5.1 Conclusions

This dissertation has presented the design and implementation of two novel distributed controllers within rooftop PV inverters. The proposed controllers did not require communication or cooperation with other PV inverters. In the presented approach, the reactive power capability of the PV inverters was exploited and the dispatch of their reactive power was calculated in an autonomous fashion. Through detailed modeling and time-series analysis, it was shown that implementation of these controllers could have a significant beneficial impacts upon the efficiency and operation of the power grid.

The most significant contributions and conclusions of this work can be summarized as follows.

- In Chapter 2, a real representative power distribution feeder model with high fidelity (in terms of electrical topology, household loads and smart appliances, and environmental parameters) was developed. This feeder model was used in performing detailed analysis of PV generation with the proposed controllers.
- In Chapter 3, we investigated the design and implementation of a voltage control loop within rooftop PV inverters to offset the voltage rise via absorbing reactive power. We conducted the analysis with detailed computer simulations of an array of the developed test feeder and other representative realistic feeders for several PV penetration levels. In addition to a sunny sky, the effect of cloud transients on distribution system performance using the proposed distributed Volt/VAr con-

troller was investigated. In all cases that were analyzed, voltage violations were completely eliminated. The simulations were run using GridLAB-D. The original inverter source code of GridLAB-D was modified to represent the proposed control. Additionally, it was observed that simple digital implementation of the droop controller leads to an undesirable oscillatory behavior between a large number of inverters connected to the grid. This phenomenon has not been previously mentioned in the PV literature, but it was revealed by our simulations. In order to mitigate this, a transfer function that helps stabilize the system by eliminating unwanted oscillatory behavior was introduced in the control path. In conclusion, this work showed that use of the proposed controller can maintain the distribution system voltages within acceptable bounds. Therefore, this approach can reduce or defer the need for new assets or grid reinforcements and will accommodate higher levels of distributed PV into the distribution system.

- A novel control scheme for PV inverters that permits residential rooftop PV systems to compensate their local reactive power consumption proposed in Chapter 4. In order to evaluate the effectiveness of the proposed controller, studies were performed by means of computer simulations of real and realistic distribution feeders with hundreds of households and their appliances modeled in high detail. Results showed that the controller is able to substantially reduce real energy losses in the feeder and reactive energy demand at the substation. Besides, it is obvious that reducing reactive demand at substation leads to loss reduction of substation transformer and transmission network. It can also maximize power transfer capability in the transmission lines. Therefore, implementing this proposed controller has significant beneficial impacts upon the efficiency of power system. Furthermore, a general framework for system stability was established using a novel distribution system analysis framework. Then it was proved that system-level voltage stability is guaranteed by using individually well-tuned controllers, which relieves the

system stability concerns for this type of controllers.

5.2 Directions of Future Research

This dissertation is not without limitations. For future research, the following directions are proposed:

- It would be interesting to integrate the aforementioned VAr compensation control in Chapter 4 with the conservation voltage reduction (CVR)[1] for reducing the induced voltage rise due to local reactive power injection. This approach can be implemented as an integrated control scheme which will monitor some or all of real-time voltages of residential loads, transmitted by smart meters via network communication. The integrated scheme can trigger sets of control commands to adjust set point and band width of substation load tap changer.
- The PV inverter can be a multi-functional device which has several operational modes such as voltage regulation and LVArC modes. For example, at normal system operation (no local voltage violation), the PV system could work in the LVArC mode (implemented in Chapter 4) to improve the operation and efficiency of the system (reducing transmission losses, maximizing power transmission capability and enhancing stability). When the inverter detects any local voltage violation it can switch to the voltage regulation mode (implemented in Chapter 3). It would be interesting to implement and test a multi-functional inverter on realistic distribution feeders for several PV penetration levels.
- The proposed LVArC controller has been claimed to be a good option to reduce congestion and losses in transmission lines. A comprehensive and accurate transmission energy loss and congestion analysis, taking into account several realistic

[1] In CVR mode, the distribution system is operated in the lower half of the acceptable voltage range (i.e., within 114–120 V in the USA), which leads to a reduction of power drawn by voltage dependent loads and to more energy savings.

feeders with the proposed controllers connected to a realistic transmission grid, is a worthwhile topic for further analysis.

- In addition, it is of significance to perform a complete economic comparison among centralized voltage regulation methods and the distributed Volt/VAr controller proposed in this work.

BIBLIOGRAPHY

[1] F. C. Brian Seal and A. Hefner, "Distributed energy management (DER): Advanced power system management functions and information exchanges for inverter-based der devices, modelled in IEC 61850-90-7," Tech. Rep., 2012.

[2] [Online]. Available: http://www.nrel.gov/gis/solar.html

[3] P. Basore and J. Gee, "Crystalline-silicon photovoltaics: necessary and sufficient," in *Photovoltaic Energy Conversion, 1994., Conference Record of the Twenty Fourth. IEEE Photovoltaic Specialists Conference - 1994, 1994 IEEE First World Conference on*, vol. 2, Dec 1994, pp. 2254–2257 vol.2.

[4] O. El Bassiouny, S. Dhople, A. Davoudi, and P. Chapman, "Energy-efficient cost-effective inverter configuration for residential photovoltaic systems," in *35th IEEE Photovoltaic Specialists Conference (PVSC)*, June 2010.

[5] A.-N. Azmi, M. Kohle, and A. Imenes, "On-grid residential development with photovoltaic systems in southern norway," in *IEEE Conference on Clean Energy and Technology (CEAT)*, Nov. 2013.

[6] "EPIA market report 2012," European Photovoltaic Industry Association (EPIA), Brussels, Belgium, Tech. Rep., Feb. 2013.

[7] "Global market outlook for photovoltaics 2013-2017," European Photovoltaic Industry Association (EPIA), Brussels, Belgium, Tech. Rep., May 2013.

[8] L. Sherwood, "U.S. solar market trends 2012," The Interstate Renewable Energy Council, Inc. (IREC), Tech. Rep., July 2013. [Online]. Available: http://www.irecusa.org/wp-content/uploads/2013/07/Solar-Report-Final-July-2013-1.pdf

[9] T. A. Short, *Electric power distribution handbook*. Boca Raton, FL: CRC Press, 2003.

[10] M. H. Bollen and F. Hassan, *Integration of distributed generation in the power system*. Hoboken, NJ: John Wiley & Sons, Inc, 2011.

[11] C. L. Masters, "Voltage rise: the big issue when connecting embedded generation to long 11 kV overhead lines," *Power Eng. J.*, vol. 16, no. 1, pp. 5–12, Feb. 2002.

[12] P. M. S. Carvalho, P. F. Correia, and L. A. F. Ferreira, "Distributed reactive power generation control for voltage rise mitigation in distribution networks," *IEEE Trans. Power Syst.*, vol. 23, no. 2, pp. 766–772, May 2008.

[13] M. Braun, T. Stetz, T. Reimann, B. Valov, and G. Arnold, "Optimal reactive power supply in distribution networks–technological and economic assessment for PV-systems," in *Proc. 24th Eur. Photov. Solar Energy Conf.*, Hamburg, Germany, Sep. 2009.

[14] L. Herman, B. Blazic, and I. Papic, "Voltage profile support in LV distribution networks with distributed generation," in *Proc. Univ. Power Eng. Conf. (UPEC)*, Glasgow, Scotland, Sep. 2009, pp. 1–5.

[15] E. Demirok, D. Sera, R. Teodorescu, P. Rodriguez, and U. Borup, "Evaluation of the voltage support strategies for the low voltage grid connected PV generators," in *Energy Conv. Congr. Exp. (ECCE)*, Atlanta, GA, Sep. 2010, pp. 710–717.

[16] M. Braun *et al.*, "Is the distribution grid ready to accept large-scale photovoltaic deployment? State of the art, progress, and future prospects," *Prog. Photovolt: Res. Appl.*, vol. 20, pp. 681–697, Nov. 2011.

[17] R. A. Shayani and M. A. G. de Oliveira, "Photovoltaic generation penetration limits in radial distribution systems," *IEEE Trans. Power Syst.*, vol. 26, no. 3, pp. 1625–1631, Aug. 2011.

[18] *American national standard for electric power systems and equipment—voltage ratings (60 hz), ANSI c84.1-2011*, American National Standards Institute (ANSI) Std.

[19] M. E. Elkhatib, R. El-Shatshat, and M. M. A. Salama, "Novel coordinated voltage control for smart distribution networks with DG," *IEEE Trans. Smart Grid*, vol. 2, no. 4, pp. 598–605, Dec. 2011.

[20] Y. Ueda, K. Kurokawa, T. Tanabe, K. Kitamura, and H. Sugihara, "Analysis results of output power loss due to the grid voltage rise in grid-connected photovoltaic power generation systems," *IEEE Trans. Ind. Electron.*, vol. 55, no. 7, pp. 2744–2751, Jul. 2008.

[21] S. B. Kjaer, J. K. Pedersen, and F. Blaabjerg, "A review of single-phase grid-connected inverters for photovoltaic modules," *IEEE Trans. Ind. Appl.*, vol. 41, no. 5, pp. 1292–1306, 2005.

[22] J. Worden and M. Zuercher-Martinson, "How inverters work," *SolarPro, Apr./May*, 2009.

[23] Inverters, converters, controllers and interconnection system equipment for use with distributed energy resources, UL 1741. [Online]. Available: http://ulstandardsinfonet.ul.com/scopes/1741.html

[24] "IEEE standard for interconnecting distributed resources with electric power systems," *IEEE Application Guide for IEEE Std 1547 (TM)*.

[25] Petra solar. [Online]. Available: http://www.petrasystems.com/

[26] Advanced energy industries. [Online]. Available: http://solarenergy.advanced-energy.com/

[27] Solaredge inverter compliance with new german grid code. [Online]. Available: http://www.solaredge.com/files/pdfs/products/inverters/se-inverter-compliance-with-lvgc.pdf

[28] T. Beach, A. Kozinda, and V. Rao, "Advanced inverters for distributed pv: Latent opportunities for localized reactive power compensation," *Cal x Clean Coalition Energy C226*.

[29] P. Jahangiri and D. Aliprantis, "Distributed Volt/VAr control by PV inverters," *IEEE Trans. Power Syst.*, vol. 28, no. 3, pp. 3429–3439, 2013.

[30] R. J. Broderick, J. E. Quiroz, M. J. Reno, A. Ellis, J. Smith, and R. Dugan, "Time series power flow analysis for distribution connected pv generation," *Sandia National Laboratories SAND2013-0537*, 2013.

[31] GridLAB-D. Pacific Northwest National Laboratory (PNNL). [Online]. Available: http://www.gridlabd.org/

[32] H. Li, F. Li, Y. Xu, D. Rizy, and J. Kueck, "Interaction of multiple distributed energy resources in voltage regulation," in *Proc. IEEE Power Energy Soc. Gen. Meet.*, Pittsburgh, PA, Jul. 2008.

[33] ——, "Adaptive voltage control with distributed energy resources: Algorithm, theoretical analysis, simulation, and field test verification," *IEEE Trans. Power Syst.*, vol. 25, no. 3, pp. 1638–1647, 2010.

[34] Integrated retail/wholesale power system operations with smart grid functionality: Project homepage. [Online]. Available: http://www.econ.iastate.edu/tesfatsi/IRWProjectHome.htm

[35] D. Aliprantis, S. Penick, L. Tesfatsion, and H. Zhao, "Integrated retail and wholesale power system operation with smart-grid functionality," in *Proc. IEEE Power Energy Soc. Gen. Meet.*, Minneapolis, MN, Jul. 2010.

[36] W. H. Kersting, "Radial distribution test feeders," in *Proc. IEEE Power Eng. Soc. Winter Meet.*, vol. 2, Columbus, OH, Jan. 2001, pp. 908–912.

[37] Distribution test feeders. IEEE PES Distribution System Analysis Subcommittee. [Online]. Available: http://www.ewh.ieee.org/soc/pes/dsacom/testfeeders/index.html

[38] K. Strunz, R. H. Fletcher, R. Campbell, and F. Gao, "Developing benchmark models for low-voltage distribution feeders," in *Proc. IEEE Power Energy Soc. Gen. Meet.*, Calgary, AB, Jul. 2009.

[39] K. Rudion, Z. A. Styczynski, N. Hatziargyriou, S. Papathanassiou, K. Strunz, O. Ruhle, A. Orths, and B. Rozel, "Development of benchmarks for low and medium voltage distribution networks with high penetration of dispersed generation," *CIGRE Report*, 2006.

[40] K. P. Schneider, Y. Chen, D. P. Chassin, R. Pratt, D. Engel, and S. Thompson, "Modern grid initiative distribution taxonomy final report," Pacific Northwest National Laboratory, Tech. Rep., Nov. 2008.

[41] K. P. Schneider, Y. Chen, D. Engle, and D. Chassin, "A taxonomy of North American radial distribution feeders," in *Proc. IEEE Power Energy Soc. Gen. Meet.*, Calgary, AB, Jul. 2009.

[42] U.S. Dept. of Transportation, Federal Highway Administration. National household travel survey (NHTS). [Online]. Available: http://nhts.ornl.gov/download.shtml

[43] T. Gönen, *Electric power distribution system engineering*, 2nd ed. CRC Press, 2007.

[44] Google earth. [Online]. Available: http://www.google.com/earth/index.html

[45] A. G. Thomas, P. Jahangiri, D. Wu, C. Cai, H. Zhao, D. C. Aliprantis, and L. Tesfatsion, "Intelligent residential air-conditioning system with smart-grid functionality," *under journal submission.*

[46] K. Fell *et al.* (2010, Mar.) Assessment of plug-in electric vehicle integration with ISO/RTO systems. KEMA, Inc. and ISO/RTO Council. [Online]. Available: http://www.isorto.org/

[47] D. Wu, C. Cai, and D. C. Aliprantis, "Potential impacts of aggregator-controlled plug-in electric vehicles on distribution systems," in *Proc. 4th IEEE workshop Comput. Adv. Multi-Sensor Adap. Process. (CAMSAP)*, San Juan, PR, Dec. 2011.

[48] M. Duoba, R. Carlson, and D. Bocci, "Calculating results and performance parameters for PHEVs," presented at the SAE World Congr. Exhibit., Detroit, MI, Apr. 2009.

[49] D. Wu, D. C. Aliprantis, and K. Gkritza, "Electric energy and power consumption by light-duty plug-in electric vehicles," *IEEE Trans. Power Syst.*, vol. 26, no. 2, pp. 738–746, May 2011.

[50] *SAE Electric Vehicle and Plug in Hybrid Electric Vehicle Conductive Charge Coupler*, Society of Automotive Engineers (SAE) Std. J1772, Jan. 2010.

[51] K. Parks, P. Denholm, and T. Markel, "Costs and emissions associated with plug-in hybrid electric vehicle charging in the Xcel Energy Colorado service territory," National Renewable Energy Laboratory, Golden, CO, Tech. Rep. NREL/TP-640-41410, May 2007.

[52] A. Brooks, E. Lu, D. Reicher, C. Spirakis, and B. Weihl, "Demand dispatch," *IEEE Power Energy Mag.*, vol. 8, no. 3, pp. 20–29, May/Jun. 2010.

[53] D. Wu, D. C. Aliprantis, and L. Ying, "Load scheduling and dispatch for aggregators of plug-in electric vehicles," *IEEE Trans. Smart Grid (Special Issue on Transportation Electrification and Vehicle-to-Grid Applications)*, to appear.

[54] C. Cai, P. Jahangiri, A. G. Thomas, H. Zhao, D. C. Aliprantis, and L. Tesfatsion, "Agent-based simulation of distribution systems with high penetration of photovoltaic generation," in *Proc. IEEE Power Energy Soc. Gen. Meet.*, Detroit, MI, July 2011.

[55] AMES wholesale power market test bed homepage. [Online]. Available: http://www.econ.iastate.edu/tesfatsi/AMESMarketHome.htm

[56] *American National Standard for Electric Power Systems and Equipment—Voltage Ratings (60 Hz), ANSI C84.1-2011*, American National Standards Institute (ANSI) Std.

[57] "EPIA market report 2011," European Photovoltaic Industry Association (EPIA), Brussels, Belgium, Tech. Rep., 2011.

[58] H. Kobayashi and H. Hatta, "Reactive power control method between DG using ICT for proper voltage control of utility distribution system," in *Proc. IEEE Power Energy Soc. Gen. Meet.*, San Diego, CA, Jul. 2011, pp. 1–6.

[59] R. Tonkoski and L. A. C. Lopes, "Impact of active power curtailment on overvoltage prevention and energy production of PV inverters connected to low voltage residential feeders," *Renew. Energy*, vol. 36, no. 12, pp. 3566–3574, Dec. 2011.

[60] M. Coddington, B. Kroposki, T. Basso, K. Lynn, C. Herig, and W. Bower, "High-penetration photovoltaic standards and codes workshop," National Renewable Energy Laboratory, Denver, CO, Tech. Rep. NREL/TP-550-48378, May 2010.

[61] M. H. J. Bollen and A. Sannino, "Voltage control with inverter-based distributed generation," *IEEE Trans. Power Delivery*, vol. 20, no. 1, pp. 519–520, Jan. 2005.

[62] R. Neal and R. Bravo, "Advanced Volt/VAr control element of Southern California Edison's Irvine smart grid demonstration," in *Proc. IEEE Power Syst. Conf. Expos. (PSCE)*, Phoenix, AZ, Mar. 2011, pp. 1–3.

[63] B. Bletterie *et al.*, "Development of innovative voltage control for distribution networks with high photovoltaic penetration," *Prog. Photovolt: Res. Appl.*, vol. 20, pp. 747–759, Nov. 2011.

[64] A. D. Domínguez-García and C. N. Hadjicostis, "Distributed algorithms for control of demand response and distributed energy resources," in *Proc. IEEE Control Decision Conf. (CDC-ECC)*, Orlando, FL, Dec. 2011, pp. 27–32.

[65] K. Schneider, J. Fuller, F. Tuffner, and R. Singh, "Evaluation of conservation voltage reduction (CVR) on a national level," Pacific Northwest National Laboratory (PNNL), Richland, WA, Tech. Rep., 2010.

[66] O. Galor, *Discrete dynamical systems.* Berlin, Germany: Springer, 2006.

[67] J. Duffie and W. Beckman, *Solar energy thermal processes.* Hoboken, NJ: John Wiley & Sons, Inc, 1974.

[68] M. D. Martz, "Photon's annual inverter market survey," *Photon Mag.*, vol. 3, pp. 66–87, 2011.

[69] P. Jahangiri, D. Wu, W. Li, D. C. Aliprantis, and L. Tesfatsion, "Development of an agent-based distribution test feeder with smart-grid functionality," in *Proc. IEEE Power Energy Soc. Gen. Meet.*, San Diego, CA, Jul. 2012.

[70] National Renewable Energy Laboratory. Measurement and instrumentation data center. [Online]. Available: http://www.nrel.gov/midc/

[71] C. Cai and D. Aliprantis, "Cumulus cloud shadow model for analysis of power systems with photovoltaics," *IEEE Trans. Power Syst.*, vol. 28, no. 4, pp. 4496–4506, Nov 2013.

[72] E. Demirok, P. Casado Gonzalez, K. Frederiksen, D. Sera, P. Rodriguez, and R. Teodorescu, "Local reactive power control methods for overvoltage prevention of distributed solar inverters in low-voltage grids," *IEEE J. Photovoltaics*, vol. 1, no. 2, pp. 174–182, 2011.

[73] Y. Xu, L. Tolbert, F. Peng, J. Chiasson, and J. Chen, "Compensation-based non-active power definition," *IEEE Power Electron. Lett.*, vol. 1, no. 2, pp. 45–50, 2003.

[74] M. H. Rashid, *Power electronics handbook*. Academic Press, 2001.

[75] C. Cai, P. Jahangiri, A. Thomas, H. Zhao, D. Aliprantis, and L. Tesfatsion, "Agent-based simulation of distribution systems with high penetration of photovoltaic generation," in *Proc. IEEE Power Energy Soc. Gen. Meet.*, Detroit, Michigan, Jul. 2011.

[76] H. Yeh, D. Gayme, and S. Low, "Adaptive VAR control for distribution circuits with photovoltaic generators," *IEEE Trans. Power Syst.*, vol. 27, no. 3, pp. 1656–1663, 2012.

[77] Y. Xu, L. Tolbert, J. Chiasson, J. Campbell, and F. Peng, "A generalised instantaneous non-active power theory for STATCOM," *IET Electr. Power Appl.*, vol. 1, no. 6, pp. 853–861, 2007.

[78] E. Malashenko, S. Appert, and W. al Mukdad, "Advanced inverter technologies report," California Public Utilities Commission Grid Planning & Reliability, Tech. Rep., 2013.

[79] GE Digital Energy. (2012) Residential electrical metering, advanced ANSI metering solutions for the smart grid. General Electric Company. [Online]. Available: http://www.gedigitalenergy.com/products/brochures/i210_family.pdf

[80] Nexus. [Online]. Available: http://www.electroind.com/nexus1252-performance-enhanced-energy-and-power-quality-meter.html

[81] Veris industries. [Online]. Available: http://www.veris.com/docs/Datasheets/E5x_d01141.pdf

[82] Wattnode. [Online]. Available: http://www.ccontrolsys.com/w/Home

[83] D. Villacci, G. Bontempi, and A. Vaccaro, "An adaptive local learning-based methodology for voltage regulation in distribution networks with dispersed generation," *IEEE Trans. Power Syst.*, vol. 21, no. 3, pp. 1131–1140, 2006.

[84] K. Rogers, R. Klump, H. Khurana, A. Aquino-Lugo, and T. Overbye, "An authenticated control framework for distributed voltage support on the smart grid," *IEEE Trans. Smart Grid*, vol. 1, no. 1, pp. 40–47, 2010.

[85] M. Farivar, R. Neal, C. Clarke, and S. Low, "Optimal inverter VAR control in distribution systems with high PV penetration," in *Proc. IEEE Power Energy Soc. Gen. Meet.*, San Diego, CA, Jul. 2012.

[86] E. Dall'Anese, S. V. Dhople, and G. B. Giannakis, "Optimal dispatch of photovoltaic inverters in residential distribution systems," *IEEE Trans. Sustainable Energy*, vol. 5, no. 2, pp. 487–497, April 2014.

[87] K. Turitsyn, P. Sulc, S. Backhaus, and M. Chertkov, "Options for control of reactive power by distributed photovoltaic generators," in *Proc. IEEE Power Energy Soc.*, June 2011.

[88] B. Zhang, A. D. Domiguez-Garcia, and D. Tse, "A local control approach to voltage regulation in distribution networks," *arXiv preprint arXiv:1307.0855*, 2013.

[89] B. Robbins, C. Hadjicostis, and A. Dominguez-Garcia, "A two-stage distributed architecture for voltage control in power distribution systems," *IEEE Trans. Power Syst.*, vol. 28, no. 2, pp. 1470–1482, 2013.

[90] M. Braun, "Reactive power supplied by PV inverters, cost-benefit-analysis," in *22nd European Photovoltaic Solar Energy Conference (EU PVSEC 2007)*, Milan, Italy, 2007.

[91] F. Vignola, F. Mavromatakis, and J. Krumsick, "Performance of PV inverters," in *Proc. of the 37th ASES Annual Conference*, San Diego, CA, 2008.

[92] W. Kersting, *Distribution system modeling and analysis*. CRC, 2006.

[93] K. Schneider and J. Fuller, "Detailed end use load modeling for distribution system analysis," in *Proc. IEEE Power Energy Soc. Gen. Meet.*, Minneapolis, MN, Jul. 2010.

[94] M. Marwali, J.-W. Jung, and A. Keyhani, "Stability analysis of load sharing control for distributed generation systems," *IEEE Trans. Energy Conversion*, vol. 22, no. 3, pp. 737–745, Sep. 2007.

[95] Y. A. R. I. Mohamed and E. El-Saadany, "Adaptive decentralized droop controller to preserve power sharing stability of paralleled inverters in distributed generation microgrids," *IEEE Trans. Power Electron.*, vol. 23, no. 6, pp. 2806–2816, Nov 2008.

[96] S. Iyer, M. Belur, and M. Chandorkar, "A generalized computational method to determine stability of a multi-inverter microgrid," *IEEE Trans. Power Electron.*, vol. 25, no. 9, pp. 2420–2432, Sep. 2010.

[97] J. Agorreta, M. Borrega, J. Lopez, and L. Marroyo, "Modeling and control of N-paralleled grid-connected inverters with LCL filter coupled due to grid impedance in PV plants," *IEEE Trans. Power Electron.*, vol. 26, no. 3, pp. 770–785, March 2011.

[98] J. Sun, "Impedance-based stability criterion for grid-connected inverters," *IEEE Trans. Power Electron.*, vol. 26, no. 11, pp. 3075–3078, Nov 2011.

[99] J. He, Y. W. Li, D. Bosnjak, and B. Harris, "Investigation and active damping of multiple resonances in a parallel-inverter-based microgrid," *IEEE Trans. Power Electron.*, vol. 28, no. 1, pp. 234–246, Jan 2013.

[100] X. Wang, F. Blaabjerg, Z. Chen, and W. Wu, "Modeling and analysis of harmonic resonance in a power electronics based AC power system," in *Proc. IEEE Energy Conversion Congr. Expos. (ECCE)*, Sep. 2013.

[101] R. Arghandeh, A. Onen, J. Jung, and R. P. Broadwater, "Harmonic interactions of multiple distributed energy resources in power distribution networks," *Electric Power Systems Research*, vol. 105, pp. 124–133, 2013.

[102] H. K. Khalil and J. Grizzle, *Nonlinear systems*. Prentice Hall, Upper Saddle River, 2002, vol. 3.

[103] J. R. Silvester, "Determinants of block matrices," *The Mathematical Gazette*, vol. 84, no. 501, pp. 460–467, 2000.